2-28-2013

Effect of Arginine and Oscillatory Ca2+ on Vascular Response Mediated Via Nitric Oxide Signaling in Normal and Salt Sensitive Hypertensive Rat Mesenteric Arterioles

Tushar V. Gadkari

tgadk001@fiu.edu

FLORIDA INTERNATIONAL UNIVERSITY

Miami, Florida

EFFECT OF ARGININE AND OSCILLATORY Ca^{2+} ON VASCULAR RESPONSE

MEDIATED VIA NITRIC OXIDE SIGNALING IN NORMAL AND SALT

SENSITIVE HYPERTENSIVE RAT MESENTERIC ARTERIOLES

A dissertation submitted in partial fulfillment of

the requirements for the degree of

DOCTOR OF PHILOSOPHY

in

BIOMEDICAL ENGINEERING

by

Tushar V. Gadkari

2013

To: Dean Amir Mirmiran
      College of Engineering and Computing

This dissertation, written by Tushar V. Gadkari, and entitled Effect of Arginine and Oscillatory Ca^{2+} on Vascular Response mediated via Nitric Oxide Signaling in Normal and Salt Sensitive Hypertensive Rat Mesenteric Arterioles, having been approved in respect to style and intellectual content, is referred to you for judgment.

We have read this dissertation and recommend that it be approved.

_____
Chenzhong Li

_____
Yen-Chih Huang

_____
Konstantinos Kavallieratos

_____
Nikolaos Tsoukias, Major Professor

Date of Defense: February 28, 2013.

The dissertation of Tushar V. Gadkari is approved.

_____
Dean Amir Mirmiran
College of Engineering and Computing

_____
Dean Lakshmi N. Reddi
University Graduate School

Florida International University, 2013

DEDICATION

गुरुर्ब्रह्मागुरुर्विष्णुःगुरुर्देवोमहेश्वरः।

गुरुरेवपरंब्रह्मतस्मैश्रीगुरवेनमः॥

'Salutation to the noble Guru, who is Brahma, Vishnu and Maheswara, the Parabrahma,

the Supreme Reality.'

To my parents, Snehal Vijay Gadkari and Vijay Mahadev Gadkari

In memory of my beloved 'amma'

ACKNOWLEDGMENTS

ABSTRACT OF THE DISSERTATION

EFFECT OF ARGININE AND OSCILLATORY Ca^{2+} ON VASCULAR RESPONSE

MEDIATED VIA NITRIC OXIDE SIGNALING IN NORMAL AND SALT

SENSITIVE HYPERTENSIVE RAT MESENTERIC ARTERIOLES

by

Tushar V. Gadkari

Florida International University, 2013

Miami, Florida

Professor Nikolaos Tsoukias, Major Professor

Hypertension, a major risk factor in the cardiovascular system, is characterized by an increase in the arterial blood pressure. High dietary sodium is linked to multiple cardiovascular disorders including hypertension. Salt sensitivity, a measure of how the blood pressure responds to salt intake is observed in more than 50% of the hypertension cases. Nitric Oxide (NO), as an endogenous vasodilator serves many important biological roles in the cardiovascular physiology including blood pressure regulation. The physiological concentrations for NO bioactivity are reported to be in 0-500 nM range. Notably, the vascular response to NO is highly regulated within a small concentration spectrum. Hence, much uncertainty surrounds how NO modulates diverse signaling mechanisms to initiate vascular relaxation and alleviate hypertension.

Regulating the availability of NO in the vasculature has demonstrated vasoprotective effects. In addition, modulating the NO release by different means has proved to restore endothelial function. In this study we addressed parameters that regulated NO release in the vasculature, in physiology and pathophysiology such as salt sensitive hypertension.

We showed that, in the rat mesenteric arterioles, Ca^{2+} induced rapid relaxation (time constants 20.8 ± 2.2 sec) followed with a much slower constriction after subsequent removal of the stimulus (time constants 104.8 ± 10.0 sec). An interesting observation was that a fourfold increase in the Ca^{2+} frequency improved the efficacy of arteriolar relaxation by 61.1%. Our results suggested that, Ca^{2+} frequency-dependent transient release of NO from the endothelium carried encoded information; which could be translated into different steady state vascular tone. Further, Agmatine, a metabolite of L-arginine, as a ligand, was observed to relax the mesenteric arterioles. These relaxations were NO-dependent and occurred via α-2 receptor activity. The observed potency of agmatine (EC_{50}, 138.7 ± 12.1 µM; n=22), was 40 fold higher than L-arginine itself (EC_{50}, 18.3 ± 1.3 mM; $n = 5$). This suggested us to propose alternative parallel mechanism for L-arginine mediated vascular relaxation via arginine decarboxylase activity. In addition, the biomechanics of rat mesentery is important in regulation of vascular tone. We developed 2D finite element models that described the vascular mechanics of rat mesentery. With an inverse estimation approach, we identified the elasticity parameters characterizing alterations in normotensive and hypertensive Dahl rats.

Our efforts were towards guiding current studies that optimized cardiovascular intervention and assisted in the development of new therapeutic strategies. These observations may have significant implications towards alternatives to present methods for NO delivery as a therapeutic target. Our work shall prove to be beneficial in assisting the delivery of NO in the vasculature thus minimizing the cardiovascular risk in handling abnormalities, such as hypertension.

LIST OF FIGURES

xiv

LIST OF ABBREVIATIONS AND ACRONYMS

Nitric Oxide	NO
Endothelium Derived Relaxing Factor	EDRF
Endothelium Derived Hyperpolarizing Factor	EDHF
Endothelial Nitric Oxide Synthase	eNOS
Smooth Muscle Cells	SMC
Endothelial Cells	EC
soluble Guanylyl Cyclase	sGC
Cyclic Guanosine Mono Phosphate	cGMP
Diacylglycerol	DAG
Inositol 1, 4, 5-triphosphate	IP_3
G-Protein Coupled Receptor	GPCR
α-2 Adrenergic Receptor	α-2 AR
oxy-hemoglobin	oxy-Hb
Acetylcholine	Ach
Spermine NONOate	SPER-NO
Norepinephrine	NE
L-NG-Nitroarginine Methyl Ester	L-NAME
DL-alpha-difluoromethyl[3,4-3H]arginine	DFMA
Ethylene Glycol Tetraacetic Acid	EGTA
Pertussis Toxin	PTx
Blood Pressure	BP
Low Salt fed Dahl Rats	DS-L

High Salt fed Dahl Rats	DS-H
Sprague Dawley	SD
Spontaneously Hypertensive Rats	SHR
Wistar Kyoto Rats	WKY
Real Time-Polymerase Chain Reaction	RT-PCR
Dulbecco's Modified Eagle Medium	DMEM
Fetal Bovine Serum	FBS
Phosphate Buffered Saline	PBS
Human Umbilical Vein Endothelial Cells	HUVEC
Dimethyl Sulfoxide	DMSO
Wall Thickness	WT
Cross Sectional Area	CSA

LIST OF SYMBOLS

m	Meter
μm	Micrometer
[X]	Concentration of X
μM	Micromolar
mM	Millimolar
nM	Nanomolar
mol	Moles
EC_{50}	Half Maximum Effective Concentration
min	Minute
D_0	External Diameter
D_i	Internal Diameter
σ_c	Circumferential Cauchy Stress
ε_c	Circumferential Cauchy Strain
P	Intraluminal Pressure
Y	Young's Modulus of Elasticity
λ_z	Axial Elongation
T	First Piola Kirchoff Stress
S	Second Piola Kirchoff Stress
D	Deformation Gradient
E	Green Lagrange Strain
W	Energy Density Work Function

CHAPTER 1

Introduction

1.1 Motivation

Hypertension has shown to play a significant role in triggering substantial health problems and targeting multiple end organs, thus leading to complex pathologies. Many factors, such as neuronal stimulus, hormonal release, cell signaling mechanisms and protein-protein interactions interplay together and make it difficult to isolate the precise cause of hypertension. Its pathogenesis thus remains intriguingly unknown.

Salt sensitivity is a measure of how the blood pressure responds to salt intake [1]. Salt sensitivity is observed in 50% of the hypertension cases [2]. High dietary sodium has been linked to multiple cardiovascular disorders including hypertension. Extensive literature and experimental data has been put forward to elucidate the mechanism of salt-sensitive hypertension [3]. However, there still exists only a vague understanding of how salt intake alters blood pressure regulation and causes hypertension.

Nitric Oxide (NO), after being identified as an endothelium derived relaxing factor (EDRF) [4], has garnered widespread attention as an endogenous vasodilator [5; 6; 7] and a putative neurotransmitter [8]. NO participates as an effector molecule in diverse and complex signaling mechanisms at various molecular levels. It serves many important biological roles in the cardiovascular physiology including blood pressure regulation. Recent studies trying the decipher the roots of hypertension have aroused significant interest in understanding mechanisms behind the L-arginine-Nitric Oxide system [9; 10; 11; 12] and pressure-volume regulation [13]. Substantial studies have reported decreased levels of NO production, reduced bioavailability or impaired cellular effects of NO in

1

hypertension leading to elevated arterial pressure. The widely accepted mechanism of NO action via the L-arginine-eNOS-NO-sGC-cGMP pathway is impaired at different levels [14; 15; 16], causing either enhanced vasoconstriction or suppressed vasodilatory effects. Vascular dysfunction is generally observed with the role of endothelium severely compromised in human as well as animal models [17; 18; 19]. There is a broad understanding about the underlying mechanisms involved in hypertension, however, the opinions seem to vary [23]. Few researchers have indicated increased NO levels, suggesting feedback mechanisms responding to hypertension [24; 25; 26; 27]. However, there is a general agreement with NO-mediated activity being significantly disrupted under hypertensive conditions.

NO is primarily synthesized in the vasculature by the oxidation of L-arginine to L-citrulline in the presence of O_2, NADPH and BH_4 in a NOS catalysed reaction. Vascular endothelium has shown to play an important physiological role in the dynamics of circulation [28]. Several theories [29; 30; 31; 32] have been proposed to elucidate the possible mechanism of NO induced vascular smooth muscle relaxation. A general consensus agrees towards NO produced in the endothelium under agonist stimulus; diffuses to the smooth muscle where it binds with high affinity to the ferrous heme of sGC to form a five coordinate Fe^{2+}-NO complex. This heme containing compound facilitates the catalytic conversion of GTP to cGMP leading to downstream phosphorylation of secondary messenger molecules and signal transduction. Modulation of calcium homeostasis plays an integral role in the downstream effect such as phospholipase C activity leading to the production of diacylglycerol (DAG) and inositol 1,4,5-triphosphate (IP_3) which triggers the activation of IP_3 receptors leading to increase

in intracellular calcium concentration modulated through the activity of ion channels. The NOS isoform expressed in the endothelial cells (eNOS), synthesizes majority of the NO produced in the vasculature [33; 34]. The eNOS, localized in the calveole [35] is inactive at the resting intracellular calcium levels, however under agonist stimulus, the intracellular calcium levels increase to facilitate complex protein-protein interactions [36] leading to calveolin-1 dissociation [33; 35], calmodulin binding and enzyme activation by phosphorylation [37; 38; 39]. When the intracellular calcium subsides and returns to basal levels it reverses the cycle to inactivate the eNOS. Several other mechanisms [37; 40] may stimulate the eNOS with transient increases in the intracellular calcium level playing an important role in regulating eNOS activity. The activation of eNOS has been reported in response to shear stress and under pulsatile conditions [41; 42].
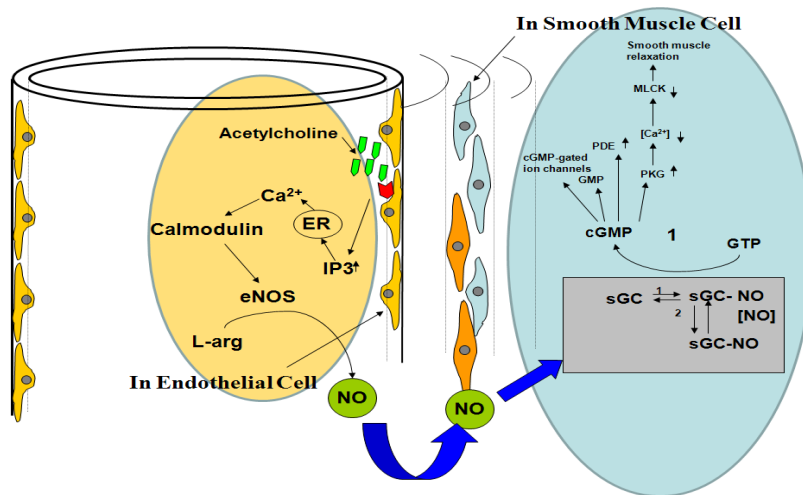
Fig 1.1 Mechanism of nitric oxide action to induce vascular relaxation

The arterioles demonstrate ability to control the vasomotor tone by modulating the vascular resistance. Increased sympathetic nerve activity is indicated to play a role in elevating vascular resistance in response to pulsatile circulation [43]. The kinetics of NO-cGMP pathway resembles a neuro-transmission mechanism, in which NO as a neuro-

modulator regulates vascular tone by activation of sGC causing cGMP accumulation [44]. Even though the mechanisms of sGC activation and deactivation are not clearly understood, it is observed that exposure to NO amplifies the sGC activity several hundred fold [45]. It is suggested that the NO binding to sGC acts as a physiological switch, where the binding of NO and the breaking of the His-Fe^{2+} bond is the first molecular event in progression of catalytic activation of sGC. In the smooth muscle, two temporally distinct states of sGC activation have been identified [46]. Initial basal levels of NO partially activates the sGC, leading to a formation of stable NO-Fe^{2+} complex, which produces low basal levels of cGMP to modulate the resting state vascular tone. A further acute increase in the NO availability follows a transient fully active enzyme which triggers increased cGMP production to facilitate phosphorylation of downstream targets leading to signal transduction and vascular relaxation [47; 48]. In addition, the desensitization of sGC is reported to cause transient and plateau patterns of cGMP responses which might play a role in selection of a particular cGMP mediated downstream signal transduction pathways [49; 50]. Under rapid dynamics the cGMP formation can be correlated to NO. The properties of sGC were observed to be different in cells and under purified condition [49]. Various binding rates of NO to sGC have been reported to provide a comprehensive NO-sGC binding kinetic analysis broadly suggesting rapid activation of sGC, typically few seconds following a much slower deactivation typically a couple of minutes [51; 52].

1.2 Frequency-Dependent Regulation of Vascular Tone

EDRF release has been reported to be modulated both by frequency and amplitude of the agonist activity such as flow, receptor binding or ion channel operation [53; 54].

There is a possibility that NO produced under such an influence may demonstrate oscillatory behavior in vivo. In response to the vasoactive stimulus, tonic oscillations of the diameter are observed in isolated arterioles [55]. The intracellular calcium is observed to follow a wave like pattern [56]. Under basal conditions, temporally coupled transient elevations of intracellular calcium are observed in vascular smooth muscle cells [57]. These synchronized calcium oscillations are regulated by endothelium derived NO. Oscillatory changes in blood pressure and flow have widely been correlated with the arteriolar tone regulation. Intracellular calcium is shown to play a crucial role is modulating the vascular tone. Vascular pulsations have shown beneficial cardiovascular effects which is linked to NO activity [58; 59].

NO availability is compromised in presence of several reactive oxygen species [60; 61]. This is accelerated even further with presence of hemeproteins in the surrounding vicinity of NO production site. Even though alternative roles of heme proteins as transporter of nitric oxide have been suggested [62; 63], oxy-hemoglobin is suggested to be the primary scavenger for nitric oxide from the biological systems [64; 65]. Palmer et.al showed that NO stimulated relaxation contracted back to basal state with a half life of 1-2 min and suggested the deactivation may be occurring by dissociation of NO from sGC [66]. Since then, various dissociation constants of NO from nitrosyl complexes of hemeproteins ranging from 1×10^{-3} to 1.8×10^{-5} sec^{-1} have been reported. Kharitonov [67; 68] measured the rate constant for NO-sGC dissociation of around 6×10^{-4} sec^{-1} at 20ºC which translates to a half life of about 2 min. Brandish et al [69] suggested that with the use of oxy-hemoglobin as a trap for NO, the rate constant for reversal for NO-sGC to ferrous sGC was 0.28 min^{-1} or a half life of 2.5 min at 37ºC. Studies have as well

5

suggested much faster dissociation rates [70] and a correlation to the acceleration of NO-sGC dissociation with the availability of substrates [69; 71]. In consensus, an overall understanding is that the sGC activation half life is relatively fast atleast an order faster in magnitude than its deactivation.

A twostate release of NO is possible with a sustained basal NO available which maintains steady vaso-dynamic tone and an oscillatory NO which occurs in burst to mimic the intracellular calcium bursting. It is likely that information is being transmitted from the endothelium to the smooth muscle in two states, a basal state facilitating a steady tone, and activated state triggering acute relaxation responses. Time-dependent NO release characteristics might play crucial role in facilitating such an activity.

In chapter 2, we tested the hypothesis previously proposed in our earlier work [72], experimentally by designing in-vitro experiments on isolated, cannulated and pressurized rat mesenteric arterioles. We demonstrated that a frequency-dependent delivery of nitric oxide achieved by modulating the NO bursting period could be a more effective way to deliver NO mediated drugs. We observed that a transient delivery of NO created by varying the NO pulse duration d over the period T exhibited a temporally dependent summation effect in achieving steady diameter tone. The observed steady states in diameter indicate a possibility that NO might escape scavenging if delivered in quick burst. A faster activation and slower deactivation of vessel might suggest a possible build up of NO activity. Since different mechanisms govern the production and consumption of NO, frequencies of burst fast enough to activate sGC might lead to a variable rate of NO accumulation in the vasculature. The pharmacological effects of such delivery may possibly perturb an intact signal transduction pathway.

Various NO donating drugs are being used with a wide range of clinical concentrations for regulating the tonic machinery in the vasculature [73]. Such drugs target the hemodynamic variables such as agonist activity, pulsatile flow, shear stress which facilitate oscillatory calcium release [74; 75]. These vasoactive agents control the vascular reactivity to achieve hemodynamic stability. However the potency of such drugs is compromised as they simultaneously influence a variety of other cellular and molecular mechanisms initiating non-specific actions. For NO based therapies to be effective in a wide range of applications, optimizing the efficiency of NO trapping and devising alternative methods of NO delivery are desirable. In this study, we illustrated the possibility that the frequency of NO bursting may have encoded information regarding vessel tone regulation. Design of drugs that incorporate the time period of NO release by modulating the frequency of NO bursts to regulate the endogenous NO bioavailability might provide a novel therapeutic technique for delivering NO in a more potent and efficient manner.

1.3 Agmatine as a mediator of L-arginine induced relaxations

L-arginine, a precursor to nitric oxide has shown to play an important physiological role in regulating the endogenous NO levels. L-arginine is required for optimal NO synthesis by nitric oxide synthase (NOS) in the rat mesenteric artery [76]. The importance of L-arginine as a therapeutic element in various physiological and pathophysiological processes such as wound healing [77; 78], protein synthesis and muscle building [79], endocrine metabolism [80], erectile dysfunction [81], cardiovascular functions [82; 83; 84] has widely been reported. It is suggested that L-arginine acts as a substrate for NOS to facilitate NO production [85]. The reported K_m

values for NOS isozymes range in 2-20 µM [85], particularly for eNOS it is reported to be 2.9 µM [86] and the intracellular L-arginine levels are in the range of 0.8 – 2 mM[87]. This would suggest that these enzymes are saturated with the substrate however it is observed that the rate of NO production varies with extracellular L-arginine concentrations [88; 89; 90]. If exogenous L-arginine acts as substrate and is present in saturating concentrations there should be a continuous production of NO. This discrepancy is widely referred to as L-arginine paradox [84]. There have been various mechanisms hypothesized to explain this behavior [91; 92; 93; 94] however there still exists an ambiguity in understanding how L-arginine mediates NO dependant relaxation. In addition to the beneficial effects of exogeneous arginine, recent study has demonstrated a possible role of agmatine as a potential vasodilator substance [95].

Agmatine [4-(aminobutyl) guanidine], a decarboxylation product of L-arginine, is produced endogenously under the activity of enzyme arginine decarboxylase (ADC) [85]. The importance of agmatine has been highlighted with its discovery as a novel neurotransmitter [96; 97] demonstrating its potential to affect multiple biological targets [98]. Various neuroprotective roles of agmatine [99], such as its role as a potential analgesic [100; 101] due to its effect of on NMDA receptor [97] or as a biphasic opoid function modulator [100] have been put forward. Agmatine has shown to reverse pain induced by inflammation [99] and provide protection to retinal ganglion cells from hypoxia [102]. The presence of agmatine in serum [103] suggested a physiological role for agmatine in the vasculature. The endothelial cells have shown to express ADC activity [104] and it has been reported that agmatine activates NOS in endothelial cells [105]. Further, agmatine shares its properties with clonidine-displacing substance [106]

and consist of a guanidium group which creates a possibility of agmatine binding as a ligand to imidazoline and α-2 type adrenergic receptors [96; 98; 104; 106; 107; 108]. In previously published data [89] we showed that L-arginine or one of its decomposition product may be initiating the NO synthesis via receptor binding and release of intracellular Ca^{2+} in endothelial cells.

In chapter 3, we presented a novel mechanism, where agmatine produced in the rat mesentery by the decomposition of L-arginine in presence of ADC activity initiates vascular relaxation. We showed that agmatine binding as a ligand on α-2 type adrenergic receptor and mediating relaxation via NO activity. To demonstrate this, we investigated the possible role of agmatine as a ligand, by performing reactivity study with intraluminally perfused exogenous agmatine and arginine. We further investigated the contribution of agmatine activity in hypertension.

1.4 Biomechanical properties of rat mesenteric arterioles

Mesenteric arterioles are referred to as resistance vessel as they contribute significantly to increased vascular resistance leading to blood pressure regulation [109]. The vascular tone and regional blood flow in the microcirculation depend on passive biomechanical properties of the vessel wall and on active constrictions of the vascular smooth muscle cells (SMC). The contractile state of SMCs depends on the intracellular calcium (Ca^{2+}) concentration and is regulated by an elaborate network of signaling pathways. In hypertension, complex remodeling of the vasculature with altered structure and mechanics of the resistance arteries is observed [110; 111; 112]. Several factors have been shown to play a role in vascular remodeling leading to morphological and functional changes in the vasculature [113; 114].

In chapter 4, we estimated the mechanical parameters of the rat mesenteric arterioles. We characterized the morphological differences in normotensive and hypertensive conditions. The pressure-diameter and pressure-thickness relationships play an important role in establishing normal blood flow conditions in the vasculature. Our understanding of physiological behavior at the tissue level in normotensive and hypertensive conditions is facilitated by obtaining pressure elongation relationships under isometric conditions. The compliance of the vasculature i.e. the slope of the pressure-diameter relationship is important in determining the non-linearity associated with the pressure flow relationship. The strain is computed from the changes in the circumferential and longitudinal displacement measurements relative to the zero stress state. We developed mathematical model to integrate the pressure-strain relationships obtained from the experiments. Inverse modeling approach enabled us to estimate the material properties such as the elasticity coefficients associated with the rat mesenteric vessels under normotensive and hypertensive conditions. This provided us a valuable insight in the abnormalities occurring in the mechanical structure of the vessel under both physiological and pathophysiological conditions. Our computational models further assisted in parameter estimation to characterize vascular properties and provided correlation between the different study groups.

1.5 Vascular reactivity study with Dahl salt sensitive hypertension model

The Dahl salt sensitive rat is a rodent model of hypertension that exhibits many phenotypic traits common with hypertensive disease observed in human populations [115]. Similarities include sodium sensitivity of hypertension and reduced renal function [116], elevated urinary excretion of protein and albumin, and a low plasma renin activity

[117], tubulointerstitial injury and the loss of nitric oxide synthase (NOS) in the development of hypertension [118]. It is suggested that the structural and functional changes that occur with vascular injury in the Dahl salt sensitive rat may contribute to the development of hypertension [18]. It is widely accepted that NO plays an important role in hypertension [8]. NO-mediated relaxation is observed to be impaired in salt sensitive hypertension [119]. Understanding the NO related mechanism in hypertension is crucial in alleviating high blood pressure related problems and designing more efficient drugs.

In chapter 5, we investigated the contribution of EDRF, EDHF and α-2 receptor mediated activity in salt sensitive hypertension. We tested the vascular responses of rat mesenteric arterioles in high salt (4% NaCl) and low salt (0.49% NaCl) fed Dahl salt sensitive rats. Our observations confirmed the possibility of multiple parallel $Ca2+$-dependent and independent pathways influencing NO induced relaxation responses.

1.6 Summary

In summary, the goal of this study was to contribute towards the understanding of NO mediated vascular tone regulation and its implications towards blood pressure regulation in physiological and pathological condition of salt sensitive hypertension.

CHAPTER 2

Frequency-dependent effect of Ca^{2+} induced nitric oxide release on the regulation of vascular tone in rat mesenteric arterioles

2.1 Introduction

Nitric Oxide (NO) as an endogenous vasodilator [5; 66] has been shown to participate in complex signaling mechanisms between endothelial cells (EC) and smooth muscle cells (SMC).NO produced in the endothelium diffuses to the smooth muscle where it modulates Ca^{2+} levels to induce smooth muscle relaxation. The NOS isoform, eNOS expressed in the endothelial cells, synthesizes majority of the NO produced in the vasculature [33].

Even though the biological role of NO and its mechanism of action are broadly established, the physiological concentration at which NO activates various signaling cascades is yet to be delineated. A wide range between picomolar to nanomolar may be regulating the tonic machinery in the vasculature [120; 121]. Recent developments have vaguely pointed the endogenous NO concentrations to range between 100 pM to 5 nM [121]. Notably, the sensitivity of the vascular response to NO is highly regulated in a small concentration spectrum. Thus, how NO initiates vascular responses in multiple pathways has remained an intriguing question.

Ca^{2+} is involved in the simultaneous regulation of many cellular processes [56; 122]. Several experiments have suggested Ca^{2+} oscillations to play a role in mediating concurrent signal transduction in different signaling cascades. Signaling between intracellular Ca^{2+} stores and Ca^{2+} channels have shown to generate intracellular Ca^{2+} oscillations in T lymphocytes [123]. Diverse cell functions are regulated by

information transmitted in the amplitude, duration or frequency of such oscillations [124]. Enzyme CaMKII has demonstrated the capability to decode the frequency of calcium oscillation into specific amount of kinase activity [125]. Konick et al [126] showed that three splice variants of β-CaMKII had different specific activity to Ca^{2+} oscillations and suggested that alternative splicing provided cells a mechanism to modulate their sensitivity to Ca^{2+} oscillations. Dolmetsch et.al [127] showed that the specificity towards a gene expression is modulated by the frequency of calcium oscillation. RasGTPases are binary switches that regulate Ras are likely to act as one of the decoder for information processing of Ca^{2+} Oscillation [128]. Ca^{2+} oscillations have shown to optimize Ca^{2+} mediated activation of Ras/ERK/MAPK pathway and facilitate its efficient activation [129]. CaMKII-PP1 exhibited switch like, all or none potentiation of individual hippocampal synapse in response to transient Ca^{2+} elevation [130].

In addition, the magnitude of contractile activity of the smooth muscle cells were determined by the frequency of calcium oscillations in rat intrapulmory arterioles [131], [132]. In the glia, intracellular Ca^{2+} facilitated intracellular IP_3 production, which resolved the information provided by a local Ca^{2+} wave into distinct spatial and temporal pattern of Ca^{2+} oscillation [133]. NO has been shown to induce smooth muscle cell relaxation by photolytic release of IP_3 with a decrease in the frequency of Ca^{2+} oscillations [134]. The eNOS may be one of the enzymes regulated by transient increases in calcium level [135]. NO produced under such influence may demonstrate oscillatory behavior in vivo.

Other theoretical studies [136; 137; 138; 139], have supported similar argument suggesting frequency of Ca^{2+} oscillations to transmit signaling information to regulate

cellular activity. Using nonlinear transformations [140], showed that biological processes with different time constants responded preferentially to different temporal stimuli. Selective regulation of different proteins was modeled by changes in bursting patterns of Ca^{2+} oscillation [137]. Empirical models have demonstrated sensitivity of enzymes such as CaMKII to optimal frequencies of Ca^{2+} oscillation [141]. Models for the kinetic activity of liver glycogen phosphorylase predicted Ca^{2+} oscillation frequency to reduce the threshold for enzyme activation [142]. Even though these studies made sound predictions, majority of them lacked experimental validation.

In our previous theoretical work, [72] has suggested that under certain conditions, transient release of NO may control the enzymatic activation of sGC. We demonstrated theoretically, a possible role for frequency-dependent control of cGMP formation under the influence of transient NO. A burst like production of NO may be observed after endothelial activation in response to periodic bursts of intracellular free Ca^{2+} [143]. The frequency of NO burst arising from the frequency of calcium oscillations in the EC may regulate cGMP formation in the SMC and control the vascular tone. We thus proposed oscillatory nature to NO activity that resulted from interaction between endothelial Ca^{2+} transients and eNOS.

In this study, we tested the vascular responses to Ca^{2+} frequency induced NO release. In-vitro experiments were performed on isolated, perfused rat resistance arterioles. We introduced oscillatory behaviour in the arterioles by modulating the pulse width of induced Ca^{2+} delivery. This could be translated to summation responses that were observed in the arteriolar tone. We showed that, frequency-dependent Ca^{2+} induced NO release may have encoded information that can be correlated to arteriolar tone.

2.2 Materials and Methods

2.2.1 Isolated Vessel Preparation

Experiments were performed on second order mesenteric arterioles (external diameter 360 ± 30 μm) isolated from male Sprague-Dwaley rats (250-300 g). The arterioles were cleaned of the surrounding tissue and cannulated with sutures on glass cannulas in a cannulation chamber. The preparation was placed in a perfusion bath maintained at 22°C and superfused with modified Krebs-Ringer buffer solution. The buffer solution (to ensure a pH of 7.4) was composed of the following (in mM): NaCl 145, KCl 5, $CaCl_2$ 2.5, $MgSO_4$ 1.2, KH_2PO_4 1.2, HEPES 20, and Glucose 10.1. The arterioles were pressurized to a constant pressure of 50 mmHg and stretched longitudinally to simulate physiological stretch condition. Only arterioles without leaks were used. Any arteriole that did not fully contract or fully relax was discarded. The preparation was allowed to equilibrate for 60 min before experimentation. Throughout the experiment, the tissue bath was continuously circulated with norepinephrine (2 μM) using a peristaltic pump. When steady constriction was established vascular reactivity was examined by intraluminal injection of solutions with an automated pressure driven system. A fast switching perfusion pencil allowed instantaneous exchange between different solutions (dead volume < 165 μl). Changes in the arteriolar diameter were recorded in real time on the stage of an inverted microscope (IX81, Olympus), fitted with a CCD video camera (1350B, QImagingRetiga) for data acquisition. The Image acquisition and post analysis of data was performed with IPLAB (BioVision Technologies) and MATLAB (MathWorks) software. The diameter at resting state was

taken as 0% relaxation obtained during precontraction to norepinephrine (2 µM). The vascular relaxation was expressed as percent increase in the resting diameter.
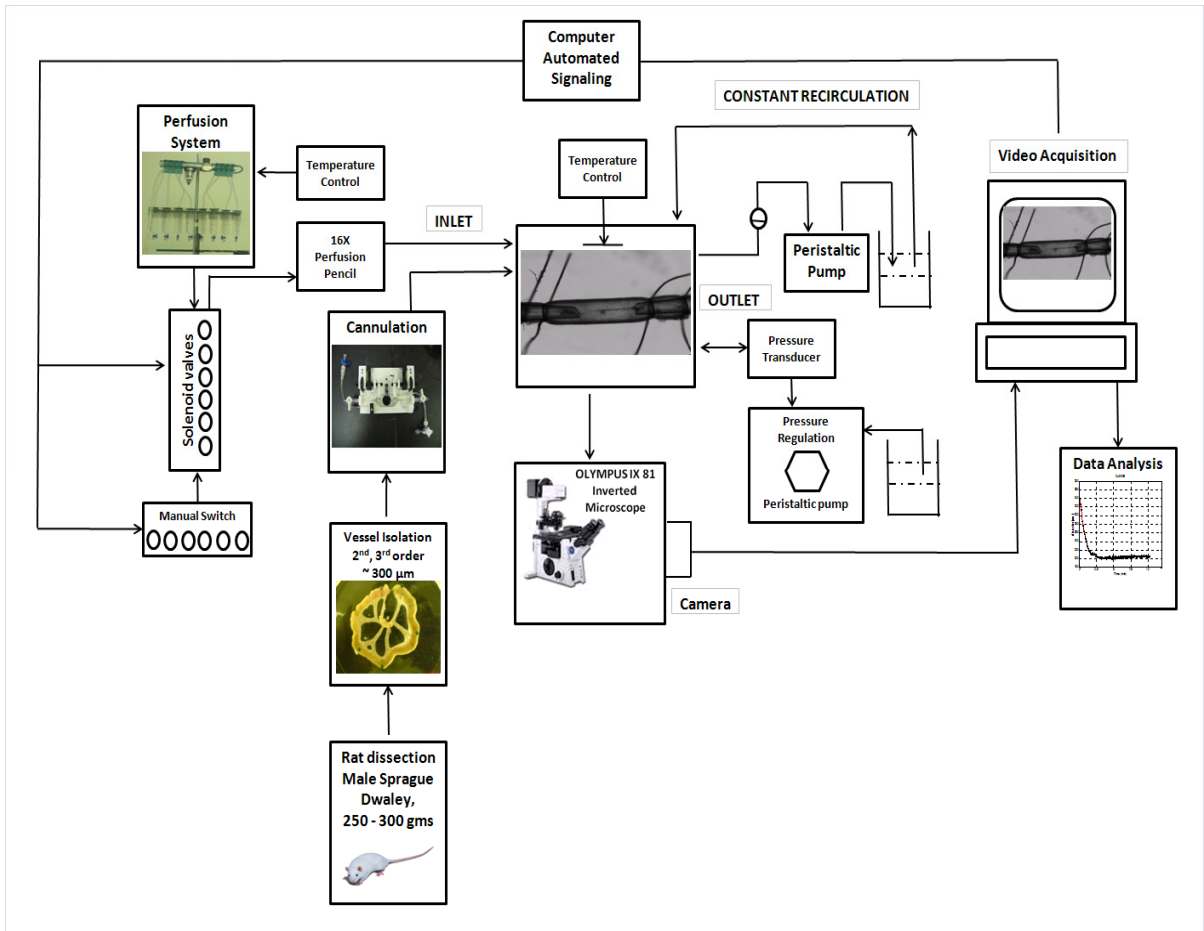
Fig 2.1. Schematic representation of the vascular reactivity methodology

2.2.2 Intraluminal loading of endothelium with fura 2-AM

To observe induced Ca^{2+} responses from the endothelium of intact arterioles, we loaded the pressurized mesenteric arteries with the ratiometeric Ca^{2+}-sensitive fluorescent dye fura 2-acetoxymethyl ester [144]. Fura 2-AM was dissolved in anhydrous DMSO at a concentration of 1 mM. Prior to loading, fura 2-AM was mixed with 10% solution of Pluronic F127 in DMSO. This solution was diluted with modified Krebs-Ringer buffer to yield a final concentration of 5 µM fura 2-AM and 0.05% Pluronic acid. Solenoid valve

operated perfusion system facilitated selective endothelial loading after delivery of fura 2-AM into the lumen for 5 min. This was followed by a 20 min washout with buffer solution to remove residual fura 2-AM from the lumen. After washout endothelial loading was visible on the luminal side of the artery in the focal plane. Similar loading protocols have previously shown that subsequent measurements are from endothelial Ca^{2+} with negligible contribution from smooth muscle [145; 146]. We assessed the changes in induced intracellular Ca^{2+} by calculating the ratio of the light emitted through a 510 nm emission filter when the vessel was illuminated at 340 and 380 nm respectively.

2.2.3 Materials

Fura 2-AM and Pluronic F127 were purchased from Molecular Probes (Eugene, OR). All other salts and drugs used in the study were purchased from Sigma, (St. Louis, MO). Male Sprague-Dwaley rats were obtained from Harlan Laboratories, (Madison, WI) and were maintained on standard pellet chow diet (2018 Teklad Global). All animal procedures were carried out in accordance with the National Institute of Health guidelines and were approved by the institutional animal care and use committee of florida international university.

2.2.4 Data analysis

Unless otherwise stated, all values are given as mean ± SE, n = number of rats. Results were presented as the normalized diameter (i.e, diameter divided by the fully relaxed diameter for the experiment). EC_{50} values were calculated by fitting concentration-response relationships to a sigmoidal curve. Statistical analysis was performed using student's t test. A P value < 0.05 was considered statistically significant.

2.2.4 Mathematical model

To assist our experimentation, we simulated the effect of frequency-dependent Ca^{2+} activity on diameter changes. We assumed the Ca^{2+} changes to induce diameter responses following a monoexponential relationship. The Ca^{2+} changes were modeled as a train of pulses described by a piecewise constant function

$$Q(t) = \begin{cases} Q_0 & iT \le t < iT + d \\ 0 & iT + d \le t < (i+1)T \end{cases} ; \quad i = 0, ..., \infty \qquad 2.1$$

characterized by period T, amplitude Q, and pulse duration d. The diameter response to Ca^{2+} resulted in vascular activation to the rising pulse $(iT \le t < iT + d)$ given by

$$D_a(t) = [D_{ss,a} - D_d(iT)](1 - e^{-k_a t}) + D_d(iT), \qquad 2.2$$

followed by vascular deactivation when the pulse subsides $(iT + d \le t < (i+1)T)$ given by

$$D_d(t) = [D_{ss,d} - D_a(iT+d)](1 - e^{-k_d(t-(iT+d))}) + D_a(iT+d), \qquad 2.3$$

where a represents the activation cycle, d describes the deactivation cycle and steady states were denoted by $D_{ss,a}$ and $D_{ss,d}$ respectively. The reaction rates, $k_a = \ln(2)/\tau_{relaxation}$ and $k_d = \ln(2)/\tau_{constriction}$ were calculated from time constants for the mesenteric arterioles obtained in our experiments.

2.3 Results

2.3.1 NO-mediated vascular activity

To establish a preconstriction concentration that gave submaximal constriction, we constructed a dose response curve to norepinephrine (Fig 2.2A). The EC_{50} value observed for norepinephrine was 0.3 ± 0.1 µM, $n = 3$. Steady constriction were retained at 2 µM, norepinephrine. In Fig 2.2B, intraluminally injected Acetylcholine [1 nM – 10 µM]

produced dose-dependent relaxation in arterioles from the resting state. Acetylcholine relaxed the arterioles with EC$_{50}$ value of 130.8 ± 0.7 nM, n = 6. The sensitivity to acetylcholine significantly decreased following treatment with L-NAME (0.5 mM), an eNOS blocker, n = 5. After eNOS blockade, maximum relaxation to acetylcholine attenuated from 92.8 ± 1.5% to 37.5 ± 5.1% demonstrating contribution of NO towards relaxation.
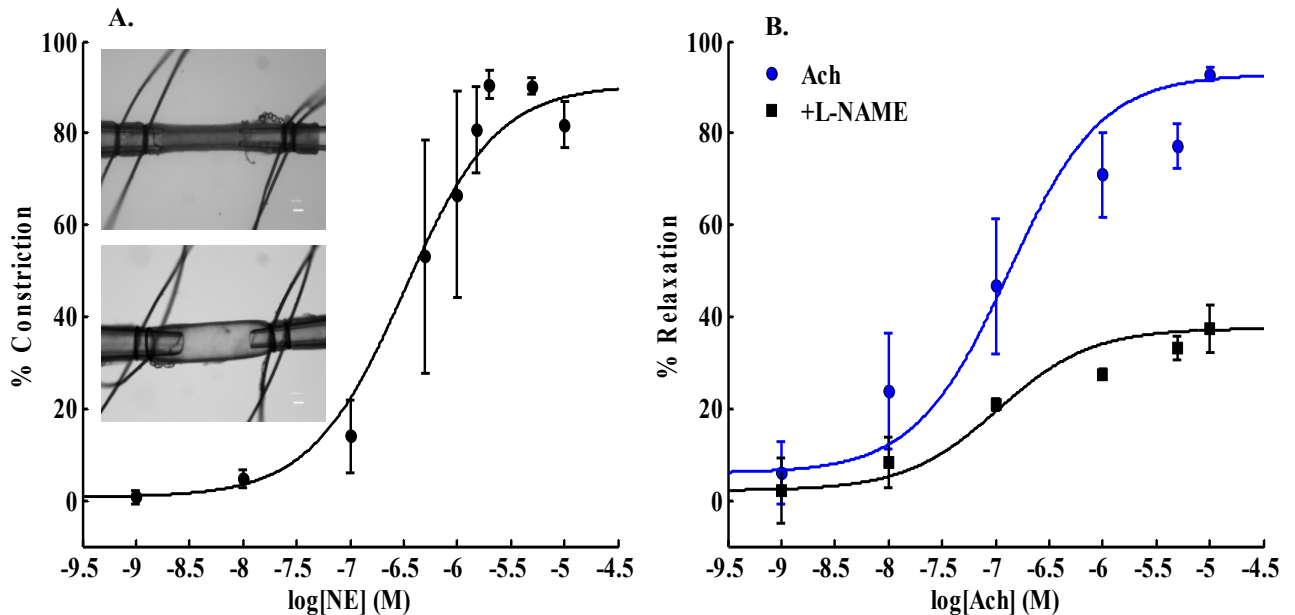
Fig 2.2. Concentration dependent relaxation responses to norepinephrine and Ach. (A). Dose-response to intraluminal perfusion of norepinephrine, NE (●, 1nM-10μM, n = 3) in Sprague Dwaley rat resistance arterioles. (B). Concentration dependent dose response curve to intraluminal perfusion of Acetylcholine, Ach (●, 1nM-10μM) in rat resistance arterioles, n = 6, along with response after inhibition with NG-nitro-L-arginine methyl ester, L-NAME (■), an eNOS blocker (0.5 mM), n = 5, demonstrating the role of nitric oxide in endothelium dependent relaxation. Inset shows arterioles constricted to 2μM NE and fully relaxed to 10μM Ach. All data are presented as mean ± SEM.

2.3.2 Time constants for rat resistance arterioles

To obtain time constants for Ca^{2+} induced vascular responses, we subjected the arterioles to intraluminal Ca^{2+} influx with A23187 (10 μM) and subsequent removal of Ca^{2+} with EGTA (500 μM) solution. In Fig 2.3 (A), we showed the vascular response to Ca^{2+} influx triggered with A23187 along with the response after eNOS blockade with L-NAME (0.5mM). In Fig 2.3 (B), we demonstrated the contribution of EDRF to relaxation by blocking the EDHF component with apamine (50 nM) and tram-34 (100 nM). Complete inhibition of relaxation was observed following a treatment with a combination of EDHF and EDRF blockers (apamine (50 nM), tram-34 (100 nM) and L-NAME (0.5mM)). The calculated time constants for these vascular responses as shown in Fig 2.3 (C-E), were $\tau_{relaxation}$ = 20.8 ± 2.2 sec, n = 5 and $\tau_{constriction}$ = 104.8 ± 10.0 sec, n = 5. We observed statistically significant difference between the time constants for arteriolar relaxation and constriction. After eNOS blockade the relaxation time constant obtained was $\tau_{relaxation}$ = 31.9 ± 4.97 sec, n = 3 and the constriction time constant was $\tau_{constriction}$ = 51.1 ± 2.5 sec, n = 3. Under similar conditions, we investigated the contribution of NO by inhibition of the EDHF component. The time constants obtained were $\tau_{relaxation}$ = 29.1 ± 4.2 sec, n = 3 and $\tau_{constriction}$ = 143.5 ± 18.2 sec, n = 3.
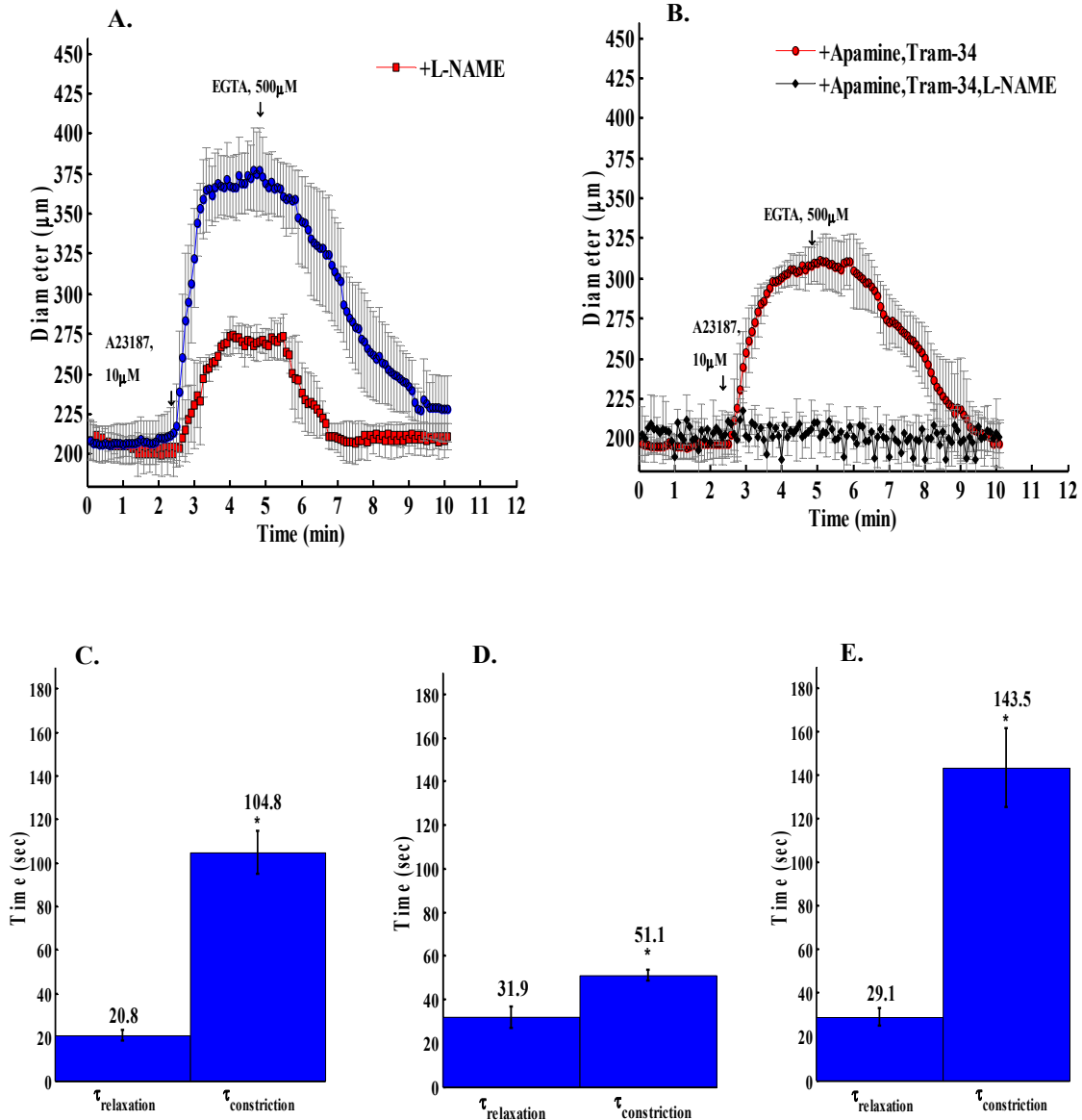
Fig 2.3. Time constant for vascular response to exogenous Ca^{2+}. (A) Vascular response to Ca2+ influx triggered by subjecting the arterioles to exogenous Ca2+ -containing (A23187, 10 µM) and Ca2+ -free (EGTA, 0.5 mM) solution; n = 5, along with EDRF blockade (L-NAME, 0.5mM, n = 3). (B) Relaxation observed after EDHF blockade (apamine; 50nM and Tram-34; 100nM, n = 3), followed by inhibition of EDHF and EDRF (apamine, 50nM, Tram-34, 100nM and L-NAME, 0.5mM, n = 3). (C) Time constants for the relaxation and constriction of the arteriole (D) after EDRF blockade (E) after EDHF blockade. The time constants were calculated by curve fitting the experimental data from Fig. 2 (A - B) with *p < 0.05 considered statistically significant for a student's t-test.

Acetylcholine has widely been reported to stimulate endogenous NO release [28]. Due to wide discrepancy in physiological concentration of NO production, endogenous mediator such as Ach provided a better choice as a source of NO. We repeated the experiment by subjecting the arterioles to intraluminal perfusion of NO stimulator (Ach, 10 µM) followed by NO scavenger (oxy-hemoglobin, 100 µM). The arterioles fully relaxed to Ach (10 µM) with $\tau_{relaxation}$ = 19.2 ± 0.9 sec, n = 9. The constriction to oxy-hemoglobin (100 µM) was much slower with $\tau_{constriction}$ = 92.6 ± 8.1 sec, n = 9. Following EDHF inhibition with apamine (50 nM) and tram-34 (100 nM), the arterioles exhibited vascular responses with $\tau_{relaxation}$ = 30.7 ± 1.7 sec, n = 4 and $\tau_{constriction}$ = 83.63 ± 8.1 sec, n = 4. After eNOS blockade with L-NAME (0.5 mM), in absence of NO, the time constants obtained were $\tau_{relaxation}$ = 34.0 ± 14.5 sec, n = 6 and $\tau_{constriction}$ = 56.1 ± 9.0 sec, n = 6. The arteriolar relaxations were completely abolished after incubation with a cocktail of apamine (50 nM), tram-34 (100 nM) and L-NAME (0.5 mM), n = 4.
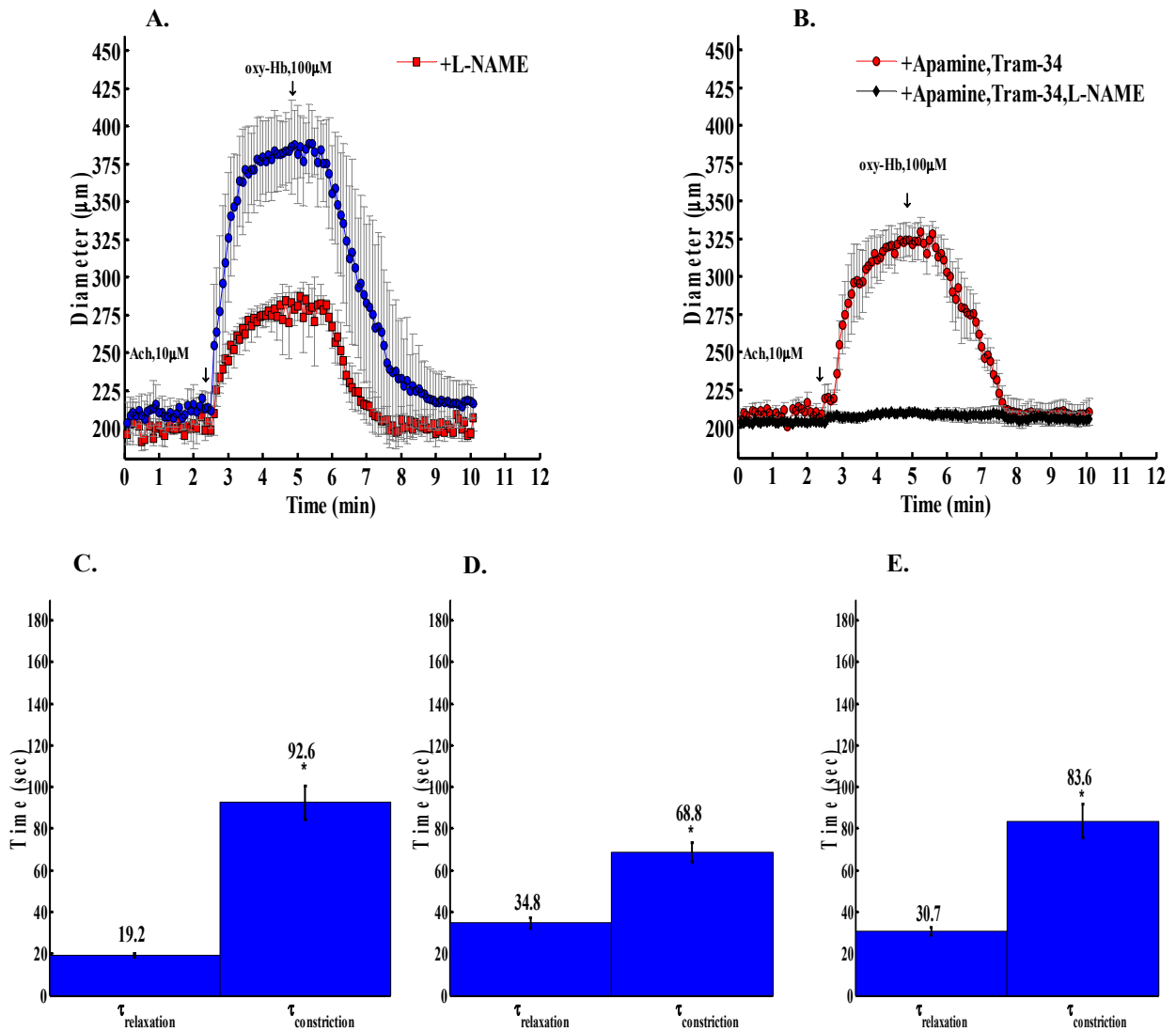
Fig 2.4. Time constant for activation and deactivation of the vessel tone response to NO release with Ach. (A): A scenario of NO delivery is created by subjecting the arteriole to NO mediator Ach, (10 μM) which stimulates endogenous NO release. This is followed by a period of no NO release, where the available NO is scavenged by intraluminal delivery of oxy-Hb (100μM). **(B):** The diameter response was observed after blockade of EDHF component with cocktail of apamine (50nM) and Tram-34 (100nM), *n* = 4, followed by a blockade of both EDHF and EDRF component with a combination of apamine (50 nM), Tram-34 (100 nM) and L-NAME (0.5 mM), *n* = 3. **(C):** Time constants for the activation and deactivation of the arteriole and **(D)** after EDRF blockade **(E)** after EDHF blockade calculated by curve fitting the experimental data from (A - B) with *p* < 0.05 considered statistically significant for a paired t-test.

23

2.3.3 Endothelial Ca^{2+} response induced by exogenous Ca^{2+} delivery

In Fig 2.5, we demonstrated endothelial Ca^{2+} response from intact pressurized mesenteric arterioles loaded with fura 2-AM. The fluorescence signal expressed as $F_{340/380}$ ratio was obtained from the vessel subjected to an induced Ca^{2+} pulse of duration $d = 10$ sec and period $T = 60$ sec. The observed Ca^{2+} response mimicked the induced Ca^{2+} delivery in the vessel with a duration of 10 sec.
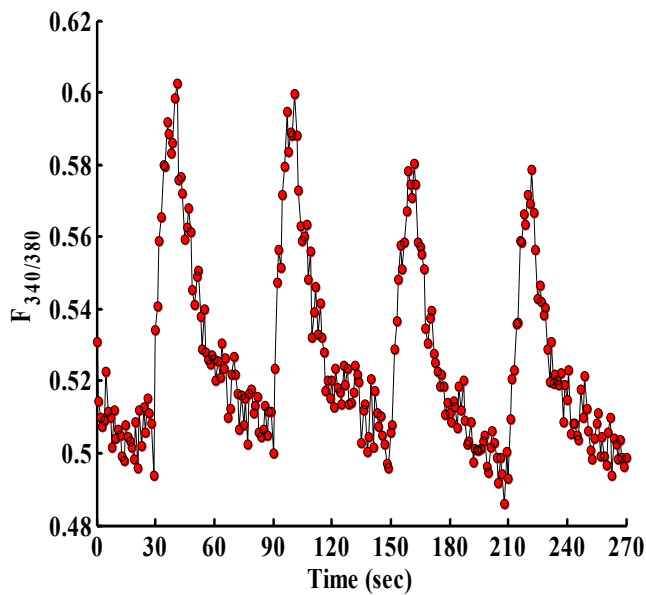
Fig 2.5. Ca^{2+} response from vessel loaded with fura2-AM. Demonstration of induced Ca^{2+} pulse scenario (duration $d = 10$ sec and period $T = 60$ sec) achieved with rapid switching of Ca^{2+}-containing A23187-4Br, 10 µM and Ca^{2+}-free (EGTA, 0.5 mM) solutions.

2.3.4 Frequency-dependent effect of endothelial Ca^{2+} induced nitric oxide release on vascular responses

In Fig 2.6, we demonstrated the frequency-dependent effect of Ca^{2+}mediated NO release on vascular responses in rat resistance arterioles. A sequential bursting of Ca^{2+} was achieved by rapid switching between a Ca^{2+} (A23187, 10 µM) and 0Ca^{2+} (EGTA,

500 µM) solution. We modulated the Ca^{2+} pulse by varying the duty cycle ratio, d/T. A duty cycle ratio d/T = 1; denoted sustained Ca^{2+} delivery, whereas, d/T < 1 indicated transient delivery of Ca^{2+}. For different duty cycle ratio the changes in diameter were tracked in real time. For a constant duration d, the duty ratio is a function of frequency (1/T). We demonstrated vascular responses for burst duration d= 10 sec and period T=15, 20, 30, and 60 sec respectively, Fig 2.6A (i -iv). To test the contribution of NO in frequency-dependent vascular responses, we repeated the experiments with EDRF blockade (Fig 2.6 B). We observed significantly compromised vascular responses following EDRF blockade. The vascular response to frequency dependent NO release was seen after EDHF blockade (Fig 2.6 C). In Fig 2.8, we presented steady state normalized diameter values calculated by fitting the data presented in Fig 2.6 (A - C) to monoexponential activation function, $\widehat{D}(t) = D_{ss} \cdot \left(1 - e^{\frac{-t}{\tau}}\right)$, where D_{ss} is the steady state diameter, τ is the time constant. The observed relaxation with duty cycle ratio, d/T = 10/15, 10/20, 10/30 and 10/60 were 92.6 ± 1.2%, 67.1 ± 1.0%, 60.2 ± 0.9%, and 31.5 ± 0.8% respectively for n = 3. After EDHF blockade with apamine (50 nM) and tram-34 (100 nM) the relaxation were 55.2 ± 0.7%, 50.6 ± 2.1%, 27.4 ± 0.4%, and 21.6 ± 0.3% respectively for n = 3. These relaxation were significantly compromised after EDRF blockade with L-NAME (0.5mM). The observed steady state values were 27.7 ± 0.5%, 19.3 ± 0.6%, 19.2 ± 1.9%, and 14.1 ± 0.3% respectively for n = 3.

Fig 2.6 A:

i.

ii.

iii.

iv.

Fig 2.6 B:

i.

ii.

iii.

iv.

Fig 2.6 C:

i.

ii.

iii.

iv.
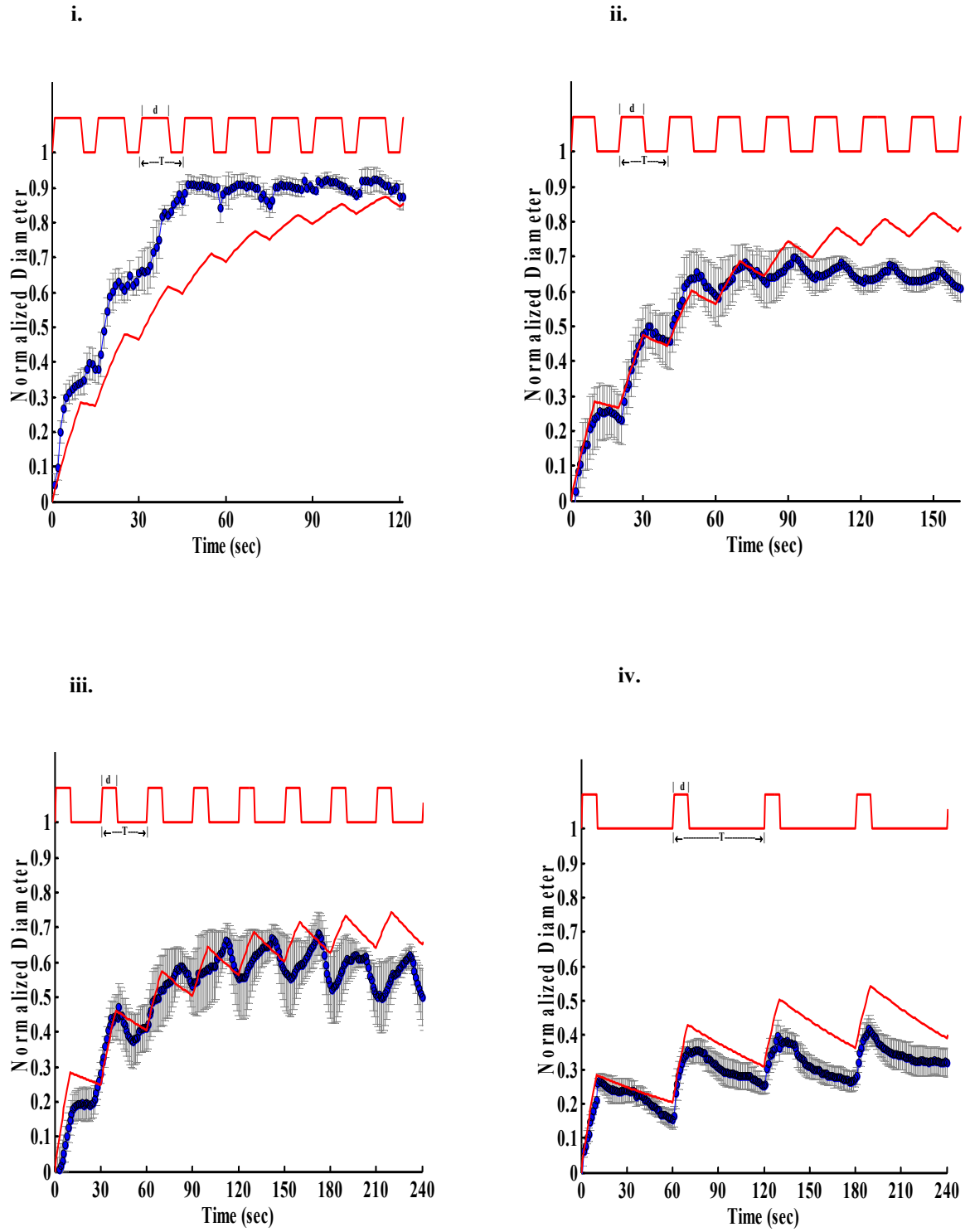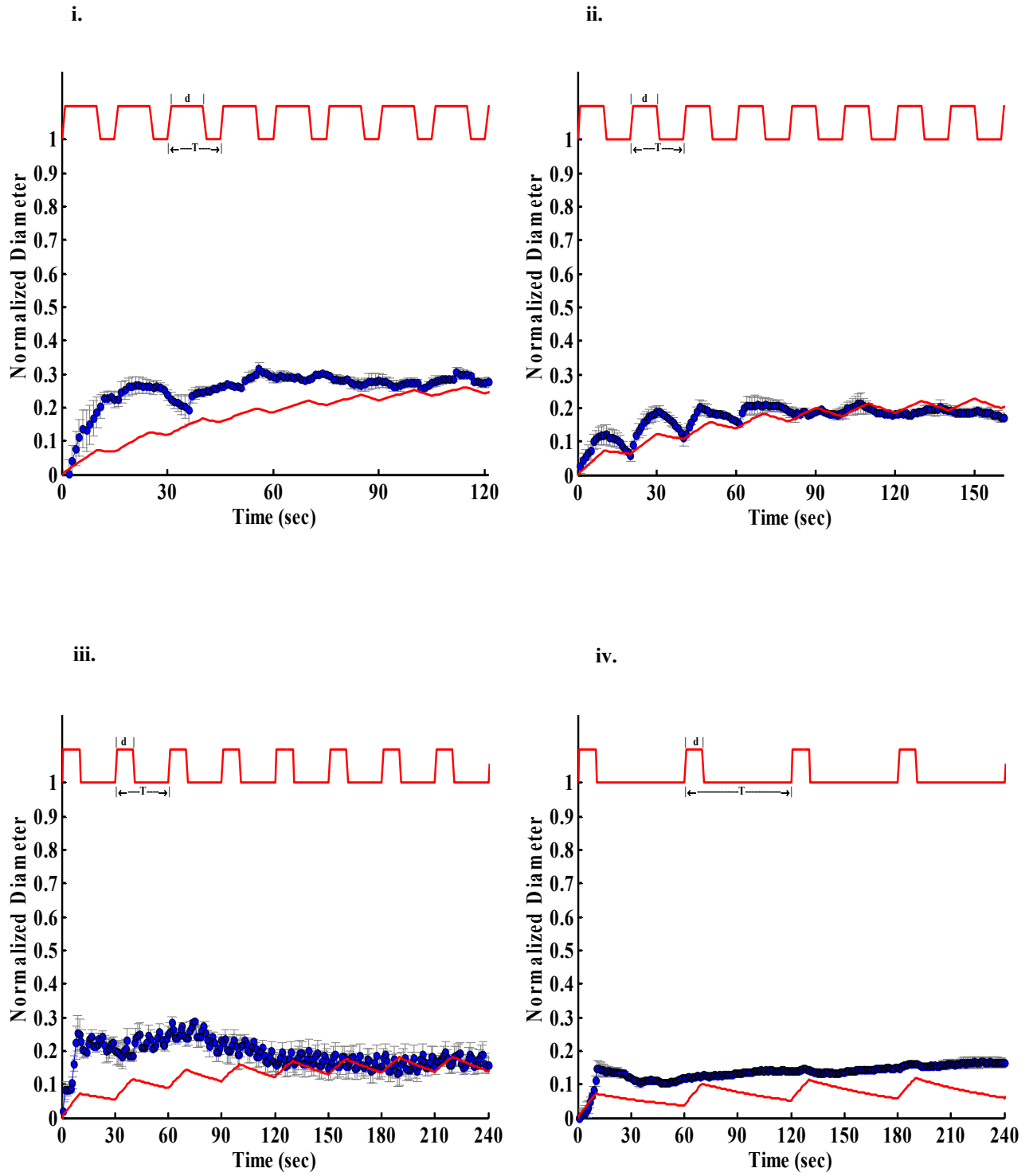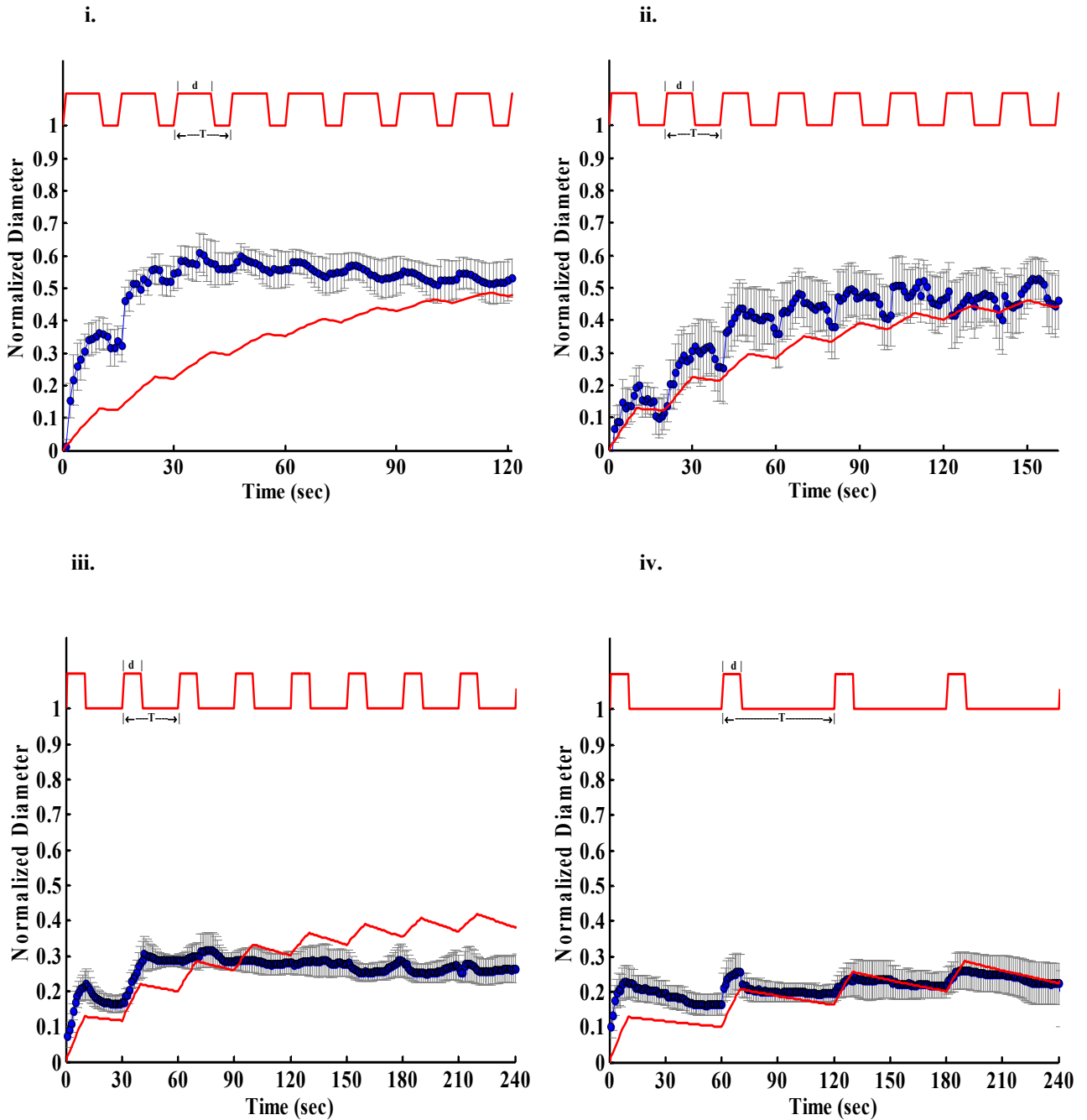
Fig 2.6. Vascular relaxation to Ca^{2+} frequency-mediated NO release. (A). Frequency-dependent Ca^{2+} delivery scenario created by varying the Ca^{2+} pulse period *T* with a constant duration *d*. A ratio of d/T = 1 denotes a continuous delivery, whereas, d/T < 1 indicates a transient delivery of Ca^{2+}. Subsection (i – iv) presents the relaxation response of the arteriole for burst period, *T* = 15, 20, 30, 60 sec respectively over a constant duration *d* = 10 sec. (B) after EDRF blockade (C) after EDHF blockade.

Similar study was repeated with endogenous source of NO, Ach (10 mM) and oxy-Hb (100 mM) as a scavenger of NO. In response to endogenous NO production stimulated with Ach, the observed steady state relaxation for duty cycle ratio d/T = 2/3, 1/2, 1/3 and 1/6 were $87.9 \pm 0.8\%$, $76.4 \pm 0.7\%$, $66.2 \pm 1.4\%$, and $51.4 \pm 2.9\%$ respectively for $n = 4$. After EDHF blockade with apamine (50 nM) and tram-34 (100 nM) the relaxation were $68.4 \pm 0.9\%$, $56.5 \pm 0.9\%$, $42.8 \pm 1.0\%$, and $35.1 \pm 2.3\%$ respectively for $n = 4$. These relaxation were significantly compromised after EDRF blockade with L-NAME (0.5mM). The observed steady state values were $21.8 \pm 0.7\%$, $12.3 \pm 0.4\%$, $10.8 \pm 0.5\%$, and $10.6 \pm 0.4\%$ respectively for $n = 4$. The results are depicted in Fig 2.7.

Fig 2.7. A:

i.
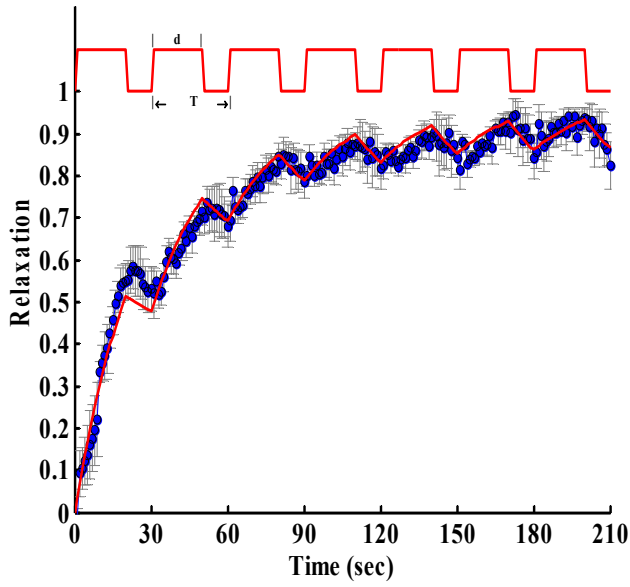
ii.
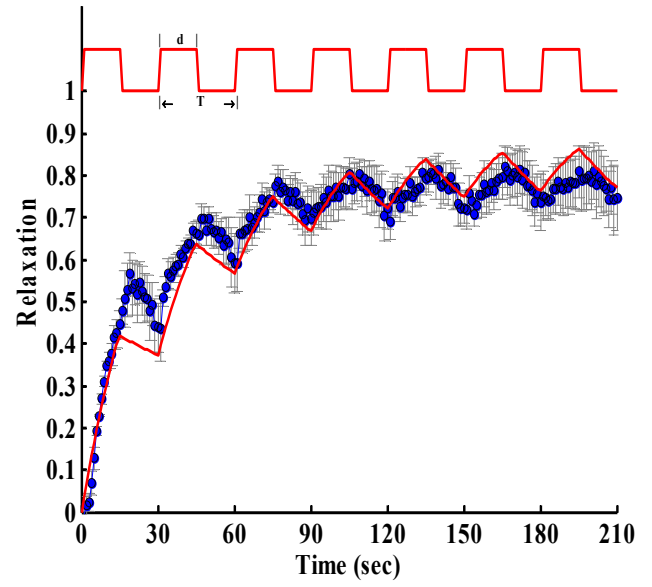
iii.
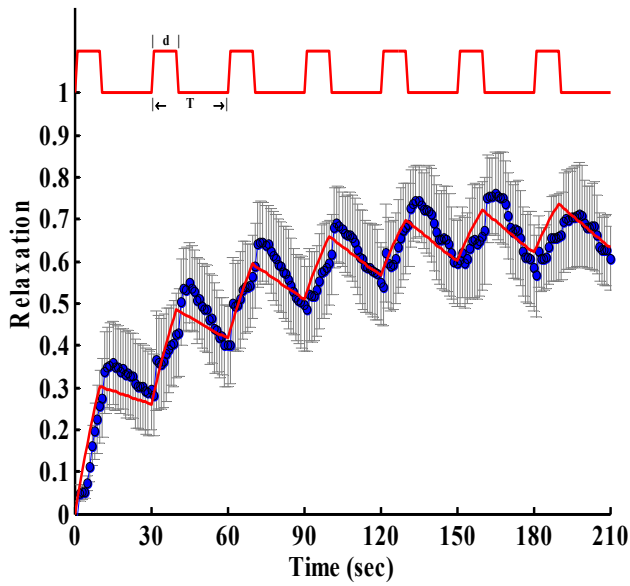
iv.
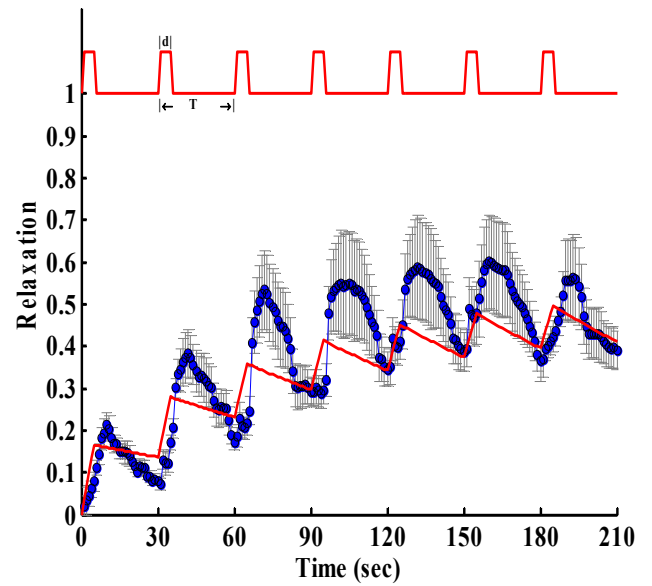
Fig 2.7. B:

i.
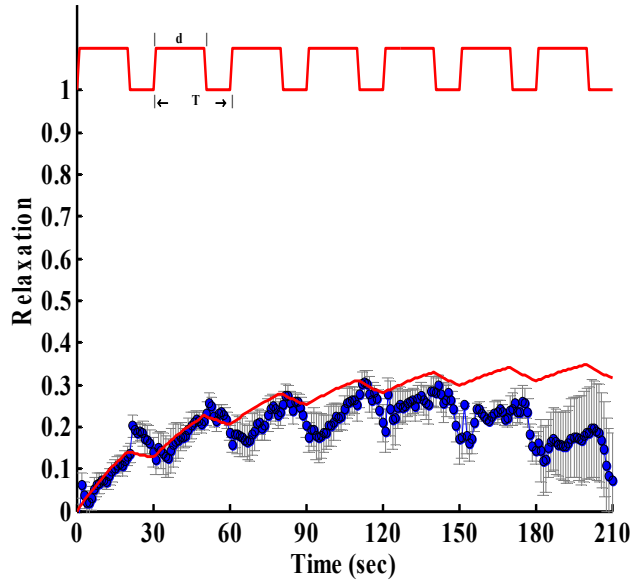
ii.
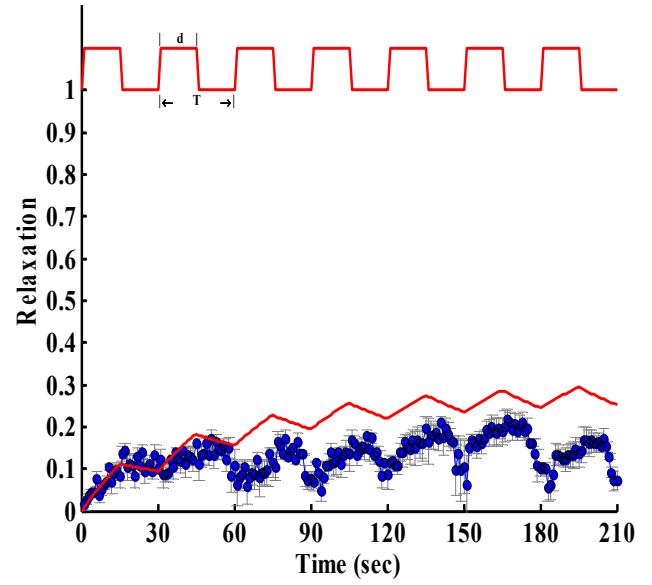
iii.
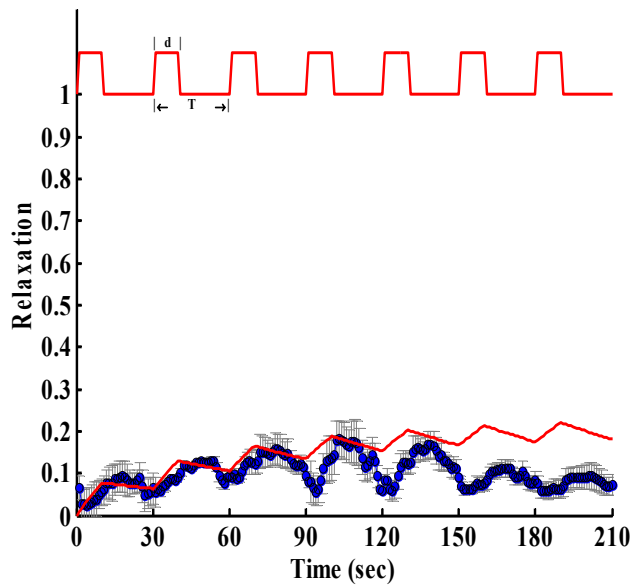
iv.
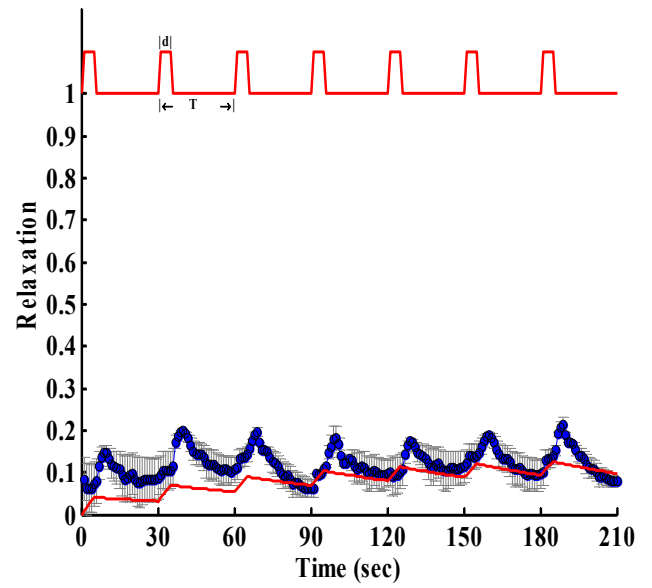
Fig 2.7. C:
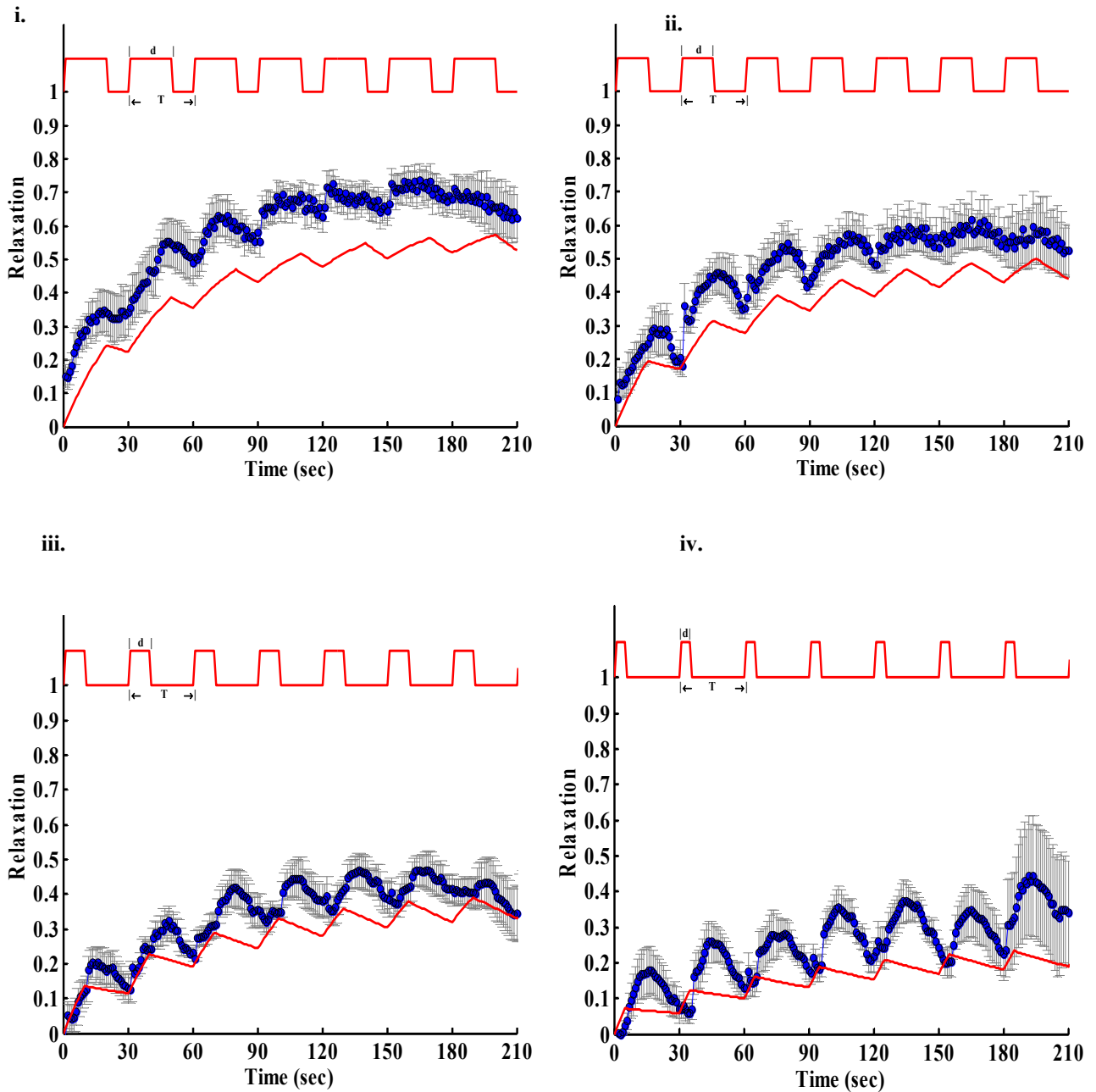
Fig 2.7. Vascular relaxation to frequency-dependent NO release. (A). Frequency-dependent endogenous NO release was induced with Ach 10 μM and NO scavenger oxyHb (100 μM). A ratio of d/T = 1 denoted a continuous NO production, whereas, d/T < 1 indicated a transient production of NO. Subsection (i – iv) presents the relaxation response of the arterioles for burst duration, _d_= 20, 10, 15, 5 sec respectively over a constant period _T_ = 30 sec. (B) after EDRF blockade (C) after EDHF blockade.

The following figure summarizes the frequency-dependent activity by Ca^{2+} induced NO release

A.

B.
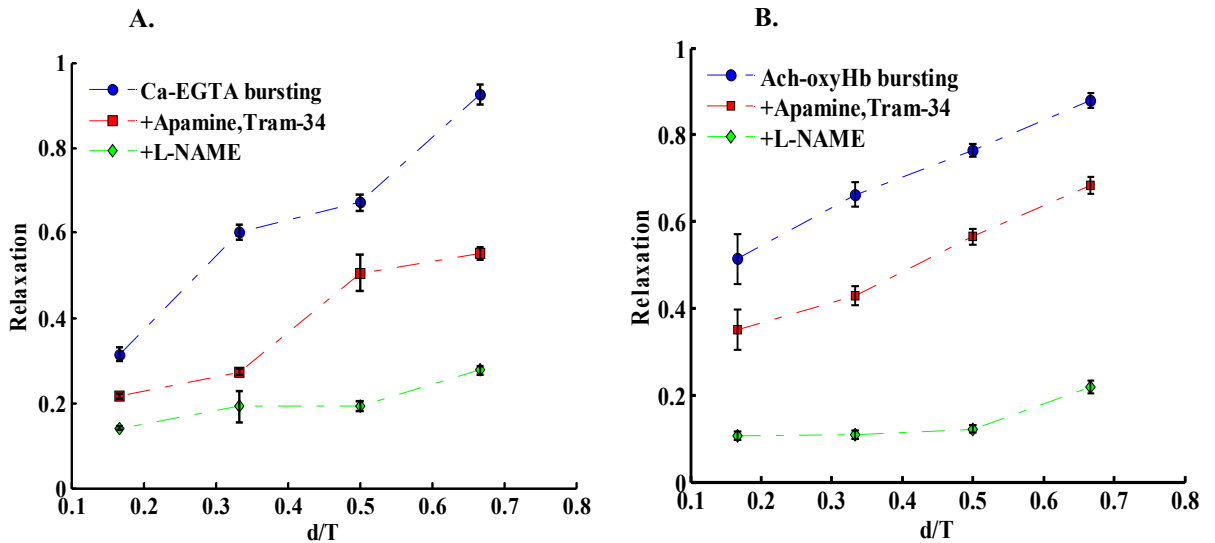
Fig 2.8. Frequency-dependent effect of induced nitric oxide release. The figures represent the steady state diameter obtained by fitting the experimental data of (A): Ca^{2+} responses (Fig. 2.6) and (B): Ach (Fig. 2.7) to a monoexponential activation function.

2.4 Discussion

Majority of the studies related to NO bioavailability have assumed constant NO production, however little emphasis has been directed towards frequency-dependent NO release. The eNOS activity could be modulated by Ca^{2+} binding which may translate oscillations in the intracellular Ca^{2+} into bursts of NO production [37; 147; 148]. This generates favorable conditions for transient release of NO. A number of studies have reported transient Ca2+-dependent release of NO [149; 150; 151]. It is likely that NO might be released in two states: a steady NO that maintained basal vaso-dynamic tone and an oscillatory NO component which occurred in bursts to mimic the intracellular calcium oscillations. The Ca^{2+} signaling efficacy and its information processing efficiency is greatly enhanced by combined amplitude and frequency modulation [152].

Several biological processes are shown to be regulated by Ca^{2+} frequency modulation such as fluid secretion by salivary glands [153], activation of cysteine protease calpin [154] or glycogen metabolism by hepatocytes [155].

The kinetics of NO binding to sGC is seen as a rate limiting step for sGC activation or deactivation leading to cGMP formation and tone regulation [52]. On similar lines, in our previous theoretical study [72], we incorporated the mechanisms of transient sGC kinetics to describe cGMP formation. Our mathematical model for NO transport in the arterioles predicted optimal conditions for transient NO release. A range of parameter values were tested for production rate, consumption rate and concentration of half maximum NO activity. Varying these parameters caused either the frequency or amplitude dependent control of cGMP formation. Significant enzyme activation was predicted under both transient (d/T < 1) and sustained (d/T = 1) NO release scenario. It was concluded that if NO release is transient and the cGMP formation is under frequency-dependent control, the system is less sensitive to the presence of NO scavengers. A transient NO released with a burst duration and period corresponding to the activation and deactivation half life of downstream targets such as sGC could trap NO [47].Modulating the frequency of such stimulus can potentially accumulate NO responses and show improved efficacy towards maintaining vascular tone. This encouraged us to design experiments to test if NO carried Ca^{2+} frequency encoded information and translated it into vascular responses.

We found that exogenous perfusion of Ca^{2+} induced rapid relaxation (time constants 20.8 ± 2.2 sec), followed with a much slower constriction after subsequent removal of the stimulus (time constants 104.8 ± 10.0 sec). On the same line, Bellamy et al. [49]

previously demonstrated that recovery from sGC desensitization resulted in a half time of 1.5 min after a rapid sGC activation by NO. Another study in the presence of NO scavenger such as oxy-hemoglobin showed that the rate constant for reversal of NO-sGC to ferrous sGC was 0.28 min^{-1} or a half life of 2.9 min at 37ºC [69]. In contrast, few studies have documented faster dissociation rates [70]. Such observations with the acceleration of NO-sGC dissociation were correlated to the availability of substrates or ligand concentrations [71]. Moreover, after the eNOS inhibition with L-NAME the fivefold difference in the time constants was significantly reduced (Fig 2), indicating NO dependent pathway mediated such responses. In addition, vascular tone has been reported to include EDHF and EDRF dependent mechanisms [156; 157]. Our results suggested 60.3% contribution to vascular relaxation from EDRF and 36.9% from EDHF. Vascular relaxation independent of EDHF and EDRF contribution has also been reported [158], however we found such contribution to be not significant. After an EDHF blockade with apamine and tram-34 combination, we observed a significant difference in the time constant for relaxation (29.1 ± 4.2 sec) and constriction (143.5 ± 18.2 sec). To confirm our findings we repeated these experiments with an endogenous source of NO (Ach, 10μM). Ach induced responses closely mimicked the observations obtained from Ca^{2+} perfusion experiments. These observations established that NO-mediated mechanisms could store time dependent information to regulate the vascular tone.

Ca^{2+} or its endothelial target NO when modulated at different frequencies could regulate vascular tone [134]. For different Ca^{2+} frequency scenario (d/T = 10/15, 10/20, 10/30, 10/60) we tracked changes in the vascular response. It was found that the arterioles exhibited summation effect with an increase in Ca^{2+} frequency and attained different

steady state tone. Such behavior might be due to an accumulation of NO response resulting from sequential Ca^{2+} bursting. In addition, an interesting observation was that a fourfold increase in the Ca^{2+} frequency improved the efficiency of arteriolar relaxation by 61.1% (Fig 2.8). This observation corroborated with Dolmetsch et al theoretical study which concluded that frequency of Ca^{2+} oscillations activated the enzymatic target more efficiently than constant Ca^{2+} signaling [136]. The frequency-dependent activity observed was significantly compromised following EDRF blockade in comparison to EDHF or a combined response.

Regulating the availability of NO in the vasculature has been demonstrated to have vasoprotective effects. In addition, modulating the bioavailability of NO by different means has proved to restore endothelial function. The complex interplay of NO mediated activity in multiple systems may suggest a wide range of stimulus to initiate physiological responses under different conditions. The efficacy of NO action thus would require a detailed attention towards achieving an optimized NO delivery mechanism that would mimic the physiological NO activity as closely as possible. In summary, we conclude by suggesting NO to encode frequency-dependent information to modulate vascular tone. Attention to the frequency aspect of NO release might provide a more efficient way to facilitate optimal NO delivery.

CHAPTER 3

Agmatine Induced NO-Dependent Rat Mesenteric Artery Relaxation and its Impairment in Salt-Sensitive Hypertension

3.1 Introduction

Over the past two decades there has been a significant interest in understanding vaso-regulation and the role of nitric oxide in mediating relaxation. Arginine, a precursor to nitric oxide has shown to play an important physiological role in regulating the endogenous NO levels. L-arginine is required for optimal NO synthesis by nitric oxide synthase (NOS) in the rat mesenteric artery wall [76]. The importance of L-arginine as a therapeutic element in various physiological and patho-physiological processes such as wound healing [77; 78], protein synthesis and muscle building [79], endocrine metabolism [80], erectile dysfunction [81], cardiovascular functions [82; 83; 84] has widely been reported.

It is suggested that L-arginine acts as a substrate for NOS to facilitate NO production [85]. The reported K_m values for NOS isozymes range in 2-20 mM [85], particularly for eNOS it is reported to be 2.9 μM [86] and the intracellular L-arginine levels are in the range of $0.8 - 2$ mM[87]. This would suggest that these enzymes are saturated with the substrate however it is observed that the rate of NO production varies with extracellular L-arginine concentrations [88; 89; 90]. If exogenous L-arginine acts as substrate and is present in saturating concentrations there should be a continuous production of NO. This discrepancy is widely referred to as L-arginine paradox [84]. There have been various mechanisms hypothesized to explain this behavior [91; 92; 93; 94]. However there still exists an ambiguity in understanding how L-arginine mediates NO dependent relaxation.

Supplying arginine to the endothelial cells and vessels contributes to the enhanced NO synthesis and vessel relaxation despite its saturating cellular levels. There have been various mechanisms hypothesized to explain this arginine paradox including endogenous NOS inhibitors and compartmentalization of intracellular L-arginine [91; 92; 93; 94; 159]. However, there still exists an ambiguity in understanding how exogenous L-arginine mediates NO-dependent relaxation. The apparent benefits of L-arginine supplementation are difficult to reconcile with a purely substrate based mechanism for NO synthesis. In addition to the beneficial effects of exogeneous arginine, recent study has demonstrated a possible role of agmatine as a potential vasodilator substance [95].

Agmatine [4-(aminobutyl) guanidine] is produced endogenously via decarboxylation of L-arginine by the endothelial arginine decarboxylase (ADC) [160] and it does not act as a substrate for NOS. A biological function for agmatine was suggested based on the observation that ADC activity transiently increased 7-fold during cerebral ischemia [161]. In addition, the importance of agmatine has been highlighted by its discovery as a novel neurotransmitter [96; 97] demonstrating its potential to affect multiple biological targets [98]. The presence of agmatine in serum [103] suggests a physiological role in the vasculature. Agmatine was demonstrated to serve as a ligand for imidazoline and/or α-2 AR [162] and α-2 AR agonists mediate endothelium-dependent relaxation in mouse and rat aorta [163]. α-2 ARs (G-protein coupled receptors) play a pivotal role in the cardiovascular system and influence vascular tone at multiple points. These receptors are targets for antihypertensive therapy and their stimulation produces long lasting drop in systemic blood pressure [164]. However, the signaling mechanisms participating in agmatine-initiated NO synthesis [165; 166] and regulation of vascular tone is little

38

understood, and the contribution of α-2 ARs is implicated in this process [165]. Compromised NO synthesis and endothelial dysfunction has been reported in the hypertensive vasculature including in salt-sensitive hypertension [167]. However, the factors that are responsible for its impaired synthesis are varied and not clearly understood. Impaired α-2 AR function has been documented in several models of hypertension [168; 169]. However, it is unknown whether this impairment is a cause or effect of hypertension.

Our hypothesis that explains arginine's NOS substrate independent actions via the activation of α-2 adrenergic receptor (α-2 AR) was demonstrated in cultured endothelial cells [165]. In this chapter, we show that arginine-mediated arteriolar relaxation are due to agmatine produced by the actions of ADC and signaling via GPCR in rat microcirculation. Evidence is also presented documenting attenuated agmatine-mediated relaxation in Dahl salt-sensitive hypertensive rat mesenteric resistant arterioles, which was attributed to reduced α-2 AR gene expression. The figure below shows the structural similarities between L-arginine and its decomposition product agmatine.
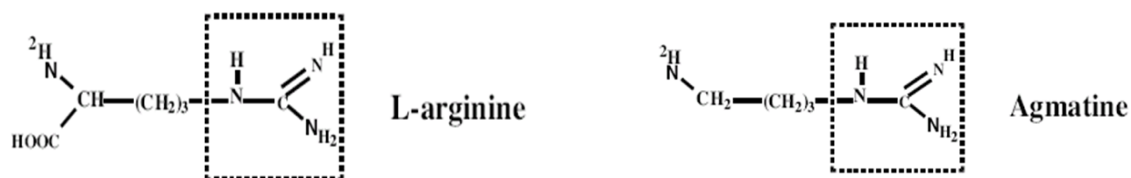
Fig 3.1. Structure of L-arginine and Agmatine, both displaying guanidinium group similar to imidazolines known to act as ligands for I-receptors and α-2 receptors, Figure taken from Joshi et al. [89].

3.2 Materials and Methods

3.2.1 Animal Model

Male Sprague Dawley and Dahl salt-sensitive (SS/JrHsd) rats and their diet were purchased from Harlan Laboratories (Madison, WI). Sprague Dawley rats were maintained on standard pellet chow (2018 Teklad Global) rodent diet whereas the Dahl salt-sensitive rats were fed 0.49% NaCl diet (Harlan Cat. #TD 96208) or 4% NaCl diet (Harlan Cat. #TD 92034).The animals were housed in temperature and humidity controlled rooms with 12 hour on/off light cycle at the animal care facility. All animal studies were performed following Institutional Animal Care and Use approved procedures.

After acclimatization for 1 week, 6-weeks old Dahl salt-sensitive rats were separated into 2 diet groups; normal salt (NS), fed 0.49% NaCl diet and high salt (HS), fed 4% NaCl diet for 5 weeks. Systolic blood pressure was measured weekly with the tail cuff method [170]. At 11 weeks old, HS rats consistently demonstrated sustained hypertension (BP > 200 mmHg) while NS rats remained normotensive (BP < 160 mmHg) (Fig. S2). The rats were euthanized and vascular reactivity assessed on isolated, cannulated and pressurized mesenteric arterioles as described above.

3.2.2 Isolated mesenteric arteriole preparation

Resistance mesenteric arterioles of the second or third order (resting diameter < 150 µM) were isolated from male Sprague-Dawley and Dahl rats (250-300 g), cleaned of the surrounding tissue and cannulated at both ends on glass cannula. The organ chamber was maintained constant at 37°C by superfusion with a modified Krebs-Ringer solution containing (mM): NaCl 145, KCl 5, $CaCl_2$ 2.5, $MgSO_4$ 1.2, KH_2PO_4 1.2, HEPES 20, and

Glucose 10.1 pH 7.4 [171]. Cannulated vessels were axially pre-stretched to remove any bents and to simulate physiological stretch conditions. The vessels were pressurized at 50 mmHg and allowed to equilibrate for 60 min before initiating the experiment. To establish a concentration that gave submaximal constriction, we constructed a dose response curve to norepinephrine. The vessels were preconstricted with continuous superfusion of norepinephrine, (NE, 2 μM) and only those that retained a constant pressure and a consistent constriction to NE, and fully responded to the agonist were included in the study (Fig. 5.2). Ach relaxation was performed on these vessels to test intact endothelium. The vessel reactivity study was carried out by intraluminal perfusion with various agonist concentrations. This was achieved by an automated solenoid valve controlled pressure driven perfusion system. Diameter measurements were tracked in real time by mounting the perfusion chamber on the stage of an inverted microscope (Olympus) fitted with a CCD camera (QImaging). Post analysis was performed with IPLAB (BioVision Technologies) and MATLAB (MathWorks) software. Chemicals NE, L-NAME, RX821002, agmatine, L-arginine were obtained from Sigma-Aldrich Co. (St. Louis, MO) and Pertussis toxin (PTx) were obtained from Tocris Bioscience (Ellisville, MO).

3.2.3 Real Time-Polymerase Chain Reaction (RT-PCR)

RT-PCR was carried out on mesenteric tissue isolated from Dahl rats [172; 173], cleaned of fat and stabilized with RNA*later*(Qiagen). RNA purification was done by homogenizing tissue (~30 mg) with a sonicator in RLT buffer (Qiagen). The lysate was repeatedly centrifuged (10,000 g) with reagents from RNeasy® Fibrous Tissue Mini Kit (Qiagen) to ensure RNA isolation. A first strand cDNA synthesis was performed by using

purified mRNA by Superscript III RT (Invitrogen) in a thermocycler (MJ Research). The new cDNA strand was purified with QIAquick® PCR Purification Kit (Qiagen). Pure cDNA (~10 ng) was reacted with Power SYBR Green PCR Master Mix reagent (Applied Biosystems) in RNase-free water in a StepOne RT-PCR system (Applied Biosystems). The relative expression of $\alpha-2_A$, $\alpha-2_B$ AR and eNOS was determined using β-actin as a housekeeping gene. The primers used were: $\alpha-2_A$; TTT GCA CGT CGT CCA TAG TG (forward) and CAG TGA CAA TGA TGG CCT TG (reverse). $\alpha-2_B$; AAA CAC TGC CAG CAT CTC CT (forward) and CTG GCA ACT CCC ACA TTC TT (reverse). eNOS; CAA CGCTAC CAC GAG GAC ATT (forward) and CTC CTG CAA AGA AAA GCT CTG G (reverse). β-actin; TCC TAG CAC CAT GAA GAT C (forward) and AAA CGC AGCTCA GTA ACA G (reverse). Standard curves (initial amount of cDNA versus Ct values) were tested for each set of primers demonstrating that for the similar range of total cDNA amplification the efficiency of target genes and housekeeping gene (β-actin) were equal. No reverse transcription control was used where the PCR reaction was run in the absence of reverse transcriptase. Expression of the gene of interest was divided by the housekeeping gene and expressed as fold-change compared with the corresponding normal-salt rat group.

3.2.4 Ca^{2+} fluorescence and HUVEC cell culture

HUVECs were obtained from American type culture collection (ATCC, Manassa, VA). The cells were cultured in media consisting of modified Kaigan's F-12 supplemented with 10% FBS along with 0.1 mg/ml heparin, 0.03 mg/ml endothelial growth supplement. Antibiotics (100 units/ml penicillin and 10 µg/ml streptomycin) were added in humidified UV irradiated hood. The cells were cultured in T75 flasks and 35mm

cell culture plates in humidified incubator at 37C and in a 5% CO_2/95% air atmosphere. For these study cells were used for eight passages. The Ca^{2+} florescence experiment were carried out with FluoForte calcium dye (4 µM). The cells were loaded for 30 min dye and Ca^{2+} responses were recorded with excitation at $\lambda = 490$ nm and emission at $\lambda = 514$ nm on an florescent microscope with video caliper.

3.2.5 Data analysis

All relaxations were expressed as percentage of norepinephrine (2 µM) induced contraction. To analyze vasodilation, we determined the maximal response and EC_{50} were calculated by fitting the concentration-response relationship to a logistic function. Amplified transcripts from RT-PCR were quantified using the comparative threshold cycle method ($2^{-\Delta\Delta Ct}$) with β-actin as normalizer and the corresponding sample from the normal salt fed rat mesentery as internal control.

All data unless stated otherwise were expressed as mean ± SEM with n representing independent rat experiments. Statistical significance was tested using a paired t - test with $p < 0.05$ considered significant.

3.3. Results

3.3.1 L-arginine-mediated relaxation is dependent upon ADC activity

We carried out relaxation studies using isolated 2nd order rat mesenteric arterioles in an intraluminally perfused vessel bath supplemented with increasing concentration of L-arginine. As shown in Fig. 1A, arginine dose-dependently relaxed the vessel with an EC_{50} value of 5.8 ± 0.7 mM ($n = 9$). The requirement of mM levels of arginine prompted us to hypothesize that the actions of arginine may be mediated via its metabolism to agmatine by ADC, which is shown to be localized in the endothelium. The relaxations to arginine

were significantly inhibited in the presence of ADC inhibitor, DFMA (Fig. 3.2A: EC_{50}, 18.3 ± 1.3 mM; n = 5). DFMA is a specific inhibitor of ADC [174; 175] and its specificity in our system was verified by the absence of any effect on agmatine-mediated vessel relaxation (Fig. 3.2B). Thus, this experiment demonstrated that the arginine's actions are mediated by the formation of agmatine.

3.3.2 Agmatine-induced vessel relaxation

To examine the effect of agmatine treatment on vessel tone, the isolated 2nd order mesenteric arterioles were subjected to different agmatine concentration by intraluminal perfusion. Agmatine relaxed the vessel in a dose-dependent fashion with an EC_{50} of 138.7 ± 12.1 µM (Fig.3.2B; n = 22). Thus, significantly less agmatine was required as compared to arginine for arteriolar relaxation. As demonstrated in Fig 1B, the agmatine-mediated relaxation was partially NO dependent as eNOS inhibitor, L-NAME (0.5 mM) significantly attenuated the relaxation (EC_{50}, 346.0 ± 19.4 µM; n = 4).
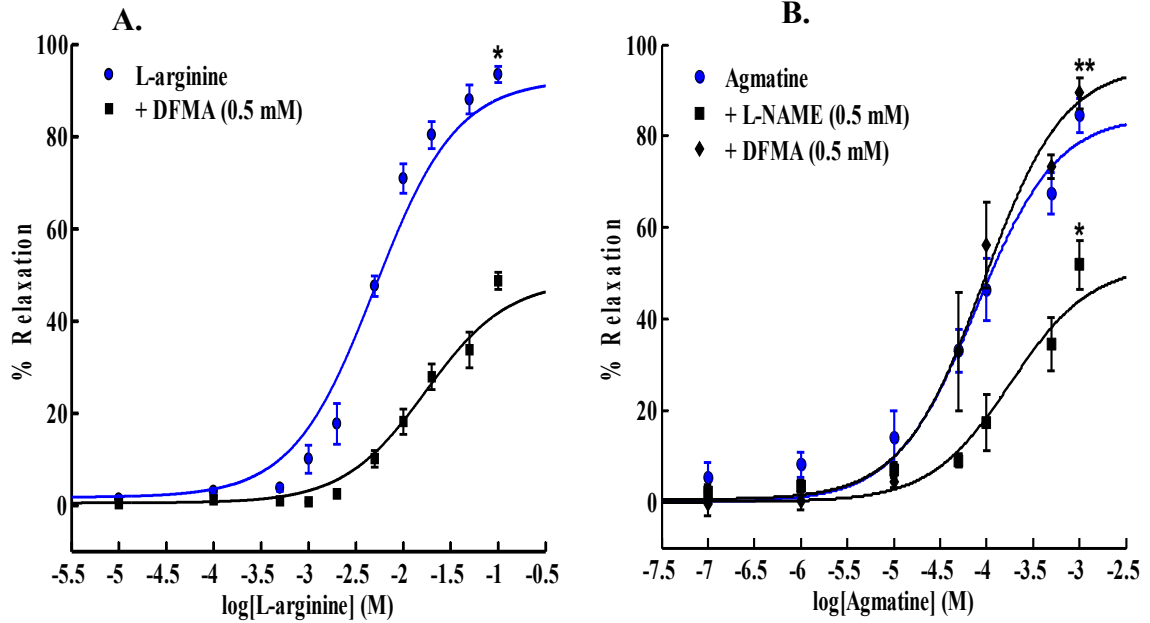
Fig 3.2. Concentration-dependant relaxation responses to L-arginine and agmatine.(A). Dose-response to intraluminal perfusion of L-arginine (n =9) in Sprague-Dawley rat mesenteric arterioles and after pre-treatment with arginine decarboxylase blocker, DFMA (0.5 mM), (n =5). *p < 0.05 vs. L-arginine + DFMA. (B). Concentration dependent dose response curve to intraluminal perfusion of agmatine in rat mesenteric arterioles in the presence and absence of an eNOS blocker, L-NAME (0.5 mM), n =4 and arginine decarboxylase blocker, DFMA (0.5 mM), n =3. Values are mean ± SE with; *p < 0.05 vs. agmatine + L-NAME; **p > 0.05 vs. agmatine + DFMA.

3.3.3 α-2 AR activity in agmatine-mediated relaxation

It has been previously reported that agmatine binds as a ligand to the α-2 ARs [106; 108]. To validate if the agmatine-induced relaxation is mediated via α-2 AR binding, we treated the vessels with agmatine in the presence and absence of RX821002, a specific antagonist of α-2 AR. As shown in Fig 3.3A, RX821002 partly attenuated agmatine-mediated relaxation (EC$_{50}$, 1498.0 ± 294.0 μM; n = 6) showing that α-2 AR may be participating in the relaxation process. These data corroborate our earlier observation in

cultured HUVECs using another selective α-2 AR antagonist, rauwolscine, where it attenuated agmatine-induced cellular NO synthesis [165].

3.3.4 Inhibition of agmatine-mediated relaxation by pertussis toxin

To narrow down the downstream mechanism that may be participating in the agmatine-induced relaxation, we examined the possible role of G-proteins. We inhibited the G-proteins by pretreating the vessel with PTx (100 nM) for 60 min at 37°C. As shown in Fig 3.3B, we observed a significantly reduced relaxation as opposed to that due to agmatine alone while the EC_{50} value increased to 1300 ± 91 μM ($n = 4$). These data show that G-proteins are mediators of agmatine-induced vessel relaxation. Similar inhibition with PTx was observed in experiments with cultured HUVECs [165].
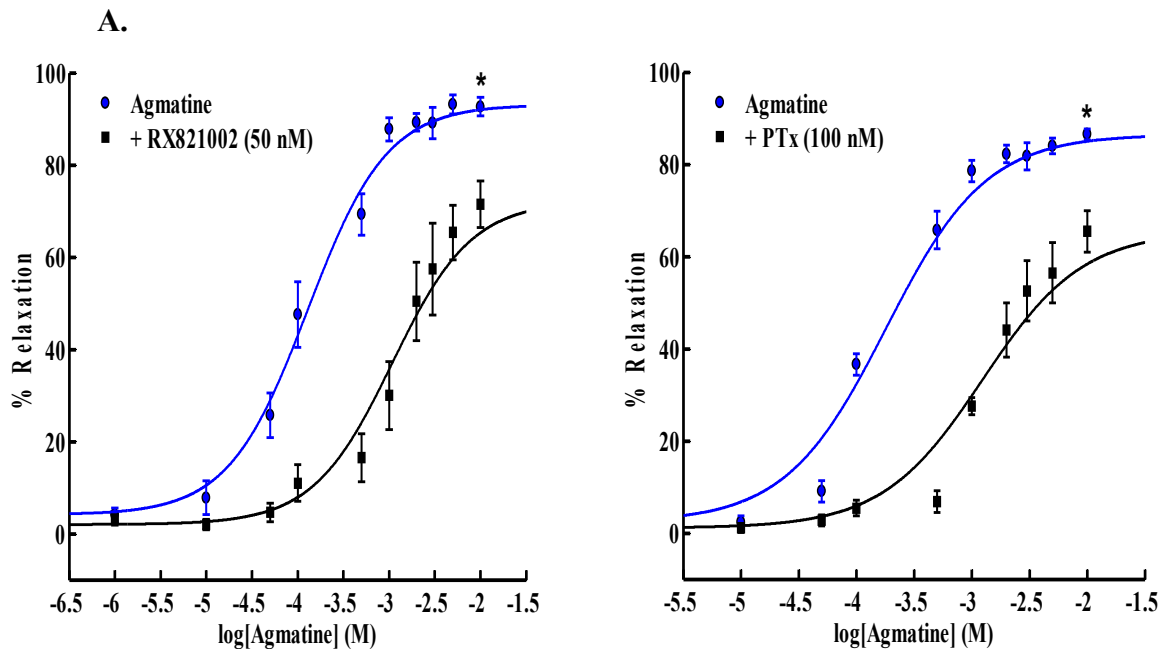
Fig 3.3. Role of α-2 AR and G-protein in agmatine-mediated relaxation. (A). Dose response to agmatine in Sprague-Dawley rat vessels was obtained in the presence and absence of an α-2 AR antagonist, RX821002 (50 nM) (n =6); *$p < 0.05$ vs. agmatine + RX821002. (B). Agmatine relaxation is mediated by G-protein activity seen after incubation with PTx (100 nM). Values are mean ± SE with n =4; *$p < 0.05$ vs. agmatine + PTx.

3.3.5 Arginine and agmatine induced Ca^{2+} responses in HUVEC

We further tested if agmatine and arginine induced Ca^{2+} responses using HUVEC. Fig 3.4 (A) shows Ca^{2+} responses to agmatine, 10 µM, n=15. We inhibited the G-proteins by pretreating the vessel with PTx (100 nM) n=8, for 60 min at 37°C. The role of α-2 receptor and PLC in agmatine induced Ca^{2+} activity was tested after incubation with a specific inhibitor, RX821002 (50 nM), n = 4 and PLC blocker U73122 (10 µM), n = 6 respectively. The Ca2+ activity from HUVEC was confirmed with Ca^{2+} ionophore, calcimycin (10 µM), n = 11, and chelation of Ca^{2+} signal with BAPTA-AM (10 µM), n = 5, as seen in Fig 3.4 (B).
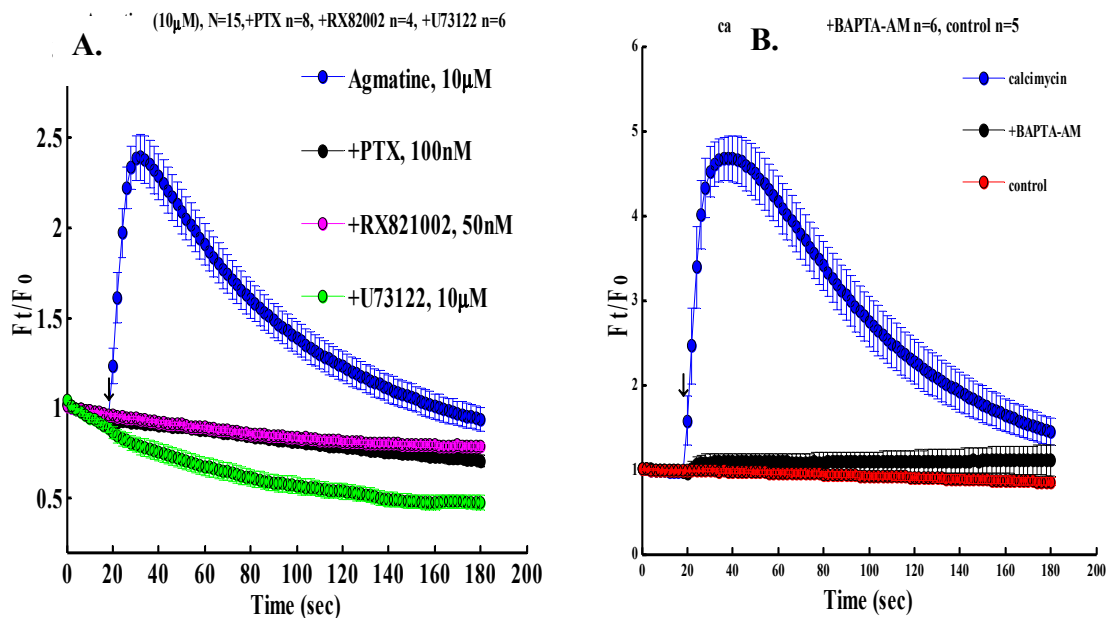
Fig 3.4.Role of α-2 AR, G-protein and PLC in agmatine-induced Ca^{2+} responses in HUVEC. (A). Agmatine stimulation of HUVEC along with incubation with α-2 AR antagonist, RX821002 (50 nM) , n = 4; G-protein inhibitor pertussis toxin, PTX (100nM), n = 8 and PLC inhibitor U73122, 10µM, n = 6 . (B). HUVEC stimulation with calcium ionophore calcimycin (10µM) along within response after calcium chelation with BAPTA-AM (10µM) and Ca^{2+} free control. Values are mean ± SE.

In Fig 3.5(A), we showed the stimulation of HUVEC with L-arginine (5 mM), n = 8. The presense of α-2 receptor activity was tested in HUVECs with α-2 receptor agonist UK14304, 10 µM, n = 3.
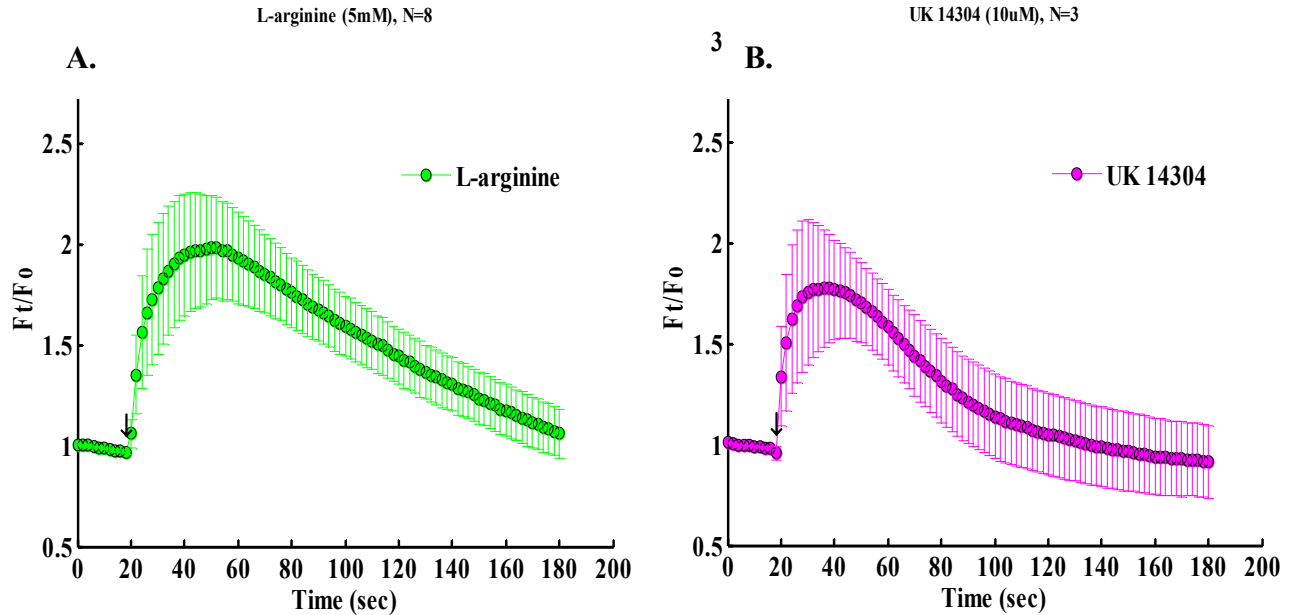
Fig 3.5. Ca^{2+} responses in HUVEC from (A) L-arginine (5mM), n=8 (B). after stimulating with α-2 AR agonist, UK14304 (10 µM) (*n* =3). Values are mean ± SE.

3.3.6 Arginine and agmatine-mediated vessel relaxation attenuated in DS rats

Small size arterioles (100-500 µm diameter) are implicated to contribute significantly to the vascular resistance [176; 177]. Accumulating evidence indicates that endothelium-dependent relaxation is impaired in salt-sensitive hypertension [178; 179; 180]. However, the underlying mechanisms have not been clearly delineated. We investigated if the agmatine-induced arterial relaxation is affected in Dahl salt-sensitive rats. 6-week old rats were placed on a diet containing either 0.49% NaCl (normal salt) or 4% NaCl (high salt) for 5 weeks and isolated mesenteric arterial relaxations were recorded in response to

agmatine. The agmatine-induced relaxation was greatly inhibited in high-salt as compared to normal salt conditions (Fig 3.7A;% max. relaxation, $90.4 \pm 1.7\%$ (NS); $19.8 \pm 2.4\%$ (HS)) with normal salt rats exhibiting relaxation to physiological agmatine concentration (EC$_{50}$, 143.9 ± 23.4 µM; $n = 5$).

Below we see representative images of HUVEC fluorescence pre and post stimulus.
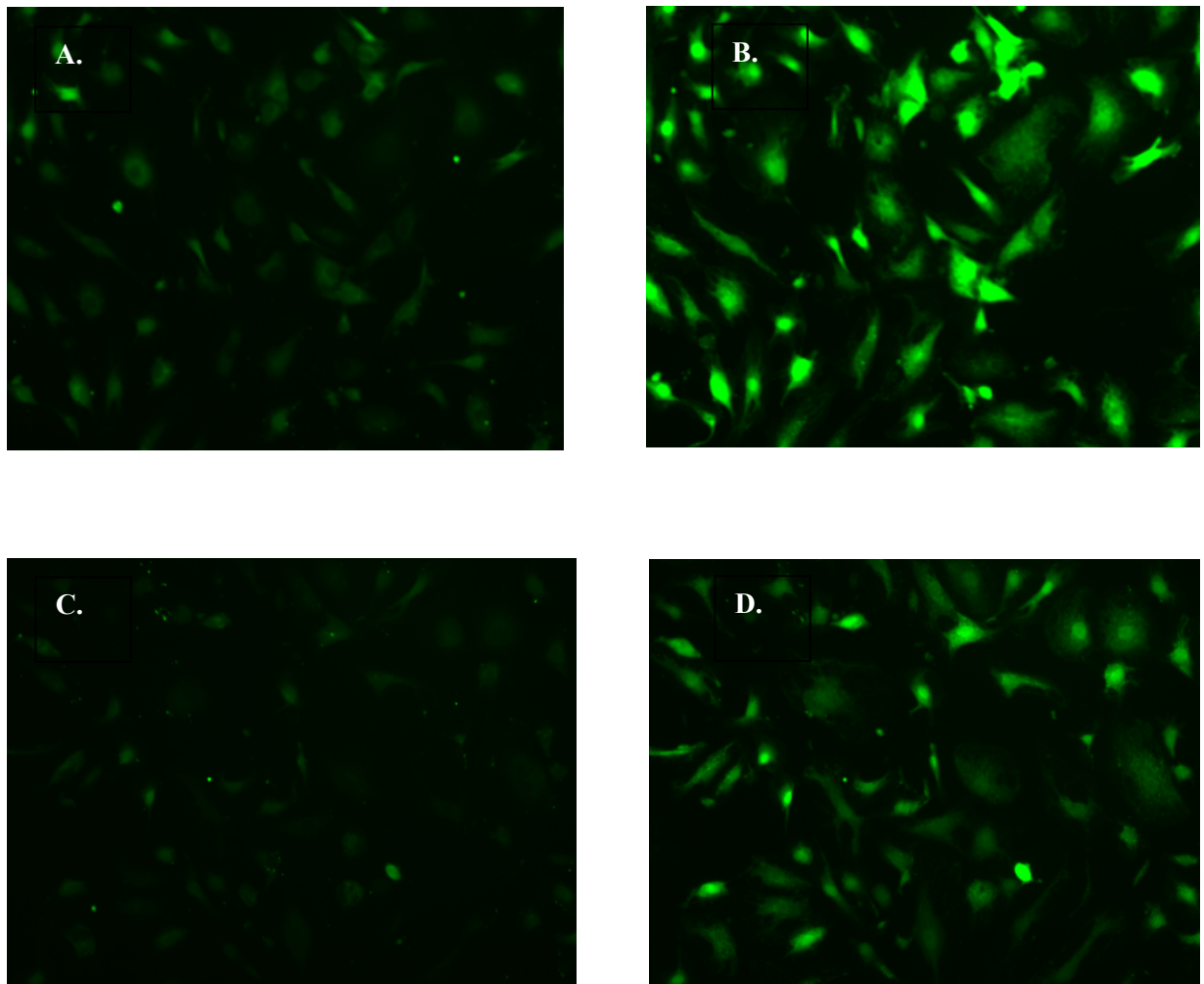
Fig 3.6. Representative fluorescent images of Ca^{2+} response with fluoforte calcium dye (4µM). (A) before and (B) after calcium ionophore A23187 (10µM) stimulus. (C) before and (D) after stimulating the HUVEC to Agmatine (10µM).

The arginine-induced relaxation was as well inhibited in high-salt as compared to normal salt conditions (Fig 3.7B;% max. relaxation, 94.7 ± 1.5% (NS); 18.4 ± 5.5% (HS)with normal salt rats exhibiting relaxation to physiological agmatine concentration (EC_{50}, 3.5 ± 0.8 mM, n = 3). Ach mediated relaxation was also impaired in vessels from high salt rats (Fig. 5.5) and thus verifying the presence of endothelial dysfunction. However, relaxation due to an NO donor, SPER-NO was not affected, showing that the signaling pathway downstream of NO synthesis is intact in Dahl hypertensive rats (Fig. 5.3). These data illustrate that agmatine-mediated signal transduction pathway leading to vascular relaxation is severely impaired in salt-induced hypertension.

A. **B.**
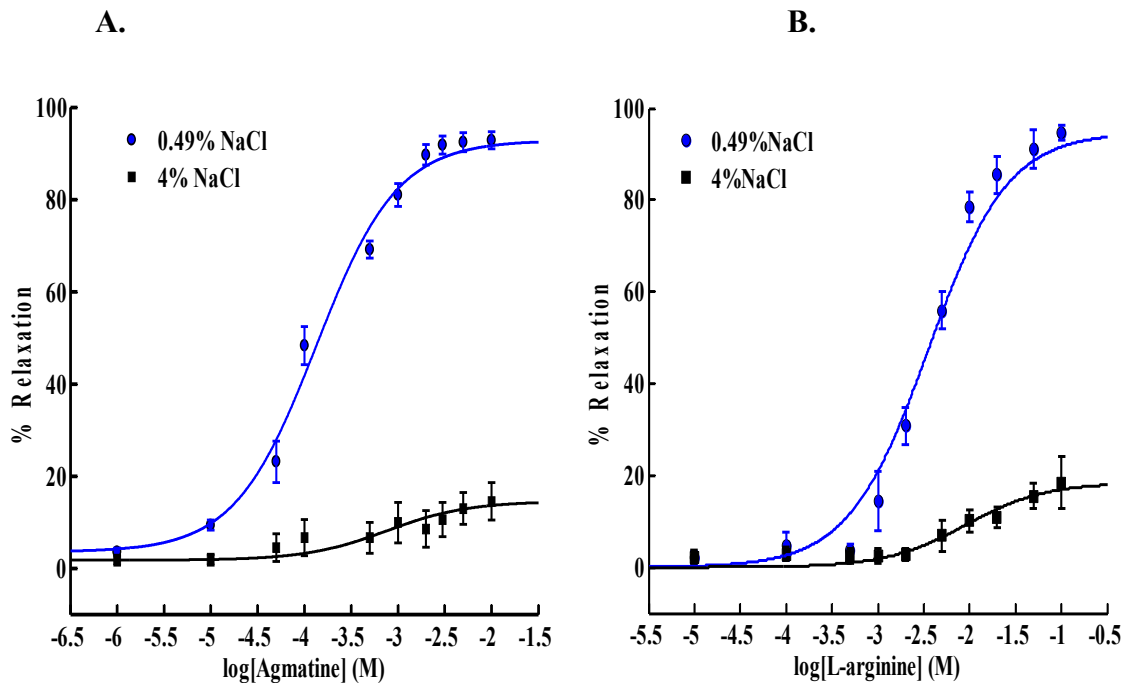
Fig 3.7.Relaxation response to agmatine and L-arginine in Dahl salt-sensitive hypertension. (A) agmatine, *n* =5 and (B) L-arginine, n = 3, mediated relaxation observed in salt-sensitive Dahl rats maintained on high salt, HS (4% NaCl) and normal salt, NS (0.49% NaCl) for 5 weeks. Values are mean ± SE.

3.3.7 Down-regulation of mesenteric artery α-2 AR mRNA expression in DS rats

Since agmatine is proposed to act via α-2 AR binding (Fig. 3.8), we carried out mRNA expression analysis of α-2 AR and eNOS in Dahl rats by real time RT-PCR. The mRNA expression of α-2$_A$, α-2$_B$ AR and eNOS were attenuated in high-salt Dahl rat mesenteric arteries (Fig. 3.7B) indicating that mRNA expression levels of these genes was reversed during the development of salt-sensitive hypertension. Among the 3 genes analyzed, there was a 10 fold under-expression of α-2$_A$ AR.
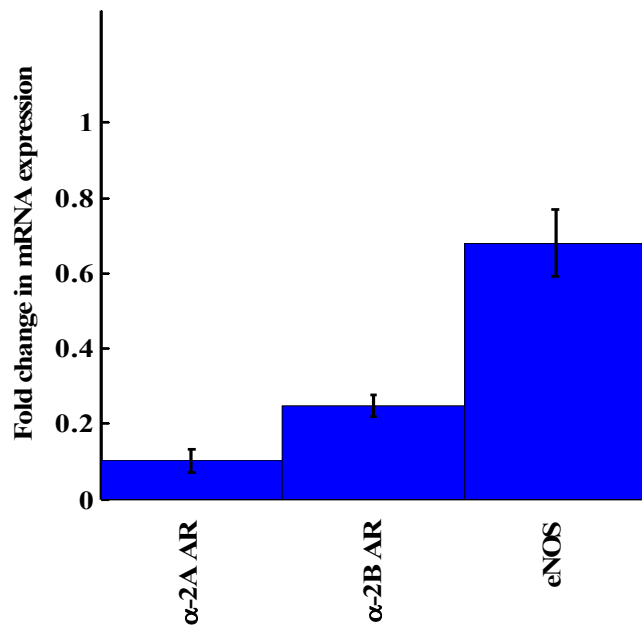
Fig 3.8.Real Time PCR data for α2$_A$ AR, α-2$_B$ AR and eNOS mRNA expression. Mesenteric artery tissue was harvested and total RNA isolated from NS and HS rats. The semi-quantitative RT-PCR was carried out using SYBR Green technology in a StepOne RT-PCR system. Values are mean ± SE with *n* =4.

3.3.8 Attenuated NO synthesis in Dahl rats

Plasma nitrite levels, as a measure of endogenous NO synthesis, were analyzed by ozone based chemiluminescence analyzer. The results indicated that NO synthesis was significantly attenuated in high salt rats as compared to normal salt rats (Fig. 3A). These data are supported by the similar observations made by Fujii et al [181].
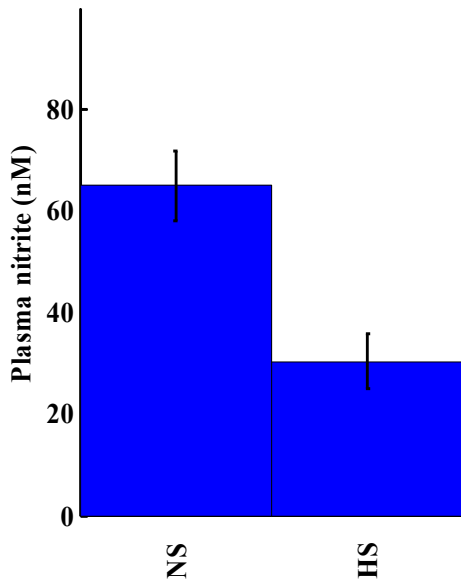
Fig 3.8.Compromised nitric oxide activity in Dahl salt-sensitive hypertension. Plasma nitrite concentrations in HS and NS fed Dahl rats ($n = 3$).

3.4 Discussion:

Although the beneficial effects of arginine in vascular relaxation are well documented and appreciated, the mechanism of its action is not clearly understood. Arginine serves a major role by acting as a substrate for NOS and synthesizing NO, which in turn participates in signal transduction of vascular relaxation. Since millimolar amounts of arginine are required to produce measurable NO levels and vasodilation, it was speculated that arginine's metabolic products could be contributing to its observed effects

[165]. We have proposed that some of the observed effects of arginine could be attributed to its conversion to agmatine by ADC.

The important finding in this investigation is that the inhibition of ADC with DFMA significantly attenuated arginine-initiated mesenteric arterial dilation, indicating arginine to agmatine conversion for the observed relaxation. The endothelium is known to possess ADC activity [160], which was documented to mediate an increased vasodilation and glomerular filtration rate following arginine infusion into animals [182]. In macrophages under inflammatory conditions, ADC was shown to modulate agmatine levels, which in turn down-regulated iNOS catalyzed NO synthesis [183]. As compared to arginine, agmatine brought about the relaxation at a significantly lower concentration (EC_{50}, 138.7 $\pm$ 12.1 μM; n = 22). The activation of vessel relaxation with μM agmatine shown here is physiologically relevant since the plasma agmatine level has been reported in the μM range [184]. Agmatine was shown to activate NO synthesis in endothelial cells but the mechanism of activation was not elucidated [166]. The partial attenuation of agmatine-initiated relaxation by L-NAME indicated that agmatine partly triggered the relaxation via NO independent pathway. Binding of agmatine to imidazoline or α-2 AR is well documented in the mammalian system. Our hypothesis that agmatine acts by receptor binding, possibly via α-2 AR, was examined by using an α-2 AR antagonist, RX821002. The observation that RX821002 did not completely attenuate agmatine-triggered relaxation implied that agmatine may be affecting relaxation partly via α-AR independent pathway. Recently, agmatine's relaxing effects in rat aorta are documented to be via small conductance Ca^{2+}-activated K^+ channel and ATP-sensitive inward rectifying K^+ channels, and idazoxan failed to inhibit these relaxations [185]. It appears that rat aorta is

devoid of I-receptors as Musgrave et al [186] have reported the absence of I-receptor antagonist effects, and it is likely that agmatine is using alternative pathways of aortic relaxation.
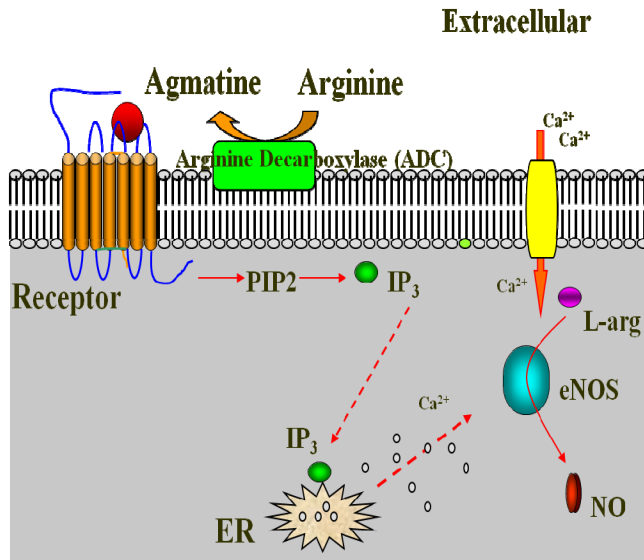
Fig 3.9.Schematic representation of the proposed receptor-mediated hypothesis for arginine/agmatine stimulation of vascular NO synthesis.

Since α-2 AR belongs to GPCR family, we tested the effects of G-protein inhibition. Pertussis toxin, a potent G-protein inhibitor, considerably attenuated agmatine-initiated relaxation. In the present investigation the inhibitory effects of α-2 AR antagonist (RX821002) and G-protein inhibitor (PTx) together provide stronger evidence for the participation of GPCR in the vasodilatory actions of agmatine. Using 2 knockout mouse models, Shafaroudi et al [163] have demonstrated the mediation of endothelial α-2$_A$ AR in vasodilation via NO-dependent mechanisms. These receptors may play important physiological functions as they're activated by the endogenous ligand norepinephrine. In addition, there is evidence for their participation in various pathophysiological

conditions. For example, blood pressure was elevated in transgenic α-2_A AR knockout mice on a normal salt diet [187], showing that α-2_A AR activation with specific agonists may serve to alleviate hypertensive conditions.

Dahl hypertensive rats are reported to exhibit endothelial dysfunction [188] and agmatine-mediated vascular relaxation could be impaired in this model. Our measurements of agmatine-initiated vessel relaxation showed that relaxation was impaired in high salt as compared to normal salt diet fed Dahl rats. This observation supports our postulation that α-2_A AR activity and associated signaling pathway is down-regulated in high salt treated rats leading to impairment of agmatine-mediated relaxation. Secondly, mRNA analysis by real time PCR showed suppression of α-2_A and α-2_B AR expression in the mesenteric artery isolated from high salt fed DS rats as compared those from normal salt fed DS rats. There was noticeably a robust 10 fold down-regulation of α-2_A AR, which could be the predominant factor responsible for the observed abolishment of vessel relaxation in HS rats. Hirano et al [189] have also observed attenuated pre- and post-synaptic α-2_A AR reactivity in DS rats fed high salt diet.

In summary, we have demonstrated the mediation of ADC in the arginine-initiated stimulation of rat mesenteric artery relaxation. Physiological concentrations of agmatine activated vessel relaxation via α-2 AR and G-protein and this was dependent on vascular NO synthesis. It relaxed the vessels at 100 times less concentration as compared to arginine and thus making it a physiologically relevant agonist at α-2 AR binding site. Most importantly, our investigations have provided a novel mechanistic explanation for the observed beneficial effects of L-arginine-initiated vessel relaxation via agmatine formation. Lastly, α-2 AR activity, mRNA expression, and agmatine-mediated

relaxations are impaired in vessels isolated from high salt loaded Dahl hypertensive rats. These findings may help define fundamental aspects of cardiovascular physiology and pathophysiology by demonstrating that many effects of arginine are due to its metabolism to agmatine. Agmatine supplementation in the diet is anticipated to alleviate the endothelial dysfunction associated with vascular hypertension.

CHAPTER 4

Determination of mechanical parameters of rat mesenteric arterioles in Dahl salt sensitive hypertension: A theoretical and experimental study.

4.1 Introduction

Mesenteric arteries have been identified as resistance vessels since they contribute significantly to overall vascular resistance [109; 190]. These vessels have been shown to adapt its vascular tone and structure to regulate blood pressure and flow [191]. Recent studies have suggested increased contribution of small resistance arteries and vascular wall mechanics towards the development of hypertension [192]. Altered morphological structure with complex remodeling of the vasculature is observed in many studies with the progression of hypertension [110; 193; 194]. Various targets have been suggested in mediating vascular effects that cause mechanical and structural changes in hypertension models of DOCA rats [195] and Dahl rats [196]. Differences in the elastin composition were reported to be a contributor of small artery remodeling in SHR model [113]. Studies on alterations in collagen, non-fibrous extracellular matrix and adhesion molecules have also been proposed in different types of hypertension [197; 198; 199].

Salt sensitivity has been associated with increased vascular resistance and volume retention [116]. Salt intake resulted in narrowing of resistance arteries and impaired distension of rat mesentery in ouabain sensitive hypertensive rats [200]. Salt sensitive Dahl rats have been consistently observed to develop hypertension when fed a high salt diet [115]. These rats frequently developed vascular injury and hardening [201]. Morphometric study from mesenteric arteries of genetically modified Dahl rat strain suggested increased smooth muscle mass, and vasoreactivity study showed impaired

relaxation capability of arteries caused by endothelial cell damage [194]. In another study, no difference in the density or diameter of small arterioles was observed in salt fed Dahl rats [202]. A study on carotid arteries showed altered mechanical properties with salt sensitivity after development of hypertension. However, these were suggested to be independent of NaCl diet or transmural pressure [203]. In DOCA-salt hypertension complex relation between arterial mechanics and sodium were pointed [110], and in another study vascular morphology was shown to be altered without altering the stiffness [195].

Arteriolar elasticity is determined by the structural composition of the vascular walls and by vascular smooth muscle tone. The mechanical properties of these arterioles are important as they characterize the stress-strain relationship in the vasculature. The vascular tone and regional blood flow in the microcirculation depend on active and passive properties of the vasculature. NO has been shown to modulate the elasticity of the arterial wall, and loss of NO affects adversely the vascular morphology and plasticity. Vascular NO release is shown to improve elastic properties in human arteries [204]. In addition, arteriolar stiffness is shown to be regulated by endothelium derived NO and hyperpolarizing factor [205]. Altered receptor-mediated responses have been linked to vascular remodeling, leading to smooth muscle cell proliferation [206] and endothelium dependent hypertension [207]. EDHF acting through Ca^{2+} activated potassium channels (K_{ca}) and NO have shown to regulate peripheral artery mechanics in vivo in humans [208] and rats [209]. Increase in smooth muscle cell length is reported to be one of the factors responsible for vascular hypertrophy in young hypertensive rats [210]. In addition, NO generating vasodilators and cGMP mediated mechanism have been shown

to function as a modulator of vascular smooth muscle cell mitogenesis and proliferation [211]. NO has been shown to play a functional role in modulating vascular stiffness and endothelial dysfunction in hypertension [212].

Our previous work has suggested compromised NO-induced vasoactivity in salt sensitive hypertension. Here we designed the study to identify the morphological and biomechanical alterations in salt loaded hypertensive Dahl rats in comparison to normotensive controls. Experiments were conducted under both active (under influence of Ca^{2+} activity) and passive (in absence of Ca^{2+} activity) conditions. We also formulated mathematical models which incorporated the experimental observations to provide parameters describing mechanical properties of vascular wall in rat mesenteric arteries. The understanding of blood pressure regulation at the tissue level could be greatly enhanced by more detailed information on mechanical properties of rat resistance arteries under physiological and salt-induced hypertensive patho-physiological condition.

4.2 Methods

4.2.1 Animal Model

Male Sprague Dawley and salt-sensitive Dahl rats (SS/JrHsd) and their diet were purchased from Harlan Laboratories (Madison, WI). Sprague Dawley rats were maintained on standard pellet chow (2018 Teklad Global) rodent diet whereas the Dahl salt-sensitive rats were fed 0.49% NaCl diet (Harlan Cat. #TD 96208) or 4% NaCl diet (Harlan Cat. #TD 92034).The animals were housed in temperature and humidity controlled rooms with 12 hour on/off light cycle at the animal care facility. All animal studies were performed following Institutional Animal Care and Use approved procedures.

4.2.2 Preparation of Resistance Arteries

Mesenteric arterioles of the second order isolated from the vascular bed were separated in cold physiological modified Krebs-Rringer solution containing (mM): NaCl 145, KCl 5, $CaCl_2$ 2.5, $MgSO_4$ 1.2, KH_2PO_4 1.2, HEPES 20, and Glucose 10.1 with pH 7.4. Second order branches of mesenteric arterioles were isolated and cleaned of surrounding fat and cannulated under dissection microscope. Buffer solutions were replaced to carry out experiments in $0Ca^{2+}$ (Ca^{2+}-free) and 2.5mM Ca^{2+} (Ca^{2+}-containing) conditions. The vessel chamber was maintained at 37^oC. The arterioles were preconditioned to obtain reproducible data. We obtained intraluminal pressure-diameter relationship with a servo-controlled pump by increasing the intraluminal pressure in 10 mmHg steps. The resting diameter was determined at 3 mmHg, and the pressures were increased upto 120 mmHg for axial prestretch $\lambda = 1.0$, 1.1 and 1.3. Vascular thickness and external diameter were calculated using a computer aided video imaging system. All data were expressed as mean $\pm$ SEM and statistical significance were compared with Student's t-test. A value of $p < 0.05$ was considered statistically significant.

4.2.3 Uniaxial tensile loading

Mechanical properties of mesenteric arteries of Sprague Dawley (SD), low salt fed Dahl rat (DS-L) and high salt fed Dahl rats (DS-H) were evaluated by tensile testing. Samples inner and outer radius and length were measured and recorded before subjecting the sample into the test. Tensile sample preparation and tests were carried out in accordance with standard ASTM, D3039M-08 protocol for biomaterials [213]. Tests were carried out using a mechanical testing device (Electroforce 3200 test instrument,

Bose Corporation, Eden Prairie, MN) in an uniaxial tensile mode using a 10 N load cell. The tests were carried out at a crosshead speed of 0.005 mm/s. Samples were placed in the saline chamber in a controlled environment where the temperature was set at 37 $^{\circ}$C. Samples from each group were tested for calculating elastic modulus. The incremental elastic modulus of the sample was determined by calculating the slope of the stress-strain curve.

4.2.3 Calculation of structural and mechanical parameters

Wall thickness (*WT*) and external diameter (*D*) of the vessel were obtained from the meta-analysis of experimental images using IPLAB (BioVision Technologies) and MATLAB (MathWorks) software. Cross sectional area (CSA) and wall to lumen ratio were calculated as follows:

Wall Thickness $WT = (D - D_i)/2$ 4.1

Lumen Diameter $D_i = (D - 2 \cdot WT)$ 4.2

Cross sectional area $CSA = \pi \cdot [(D - WT) \cdot WT]$ 4.3

Wall to Lumen Ratio $= (D - D_i)/2 \cdot D_i$ 4.4

The stress strain relationship was observed to be non-linear. The stress-strain data were fitted by the exponential function by adjusting material constants σ_0 and β:

$$\sigma = \sigma_0 \cdot e^{\beta \cdot \varepsilon} \qquad\qquad 4.5$$

The circumferential and axial Cauchy strains were calculated from experimental data as experimental as:

$$\varepsilon_c = (D - D_0)/D_0 \text{ and } \varepsilon_z = (L - L_0)/L_0 \text{ 4.6}$$

where D_0 is the diameter observed at 2 mmHg intraluminal pressure in the vessel. L_0 is the initial axial length. The Cauchy stress was calculated as

$$\sigma_c = (P \cdot D_i)/2 \cdot WT \text{ and } \sigma_z = F/CSA, \qquad 4.7$$

where P is the intraluminal pressure applied with the aid of servo-controller assembly and F is the axial load on the vessel. The compliance of the vasculature, i.e. the slope of the pressure-diameter relationship, is important in determining the non-linearity associated with the stress-strain relationship. This is characterized by incremental elasticity modulus which is the slope of the stress-strain curve. We obtained a tangential or incremental elasticity modulus by determining the slope of the stress-strain relationship. At any given point incremental Young's modulus (Y_{inc}) is directly proportional to β. An increase in β implies an increase in Y_{inc}, which translates to an increase in stiffness calculated by

$$Y_{inc} = \beta \cdot \sigma. \qquad 4.8$$

4.2.4 Constitutive 4 parameter finite element model

We further extended the study by considering the stress-strain relationship to observe a non-linear continuum mechanics with arteriole treated as a hyperelastic material described by [214]

$$S = \frac{\partial W}{\partial E}, \qquad 4.9$$

where S is the second Piola-Kirchhoff stress tensor. We constructed a 2D axisymmetric finite element model in *COMSOL* to describe the integrative vascular biomechanics with active and passive components.

The total strain energy density function of the NE induced active vessel is given by

$$W_{total} = W_{active} + W_{passive}. \qquad 4.10$$

The generalized passive strain energy density function is given by [215]

$$W_{passive} = \frac{1}{2}C_p\left(e^Q - 1\right),$$

$$Q = \frac{1}{2}a_{KLMN}E_{KL}E_{MN}.$$

4.11

Where

$$Q = a_1 E_{RR}^2 + a_2 E_{\Theta\Theta}^2 + a_3 E_{ZZ}^2 + 2a_4 E_{RR}E_{\Theta\Theta} + 2a_5 E_{ZZ}E_{\Theta\Theta} + 2a_6 E_{RR}E_{ZZ} + a_7\left(E_{R\Theta}^2 + E_{\Theta R}^2\right)$$
$$+ a_8\left(E_{Z\Theta}^2 + E_{\Theta Z}^2\right) + a_9\left(E_{ZR}^2 + E_{RZ}^2\right),$$

whereCp, $a_1 = a_2 = a_3$, $a_4 = a_5 = a_6$, and $a_7 = a_8 = a_9$ represent the passive, orthotropic, compressible material constants. The active strain energy function to incorporate the SMC activity is given by:

$$W_{active} = C_a\left[Erf\left(Q'\right) - 1\right], with\ Q' = \frac{\lambda_\theta}{b_1} + \frac{\lambda_z}{b_2} - b',$$

4.12

whereC_a, b_1, b_2 and b' are material constants and Erf(X) is a Gaussian error function.

4.2.4 Parameter Estimation

Case i. Parameter identification from deterministic scenario

We tested the performance of the model and optimization procedure by implementing a deterministic scenario with known parameter values Θ_k.

We implemented optimization algorithm which minimized the following least squares cost functions.

$$\min_{\theta_{k,passive}}\left(c_{IS}\right)$$

4.13

$$where\ c_{LS}\left(\theta_{k,passive}\right) = \sum_j \left\|\left(y_{MODEL}\left(p_j, \hat{\theta}\right) - y_{MODEL}\left(p_j, \Theta_{k,passive}\right)\right)\right\|_2^2$$

where $y_{MODEL}\left(p_j, \Theta_k\right)$ is the Green Lagrange strain vector computed from Eqs 4.11-12

for pressure range p_j

At each pressure, mean strain was calculated as:

$$y_{MODEL}\left(p_j\right) = \left[\frac{1}{n_E} \sum_{i=1}^{n_E} \left[y_{MODEL}{}^T\left(r_1, p_j\right), ..., y_{MODEL}{}^T\left(r_{n_E}, p_j\right)\right]\right], \qquad 4.14$$

In similar way we have identified parameters describing the active component:

$$c_{LS}\left(\theta_{k,active}\right) = \sum_j \left\|\left(y_{MODEL}\left(p_j, \hat{\theta}\right) - y_{MODEL}\left(p_j, \Theta_{k,active}\right)\right)\right\|_2^2, \qquad 4.15$$

where n_E is the number of points along vessel over which the strain was averaged. Quasi

Newton method was implemented to perform the minimization in MATLAB. To test the

robustness of the identification method runs with random starting points were carried

within chosen parameter bounds. The obtained parameter values from the deterministic

scenario implementation are presented in Table 1.

Case ii. Parameter identification from experimental data

To obtain the unknown parameters we used the optimization algorithm described in Case

i, which minimized the following least squares cost functions.

$$c_{LS}\left(\theta_k\right)_{passive} = \sum_j \left\|\left(y_{MODEL}\left(p_j, \hat{\theta}\right) - y_{EXPERIMENT}\left(p_j\right)\right)_{passive}\right\|_2^2, \qquad 4.16$$

We first obtained the passive parameters and used them as constants while estimating the

active parameters.

$$c_{LS}(\theta_k)_{active} = \sum_j \left\| \left(y_{MODEL}\left(p_j, \hat{\theta}\right) - y_{EXPERIMENT}\left(p_j\right)\right)_{active} \right\|_2^2 ,$$

4.17

where θ_k is the vector of constitutive k parameters for identification, p_j is the intraluminal pressure applied to the mesenteric arterioles over range index j.

We obtained set of circumferential strain measurements for different axial stretch from isolated mesenteric arterioles of Sprague Dawley and salt sensitive Dahl rats. The lumped experimental strain measurements $y_{EXPERIMENT}$ were:

$$y_{EXPERIMENT}(p_j) = \left[\frac{1}{n_E} \sum_{i=1}^{n_E} \left[y_E{}^T\left(r_1, p_j\right), ..., y_E{}^T\left(r_{n_E}, p_j\right)\right]\right], \qquad 4.18$$

The obtained parameter values for the active and passive case from the experimental measurements are presented in Table 2.

4.3 Results

After 5 weeks of salt feeding the high salt Dahl rats consistently developed hypertension. These vessels exhibited reduction in lumen diameter and increased vascular wall thickness. In addition to testing the morphological characteristics of resistance arterioles in the three groups, we determined the mechanical properties from salt fed Dahl rats. In fig 4.1, we see the representative strain obtained from 2D axial symmetric finite element model for vascular thickness 25μM (Control condition) and 45μM (High salt condition).
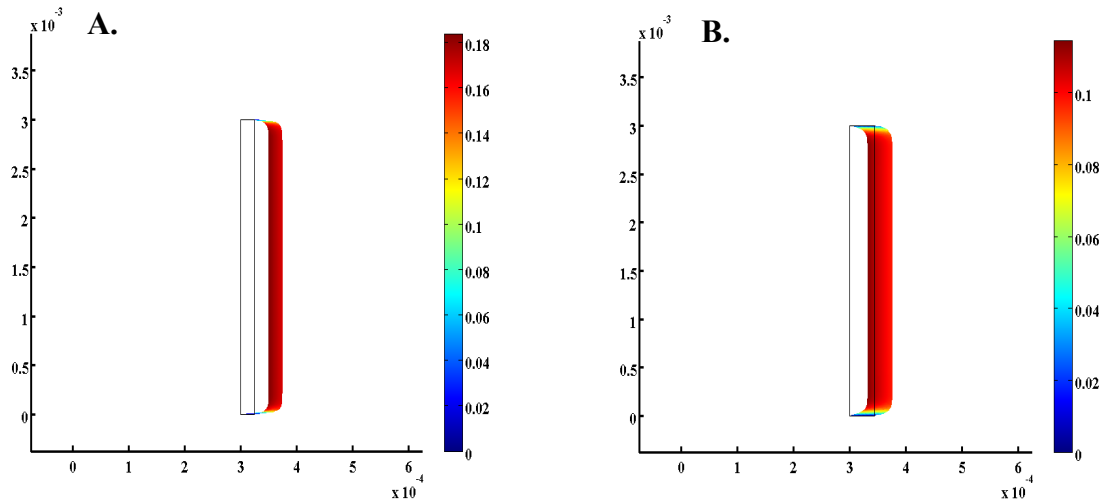
Fig 4.1. Representative strain measurements obtained from 2D finite element, axis symmetric rat mesenteric arteriole model of thickness (A) 25µM (Control) and (B) 45µM (High salt) experiencing 50 mmHg intravascular pressure.

In Fig 4.2, we showed the morphological characteristics under passive ($0Ca^{2+}$) conditions. The variation in vascular diameter and thickness were plotted against increased intraluminal pressure. We obtained these relationships for three different axial elongations ($\lambda = 1.0$, 1.1 and 1.3). We observed increased external diameter and thickness in high salt fed Dahl rats (DS-H) as compared to low salt fed Dahl rats (DS-L) and Sprague Dawley (SD) rats.

In Fig 4.3, we plotted the cross sectional area (CSA) and the wall to lumen ratio obtained along with change in intraluminal pressure. We observed the hypertensive DS-H rats to have a larger CSA and increased wall to lumen ratio as compared to its corresponding normotensive controls.

4.3.1 Characterization of passive mechanical properties
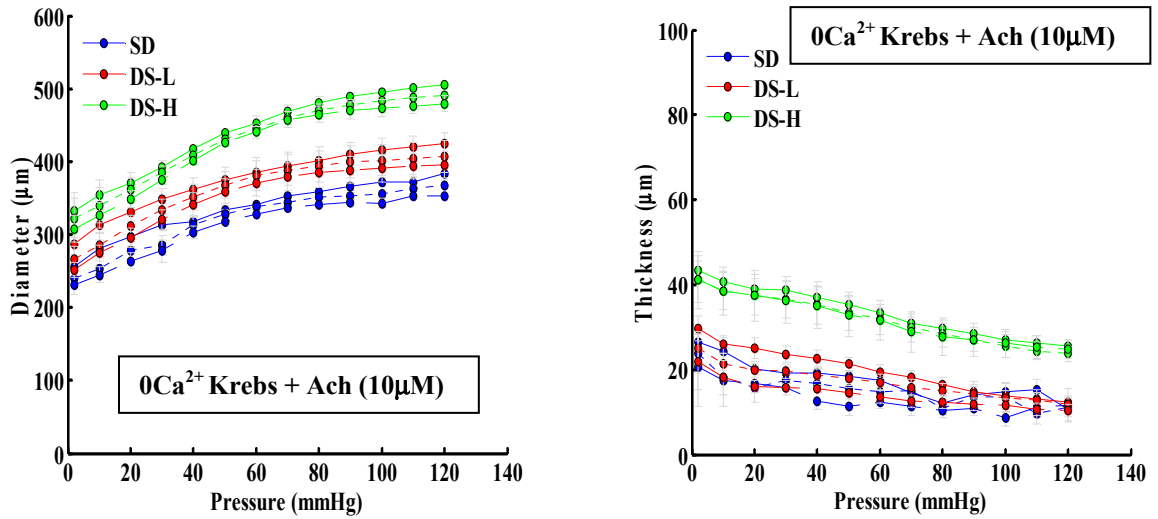
Fig 4.2. Variation of diameter and thickness with the intraluminal pressure at various longitudinal stretch ratios: λz = 1.0, λz = 1.1 and λz = 1.3 in mesenteric arterioles of Sprague Dawley (SD), low salt fed Dahl rats (DS–L) and high salt fed Dahl rats (DS-H). Data is mean ± SEM, n = 3 rats.
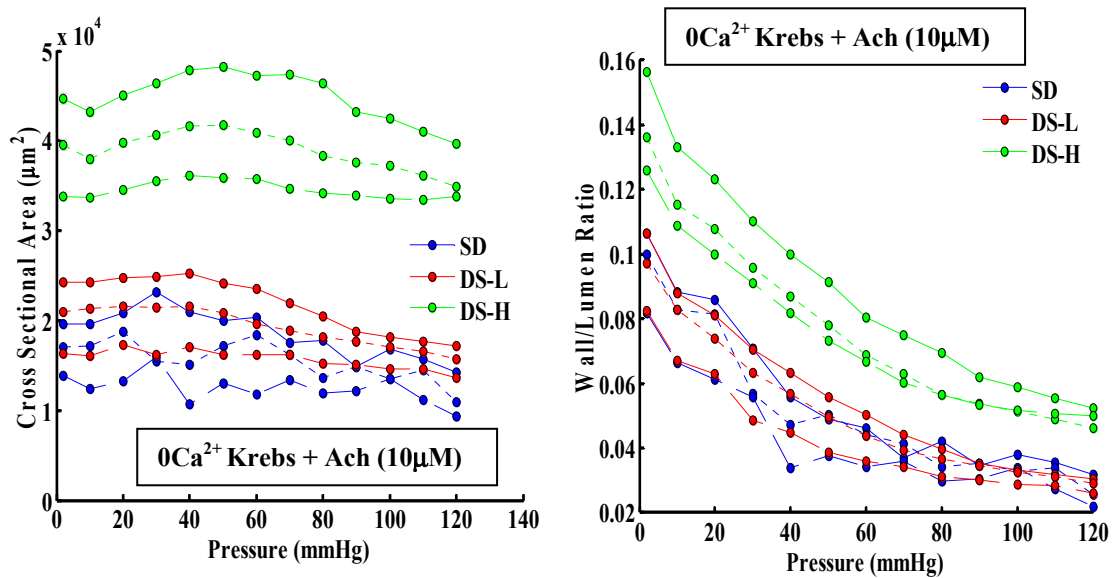
Fig 4.3. (A) Intraluminal pressure - Cross sectional area and (B) intraluminal pressure - wall to lumen ratio relationship at various longitudinal stretch ratios: λz = 1.0, λz = 1.1 and λz = 1.3 in mesenteric arterioles of Sprague Dawley (SD), low salt fed Dahl rats (DS–L) and high salt fed Dahl rats (DS-H). Data is mean ± SEM, n = 3 rats.

4.3.2 Characterization of active mechanical properties

Identical study was performed for 3 different axial elongation (λ = 1.0, 1.1 and 1.3) under active stress conditions in presence of 2.5mM Ca^{2+} and 2.5mM Ca^{2+} + 10µM NE. Here below we demonstrated the morphological characteristics under active stress conditions. In Fig 4.4 and Fig 4.5 we see the diameter and thickness relationship under active stress conditions.
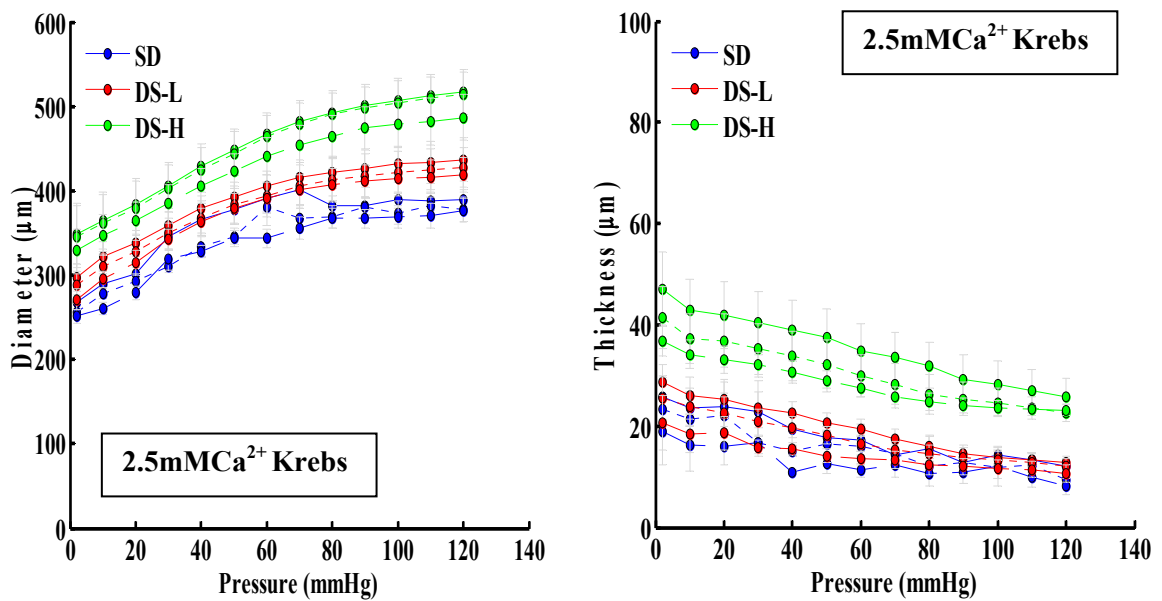
Fig 4.4.Variation of diameter and thickness with the intraluminal pressure at various longitudinal stretch ratios: λz = 1.0, λz = 1.1 and λz = 1.3 in mesenteric arterioles of Sprague Dawley (SD), low salt fed Dahl rats (DS–L) and high salt fed Dahl rats (DS-H). Data is mean ± SEM, n = 3 rats.

In Fig 4.5, we showed the arterioles subjected to active stress induced by 10µM NE in presence of 2.5mM Ca^{2+}. The arterioles demonstrated significant active tension under 10µM NE. We observed decreased diameter and increased thickness under 10µM NE.
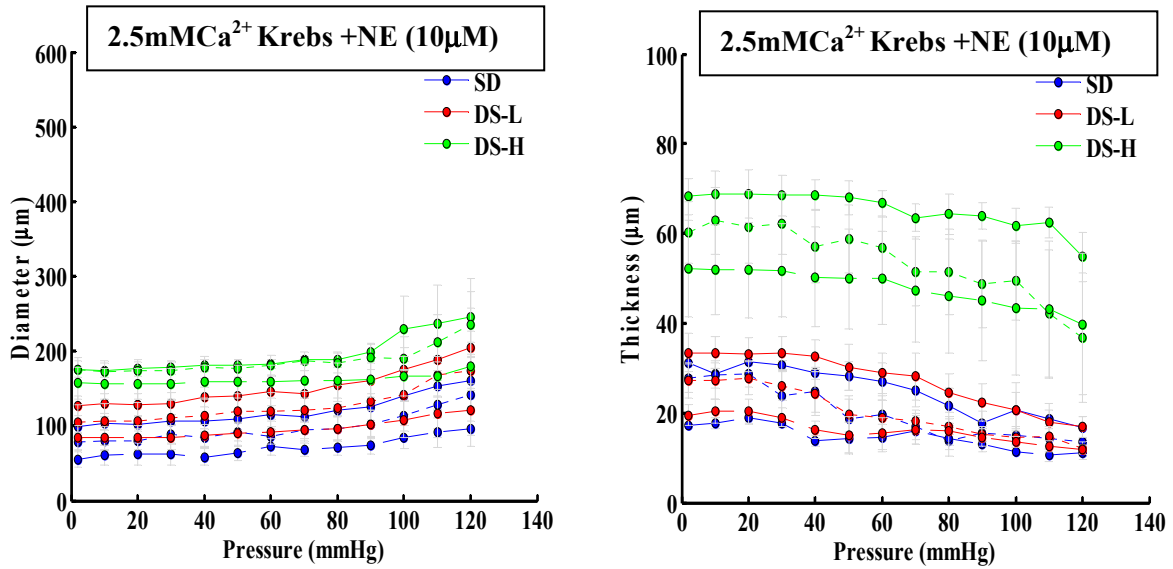
Fig 4.5. Variation of diameter and thickness with the intraluminal pressure at various longitudinal stretch ratios: λz = 1.0, λz = 1.1 and λz = 1.3 in mesenteric arterioles of Sprague Dawley (SD), low salt fed Dahl rats (DS–L) and high salt fed Dahl rats (DS-H). Data is mean ± SEM, n = 3 rat.

Fig 4.6. Intraluminal pressure - Cross sectional area and intraluminal pressure - wall to lumen ratio relationship at various longitudinal stretch ratios: λz = 1.0, λz = 1.1 and λz = 1.3 in mesenteric arterioles of Sprague Dawley (SD), low salt fed Dahl rats (DS–L) and high salt fed Dahl rats (DS-H). Data is mean ± SEM, n = 3 rats.

In Fig 4.6 and Fig 4.7 we showed the cross sectional area and lumen to diameter relationship under active stress conditions in presence of 2.5 mM Ca^{2+} and under active tension from 10μM NE.
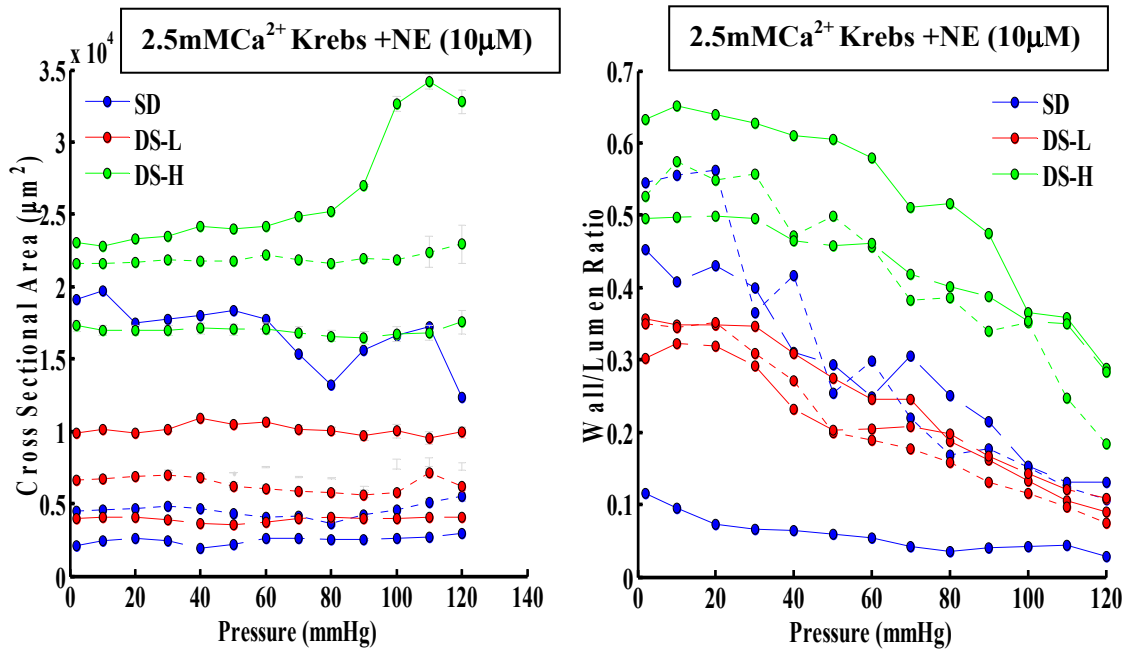
Fig 4.7. (A) Intraluminal pressure - Cross sectional area and (B) intraluminal pressure - wall to lumen ratio relationship at various longitudinal stretch ratios: λz = 1.0, λz = 1.1 and λz = 1.3 in mesenteric arterioles of Sprague Dawley (SD), low salt fed Dahl rats (DS–L) and high salt fed Dahl rats (DS-H). Data is mean ± SEM, n = 3 rats.

Under active tension we observed increased wall to lumen ratio and decreased cross section area. Further, we demonstrated the stress strain relationship that characterizes the material properties.
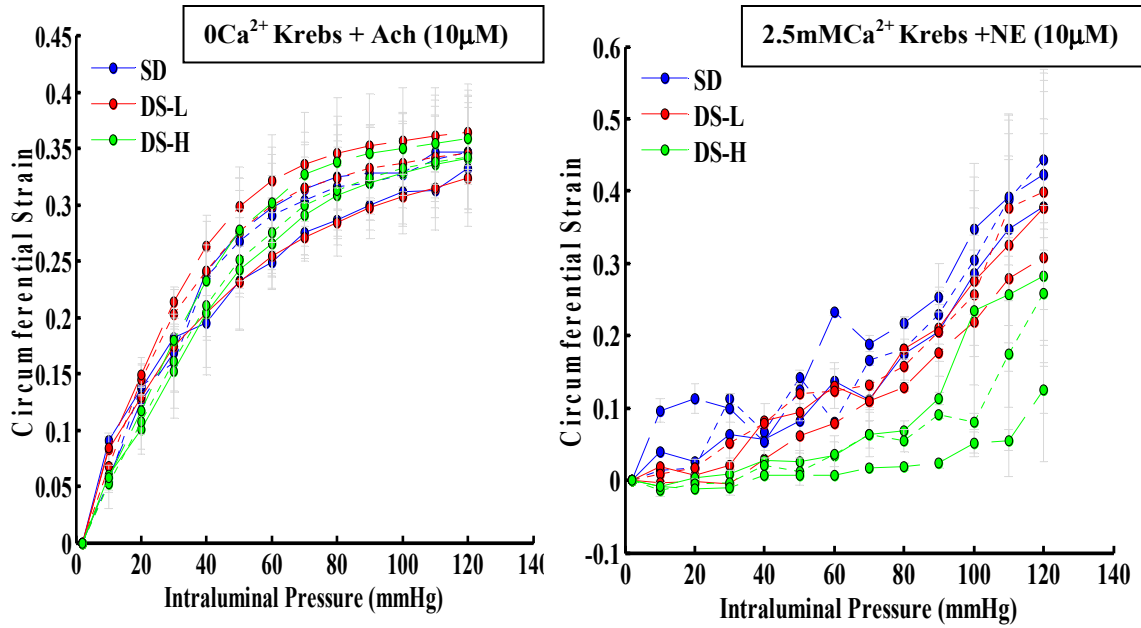
Figure 4.8. Intraluminal Pressure and Circumferential Strain curves for various longitudinal stretch ratios: $\lambda_z = 1.0$, $\lambda_z = 1.1$ and $\lambda_z = 1.3$ in mesenteric arterioles of Sprague Dawley (SD), low salt fed Dahl rats (DS–L) and high salt fed Dahl rats (DS-H). Data is mean ± SEM, n = 3 rats.

In Fig 4.8, we showed the circumferential pressure and strain relation for passive and active $0Ca^{2+}$ and 2.5 mM Ca^{2+} conditions.
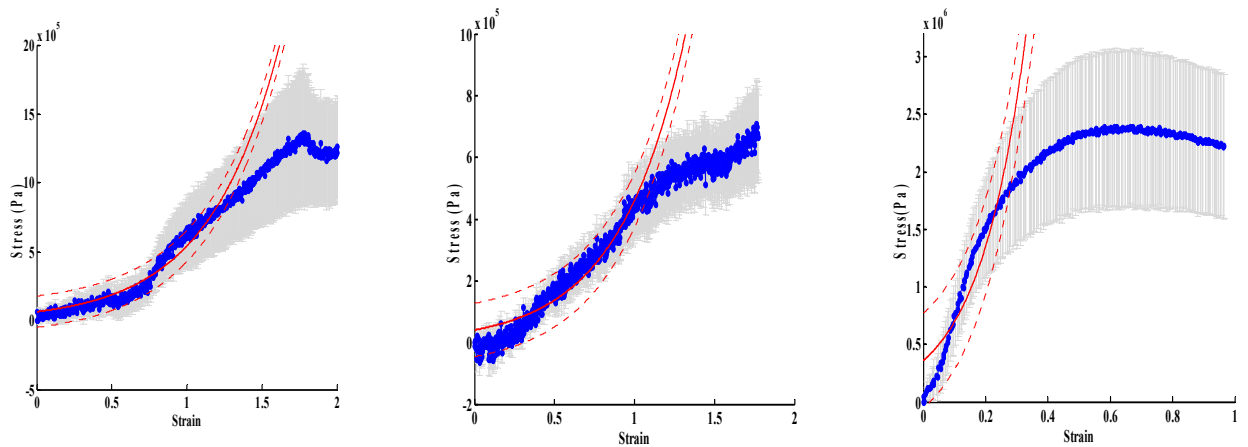
Fig 4.9. Axial stress – Axial strain curve in uniaxially loaded mesenteric arteries from Sprague Dawley, LS fed Dahl rats and HS fed Dahl rats, n = 5 vessels. Data is mean ± SEM.

In fig 4.9, we plotted the axial stress-strain relationship for the three different groups of rats. The difference in stiffness was characterized by β as described earlier. The obtained results were tabulated in the following table 4.1:

	Wall Thickness (WT, µm)	Axial β	Circumferential β
SD	18.52 ± 1.26	2.344 ± 0.22	2.256 ± 0.60
DS-L	21.30 ± 1.98	2.188 ± 0.38	1.921 ± 0.38
DS-H	35.31 ± 2.44	3.713 ± 0.80	1.895 ± 0.42

Table 4.1.Wall thickness and βvalues for SD, DS-L and DS-H rats.

4.3.3 Parameter Estimation:

The parameters obtained from the estimation are tabulated below:

Case i. Deterministic Scenario

Table 4.2 A. Passive condition:

True Value:Cp = 80.568kPa, a1 = 0.521, a4 = 0.251, a9 = 0.391.

Trial	a1	a4	a9	Cp*100kPa
1	[0.46935	0.24112	0.40002	0.84892]
2	[0.53995	0.13283	0.43322	0.92103]
3	[0.53822	0.24651	0.50981	0.92190]
4	[0.63975	0.13069	0.33109	0.72203]
5	[0.71210	0.21991	0.38001	0.78143]

Table 4.2 B. Active Condition:

True Value: Ca = 4.41 kPa, b1 = 0.117, b2 = 0.207, b' = 20.5. {Parameters obtained from Kassab et al. [215]}

Trial	Ca *10kPa	b1	b2	b'*100
1	[0.62001	0.1997	0.30103	0.18192]
2	[0.43301	0.23018	0.20502	0.20495]
3	[0.42087	0.18283	0.21196	0.19236]
4	[0.50123	0.21009	0.47530	0.31576]
5	[0.38112	0.10283	0.28201	0.21765]

Case ii. Parameter identification from experimental data

Minimizationperformed on mean data from N=3 rats in each group

Table 4.3 A. Passive Condition:

Rat	a1	a4	a9	Cp*100kPa
SD	[0.33190	0.38173	0.12911	0.54210]
DS-L	[0.48721	0.47903	0.24236	0.40331]
DS-H	[0.73115	0.68311	0.11173	0.79300]

Table 4.3 B. Active Condition:

Rat	Ca*10kPa	b1	b2	b' *100
SD	[0.67210	0.17060	0.11380	0.30595]
DS-L	[0.51480	0.31559	0.41750	0.18890]
DS-H	[0.30991	0.61981	0.54201	0.04211]

4.3.4 Statistical Analysis:

To quantify the 'goodness of fit', comparison were made between the experimental values and the theoretical predictions with best fit material constants, i.e. RMSE were calculated for the fitting.

4.4 Discussion

The pressure-lumen relationship of the resistance arterioles play a critical role in maintaining normal blood flow conditions in the vasculature [190]. Altered mechanics may lead to arteriolar resistance increases due to vasoconstriction and structural changes. Increased resistance of the mesenteric vessels is associated with hypertension, which may result from a decrease in the lumen size induced by the contraction of the smooth muscle. Pathogenetic malfunction such as impaired endothelium may further augment complex remodeling of the vasculature [194]. Under hypertensive conditions, studies have suggested that changes in pressure-diameter relationship are influenced with increased distensibility in small arteries [217]. Changes in the vascular reactivity could be preceded by elevation of vascular resistance and arterial pressure in salt sensitive hypertension [192]. In addition, in vivo vessels experience axial strain, and thus characterizing circumferential and axial stress-strain aspect associated in mesenteric vessels is fundamental to provide better understanding of the patho-physiology of hypertension.

Microvascular tone and blood flow are determined by passive biomechanical properties of the vessel wall and by active constrictions of the vascular smooth muscle cells (SMC). In the vascular smooth muscle cells, increased expression of Ca^{2+} activated K^+ channels (IKCa) is associated with smooth muscle cell proliferation [218; 219]. The intracellular calcium concentration in SMC is the major determinant of the active tone

74

and is controlled by a complex system of intracellular and intercellular signaling pathways [156]. The contractile state of SMCs depends on the intracellular Ca^{2+} concentration and is regulated by an elaborate network of signaling pathways. The SMC-EC network plays an integral role in modulating signal transmission. Several Ca^{2+}dependent channel operations are altered due to changes in vascular morphology. Ca2+-dependent volume regulated chloride channel activity is shown to be compromised in rat cerebrovascular smooth muscle cell during hypertension [220]. β-adrenergic regulation of Na-K-Cl ion transport abnormality was correlated to cytoskeletal and smooth muscle altered cell morphology [221]. The glycoprotein tenasin associated with remodeling events is expressed in smooth muscle cells of spontaneously hypertensive rats [222]. Changes in expression and function of Ca2+-dependent K^+ channels is reported to be associated to wall structure in hypertension [110; 111]. The intracellular Ca^{2+} thus not only regulates the intracellular contractile response of smooth muscle cell [223] but it also causes long term morphological changes by altering gene expression [224] that might alter the vascular tone in normotensive [109] and hypertensive conditions [209]. Arteries of hypertensive animals have shown increased smooth muscle cell mass as compared to normotensive controls which might trigger enhanced vasoconstriction [193]. Changes in the contractile properties are reported in resistance arteries of SHR and normotensive rats [225]. In animal models, significant changes in the viscoelastic properties of the arteries were observed in Goldblatt hypertension [226] and in SHR [227] rats. Wall stress generated by intraluminal pressure was significantly smaller with reduced elasticity modulus in another study with SHR hypertension model [228]. The

differences in the elastic properties are suggested to be a consequence rather than precursor to hypertension [113].

In this study, we identified whether the passive and active biomechanical properties of mesenteric resistance arterioles are altered in Dahl salt sensitive hypertension active. We presented material properties of rat mesenteric arterioles in high salt fed hypertensive (DS-H) rats in comparison to normotensive low salt fed Dahl rats (DS-L) and Sprague Dawley as controls. The salt sensitive hypertension is associated with alteration in the morphology of the carotid arterial wall [203]. We examined whether morphological alteration occurred in rat mesenteric arteries after salt loading in HS Dahl rats as compared to LS and Sprague Dawley as controls.

Our evaluation of the mechanical properties of the mesenteric arteries in HS fed Dahl rats along with LS fed Dahl rat and Sprague Dawley as control suggested morphological changes in HS fed hypertensive rats which included increase in media width and CSA, both indicators of vascular growth. Our study with salt sensitive Dahl hypertension model demonstrated increased vascular growth with thicker vessel walls. We observed that salt loading resulted in vascular remodeling. Our experiments suggested that treatment with high salt decreased the lumen to external diameter ratio. The strain was computed from the changes in the displacement measurements relative to the zero stress state. From the obtained stress-strain relationship we estimated the material properties such as the elasticity coefficients associated with the rat mesenteric vessels under normotensive and hypertensive conditions. Increased elastic modulus was observed in HS Dahl rats suggesting significant changes in the stiffness of the arterial wall components.

The mathematical model could be used to simulate agonist-induced vasorelaxation and vasoconstriction, conducted vasoreactivity, myogenic tone and pressure-induced diameter changes. This model can also be used to test hypotheses about tone regulation, such as the role of myoendothelial projections and extracellular potassium in endothelium derived hyperpolarizing factor. Disease-specific changes at the subcellular level can be incorporated into the model to predict their effect on responses at the vessel level. These observations could facilitate an insight in the pathophysiology of salt sensitive hypertension thereby giving us a valuable insight in the abnormalities occurring in the mechanical structure of the vessel under hypertensive conditions. This occurs through a wide variety of mechanical and biochemical mechanisms that maintain cardiovascular equilibrium. An understanding of the physiological factors that regulate the resistance in arteriolar circulation is thus important to identify the pathological basis of cardiovascular risk such as hypertension.

In conclusion, we developed a forward mathematical model to simulate the abnormality such as salt sensitive hypertension in rat mesenteric arteriole. Further, we proposed an inverse computational model for estimating the elasticity profile of the mesenteric arteriole in normotensive and salt sensitive conditions. Our identification of coefficients which represented salt sensitivity in mesenteric arterioles can provide an insight to streamline causes of salt sensitive hypertension.Thus, the integration of subcellular data into a computational model can allow the analysis of complex microcirculatory function in health and disease, hypothesis testing, and guide new experimentation.

CHAPTER 5

Vascular reactivity study on isolated Dahl rat mesenteric arterioles: A role of EDHF, EDRF and α₂-adnergic receptor in salt sensitive hypertension

5.1 Introduction

Salt sensitivity possesses a significant health risk as it appears in more than half of the hypertension cases. It acts a marker for increased cardiovascular risk in patients with essential hypertension. It leads to susceptibility of endothelial dysfunction and vascular damage. Many elementary questions regarding the pathophysiology of salt sensitive hypertension are vaguely addressed. The mechanisms by which salt intake increases peripheral vascular resistance leading to arterial constriction and increase in blood pressure have not been clearly understood.

It is widely accepted that NO plays an important role in salt sensitive hypertension. The L-arginine/NO pathway particularly NO as an EDRF has been the area of keen interest. L-arginine supplementation has shown beneficial effects with increased NO production in Dahl salt sensitive rats [229; 230]. On the other hand, chronic inhibition of NO induced salt sensitive hypertension in control rats [231]. Suppression of L-arginine-NO system [232] has emerged as one of the major component in the pathophysiology of salt sensitivity. Compromised endothelium-dependent vasodilation has been reported in salt sensitive humans [233] and animal models [234; 235].

The mechanisms that link salt sensitivity to altered NO activity have not been resolved. Recent studies have suggested decreased expression of eNOS, increased NO scavenging and decoupling of eNOS in salt sensitivity. Limited NO availability has shown to precede development of hypertension [236]. It is not clear if compromised NO

bioactivity plays a major role in the pathogenesis of hypertension or if it is a result of elevated blood pressure. On the other hand there are experimental findings that have suggested NO is not an essential factor for the development of hypertension [237; 238]. Both upregulation and downregulation of NO activity has been reported in hypertension and there are contradictory reports regarding the role of NO in both humans [239] and in hypertensive animal models [240; 241]. In SHR model studies have reported decreased endothelium derived relaxation in different vessels including the aorta [242], coronary arteries [243], and mesenteric arterioles [244]. These results imply decreased NO mediated activity in SHR. On the other hand studies have as well reported no change [240] or enhancement [245] of the endothelium dependent relaxation, increased expression of eNOS [246] and enhanced overall NO activity of SHR in vivo [247].

Distinct endothelial impairment is seen in coronary microvessels from hypertensive Dahl rats [17]. Endothelium dependent relaxations are primarily mediated by the release of NO (EDRF), prostacyclin or endothelium derived hyperpolarizing factor (EDHF) [248]. The relative contribution of EDHF and NO in endothelium dependent relaxation has been a subject of wide interest [249]. Observation that EDHF is distinct from NO has suggested benefits towards vascular control mechanisms. If one system fails then a parallel or back up system could compensate in the vasomotor responses. NO pathway and EDHF mechanisms have demonstrated to work in a feed forward associative and feedback compensatory mechanisms. Such parallel or backup controls could be produced by different signal transduction pathways and may have different downstream effectors. Studies have documented inhibitory actions of NO in the production and/or action of EDHF suggesting it to follow a negative feedback mechanism [250; 251]. Another study

on rat cerebral vessel demonstrated that EDHF responses were not suppressed by NO thereby suggesting a functional role for EDHF [252]. NO has as well shown to contribute to EDHF responses in small rat arteries [253].

In addition, Chang et.al [254] pointed out that vast majority of the experimental studies utilize vascular rings of large vessels and not vessels from microcirculation, where the blood flow and pressure are mostly controlled. Large arteries may behave significantly differently from the smaller resistance arterioles. In this chapter, we hence try to develop a better fundamental understanding of the signal transduction events that are involved in the vascular tone regulation in small resistance arterioles of salt sensitive hypertensive Dahl rats.

5.2 Methods

5.2.1 Animal Model

Dahl salt-sensitive (SS) rats and their diet were purchased from Harlan Laboratories (Madison, WI). Dahl salt-sensitive rats were fed 0.49% NaCl diet (Harlan Cat. #TD 96208) or 4% NaCl diet (Harlan Cat. #TD 92034).The animals were housed in temperature and humidity controlled rooms with 12 hour on/off light cycle at the animal care facility. All animal studies were performed following Institutional Animal Care and Use approved procedures.

After acclimatization for 1 week, 6-week old Dahl salt-sensitive rats were separated into 2 diet groups; normal salt (NS), fed 0.49% NaCl diet and high salt (HS), fed 4% NaCl diet for another 5 weeks. Systolic blood pressure was measured weekly with the tail cuff method [170]. At 11 weeks old, HS rats consistently demonstrated sustained hypertension (BP > 200 mmHg) while NS rats remained normotensive (BP < 160

mmHg). The rats were euthanized and vascular reactivity assessed on isolated, cannulated and pressurized mesenteric arterioles as described below.

5.2.2 Isolated mesenteric arteriole preparation

Mesenteric arterioles of the 2nd order with external diameter of 380 ± 30 μm were isolated from male Dahl rats (250-300 g), cleaned of the surrounding tissue and cannulated at both ends on glass cannula (O.D. 200 ± 25 μm). The organ -chamber was maintained constant at 37°C by superfusion with a modified Krebs-Ringer solution containing (mM): NaCl 145, KCl 5, $CaCl_2$ 2.5, $MgSO_4$ 1.2, KH_2PO_4 1.2, HEPES 20, and Glucose 10.1 pH 7.4 [171]. Cannulated vessels were axially pre-stretched to remove any bents and to simulate physiological stretch conditions. The vessels were pressurized at 50 mmHg and allowed to equilibrate for 60 min before initiating the experiment. The vessels were preconstricted with continuous superfusion of norepinephrine, (NE, 2 μM) and only those that retained a constant pressure and a consistent constriction to NE, and fully responded to the agonist were included in the study. The vessel reactivity study was carried out by serial addition of various agonist concentrations to the vessel chamber. Diameter measurements were tracked in real time by mounting the vessel chamber on the stage of an inverted microscope (Olympus) fitted with a CCD camera (QImaging). Post analysis was performed with IPLAB (BioVision Technologies) and MATLAB (MathWorks) software. Chemicals: All Chemicals were obtained from Sigma-Aldrich Co. (St. Louis, MO)

5.3 Results

5.3.1 Systolic blood pressure of Dahl rats during the 5-week salt treatment

High salt diet (HS: 4% NaCl) fed for 5 weeks resulted in significant increase in systolic blood pressure (212 ± 4 versus 154 ± 3 mm Hg; $P < 0.05$) in HS Dahl rats as compared to Low Salt (LS: 0.49% NaCl) fed Dahl rats.
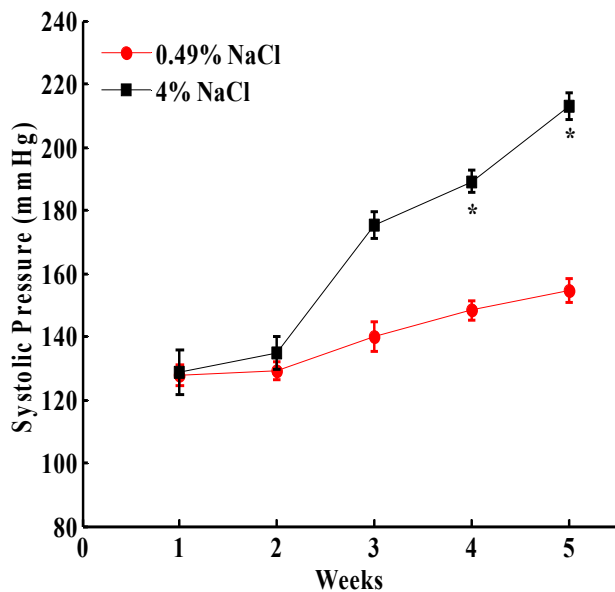
Fig 5.1. Time course of systolic blood pressure measured by tail cuff method in Dahl rats placed on LS (•) and HS (■) diet for 5 weeks, n=11. The data are expressed as mean ± SEM. #P<0.05 vs. LS considered significant.

5.3.2 Norepinephrine induced vascular constriction

To establish a concentration that gave submaximal constriction, in Fig5.2, we constructed a dose response curve to norepinephrine. The EC_{50} value observed of norepinephrine for LS dahl rats was 0.641 ± 0.17 μM, $n = 3$and that of HS dahl rats was 0.457 ± 0.29 μM, $n = 3$.Exogenously applied norepinephrineinduced consistent 80% constrictions at 2μM concentration. This was considered as preconstriction diameter for

the relaxation experiments. In our experiment, no significant difference was observed in the vascular responses to norepinephrine in both group of rats.
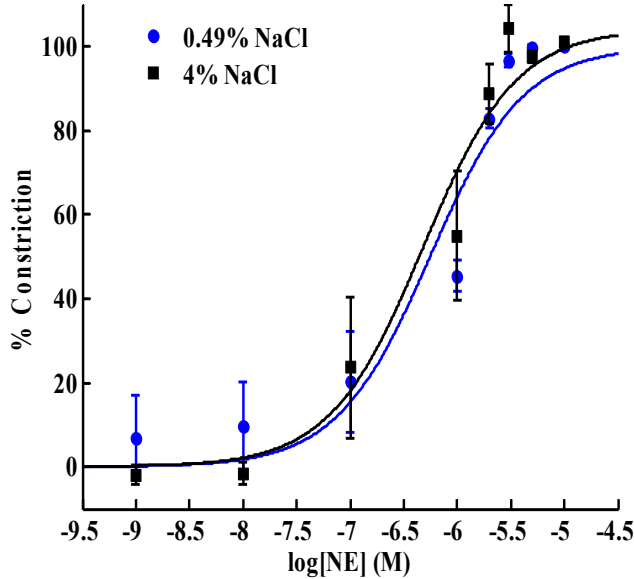
Fig 5.2. Contractile response of mesenteric arterioles to norepinephrine in LS (•) and HS (■) fed Dahl rats, n=3. The data are expressed as mean ± SEM.

5.3.3 Vascular response to Sper-NO and calcimycin

We investigated vascular responses to exogenous NO (Sper-NO) and exogenous Ca^{2+} influx with calcimycin in the two rat groups. We observed maximal relaxation elicited in both groups in response to Sper-NO and calcimycin. The relaxation observed to Sper-NO in LS fed rats was ($100 \pm 3\%$, $n= 3$) as opposed to high salt fed rats ($98 \pm 3\%$, $n = 3$). Calcimycin induced relaxation was ($86 \pm 6\%$, $n = 3$) in low salt and ($87 \pm 8\%$, $n = 3$) in HS fed dahl rats.
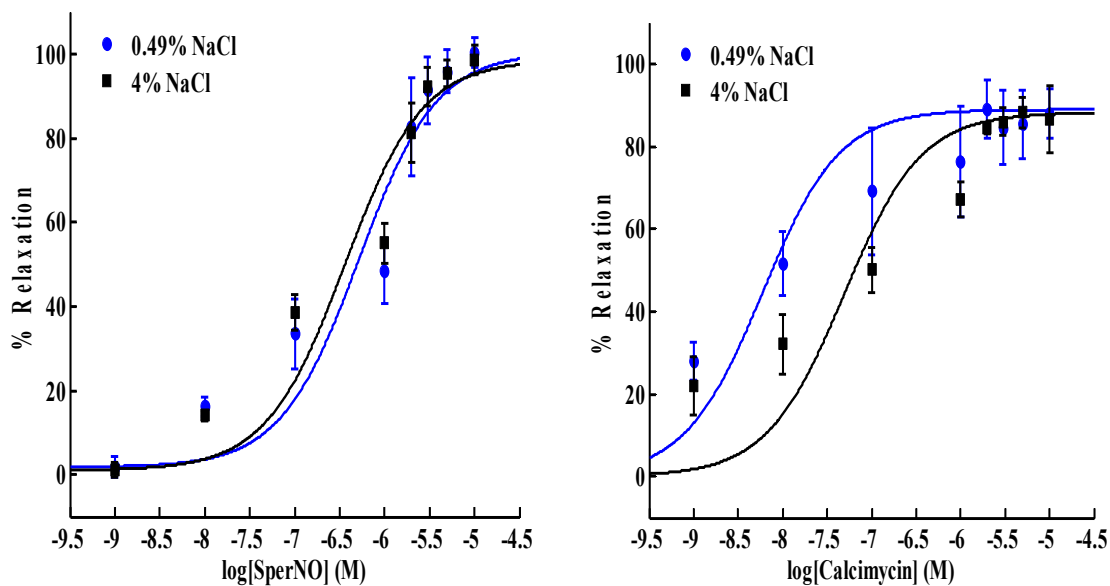
Fig 5.3. Relaxations to SperNO and calcimycin in 2µM, NE preconstricted mesenteric arterioles of LS and HS fed Dahl rats, n=3. The data are expressed as mean ± SEM.

5.3.4 Vascular response to α-2 receptor agonist (UK14304)

The application of α-2 receptor agonist (UK14304) evoked dose dependent relaxation in both groups with a maximum relaxation of (41 ± 3%, *n* = 3) in LS fed dahl rats. These relaxation were significantly compromised in HS fed rats with a maximum obtained response of (19 ± 8%, *n* = 3).
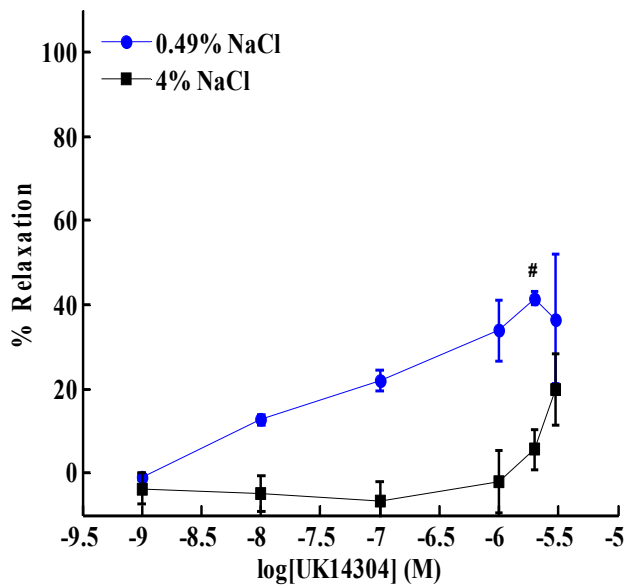
Fig 5.4. Concentration dependent relaxation response to α-2 receptor agonist (UK14304) in 2µM, NE preconstricted mesenteric arterioles of LS and HS fed Dahl rats, n=3. The data are expressed as mean ± SEM.

5.3.5 Vascular responses to Ach in salt sensitive hypertension

The endothelium dependent relaxations evoked by Ach were significantly suppressed in mesenteric arteries of HS fed Dahl rats as compared to those of LS Dahl rats. The maximal relaxation to Ach was ($71 \pm 4\%$, $n = 3$) in HS group as compared to ($95 \pm 9\%$, $n = 3$) in LS group. We investigated the relative contribution of NO and EDHF in acetylcholine mediated smooth muscle relaxation. The NOS inhibitor L-NAME (0.5mM) reduced the acetylcholine evoked endothelium dependent in both the groups. After L-NAME treatment, we observed that acetylcholine induced relaxation were ($62 \pm 4\%$, $n = 3$) in LS fed rats which were compromised significantly ($48 \pm 9\%$, $n = 3$) in HS fed rats as compared to LS group. These relaxations were completely blocked after a combined NOS and EDHF blockade with a cocktail of L-NAME (0.5mM), apamin (50nM) and TRAM-34 (100nM).
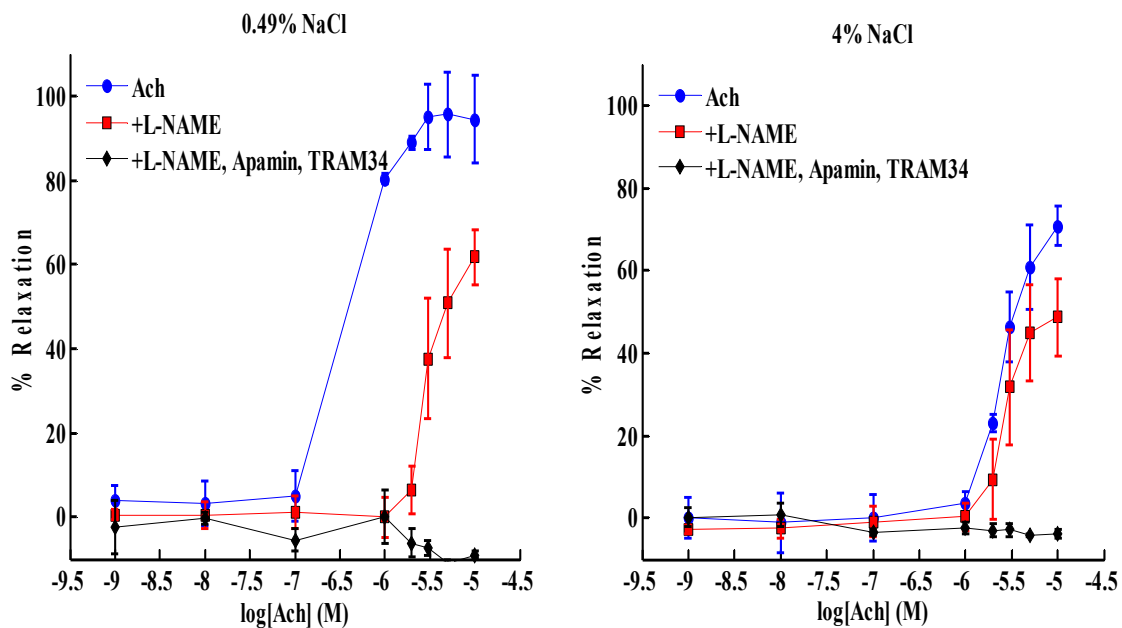
Fig 5.5. Concentration dependent relaxation response to acetylcholine in preconstricted mesenteric arterioles of LS and HS fed Dahl rats, n=3 with EDRF blockade (■) and combined EDRF, EDHF blockade (♦). The data are expressed as mean ± SEM.

5.4 Discussion

Salt sensitive hypertension is associated with impaired endothelial function [23]. The mechanisms that contribute to such susceptibility remain largely unresolved. A relationship between salt sensitivity and hypertension has not been precisely identified. The signaling pathways by which salt intake elevates blood pressure have also not been clearly elucidated. Hence, to develop a better fundamental understanding we investigated the contribution of EDRF, EDHF and α-2 receptor mediated activity in salt induced hypertension.

5.4.1 Effect of α-2 adreno receptors on vascular responses in SS hypertension:

The α-2 adreno receptors are shown to initiate nitric oxide mediated vascular relaxation in rats [255]. Such relaxations were initiated by binding of different agonist to cell membrane receptors. These responses were observed to be independent of EDHF mechanism, primarily mediated via G proteins and EDRF action [256]. Altered α-2 adreno receptor expression is reported with salt loading in salt sensitive hypertension. Studies have demonstrated both upregulation and downregulation of α-2 adreno receptor expression [257; 258; 259; 260]. In SHR model dose dependent relaxation was observed to α-2 adreno receptor agonist, UK14304, in normotensive wistarkyoto rats (WKY) which was significantly compromised in SHR rats.

We tested the role of α-2 adreno receptors with a selective and potent agonist, UK14304 in salt sensitive dahl rats. We observed that UK14304 only partially relaxed the arterioles in LS fed dahl rats. These relaxation were significantly compromised in HS Dahl rats. This suggested that α-2 receptor mediated pathways are significantly compromised downstream of α-2 adreno receptor in salt induced hypertension.

5.4.2 Effect of exogenous NO on vascular responses in SS hypertension

Exogenous NO delivery has shown to alleviate hypertension in multiple rat models [261]. Though wide uncertainty surrounds the precise mechanism of action, the potency of its action is widely accepted. Various precursors of NO such as L-arginine when supplemented or fed as treatment have produced antihypertensive effects [230; 262]. Previously studies have reported significant improvement in relaxation responses to NO donating agents in hypertension [73; 263]. We tested the potency of NO donor (Sper-NO) in causing an effect in salt loaded Dahl rats. We observed that Sper-NO fully reversed the

hypertensive effects. Though ambiguity surrounds the mechanism or its action, it is possible that under compromised NO machinery, Sper-NO or NO might initiate responses by triggering EDHF -like mechanisms [253; 264; 265; 266]. Sper-NO has shown to reduce chloride absorption and improve salt sensitivity in thick ascending limb from HS rats [267]. We observed in our experiment that Sper-NO fully recovered the relaxation in HS fed Dahl rats. In another salt induced hypertension study, similar observations were reported with NO donor sodium nitroprusside[117]. Our observation can provide significant insights in designing medications to reverse hypertension.

5.4.3 Effect of extracellular Ca^{2+} influx with calcimycin on vascular responses in SS hypertension

Calcimycin, a calcium-mobilizing agent has been reported to cause endothelium dependent dilation in the rat mesenteric arteries [268]. EDRF was shown to be a candidate in mediating these relaxation responses [269]. The concentration dependent relaxation curve of calcimycin is shown to shift to the right following inhibition with NOS blocker, NG-nitro-L-arginine [270]. NO has as well been measured directly in-situ in rat mesentery after maximal stimulation with the calcium ionophore ($10\mu M$) [271]. In addition, these relaxations were suggested to be via NO independent mechanism with increases in extracellular potassium concentration reflecting EDHF action [272; 273].

Extracellular Ca^{2+} influx is a major determining factor in endothelium dependent vascular relaxation. It stimulates the release of both EDRF and EDHF mediated relaxation machinery. Contradictory reports have been presented with actions of calcimycin in hypertension. In SHR model calcimycin responses are observed to be partially compromised and suggested to be a result of decreased NO availability due

88

scavenging of NO rather than reduced NO bioavailability [271]. Decreased constitutive endothelial NOS activity is also reported in an extracellular Ca^{2+} dependent manner [274]. The effect of calcimycin was different in various models of hypertension. The relaxation to calcimycin was impaired in angiotensin II induced hypertension but was unaltered in NE induced hypertension [275]. In DOCA-salt hypertension the endothelium dependent dilations to calcimycin were very minimally altered and were reported to be not significant [276]. Other study in the same rat model has shown partial inhibition of vascular response which was improved after treatment with medication [277].

We tested the effect of Ca^{2+} induced dilations in salt fed Dahl mesenteric arterioles. The full relaxation observed to calcimycin in both the groups may be a result of Ca^{2+} mediated compensatory mechanisms between EDHF and EDRF.

5.4.4 Contribution of EDRF and EDHF in salt sensitive hypertension

Ach has widely been reported to induce relaxation by endogenous NO release and EDHF activity [121]. Ca^{2+} activated K^+ channels (K_{Ca}) in particular the small and intermediate K_{Ca} (SK_{Ca} and IK_{Ca}) channels are identified as key players in EDHF mediated relaxations of rat resistance arteries [278]. Reduced expression of IK_{Ca} and SK_{Ca} are reported in resistance arteries of angiotensin II induced [279] and high salt fed hypertensive rats [280] . Compromised EDHF mediated relaxation to Ach in rat mesenteric arteries from angiotensin II treated rats [281], SHR [282] in comparison to control rats are reported. In HS fed Dahl rats partial impairment of relaxation to Ach was observed in mesenteric arteries [283], renal arteries [178] and aortic rings [284; 285]. Studies have as well reported no difference in relaxation to Ach in mesenteric arteries between low salt and high salt fed Sprague Dwaley [286] and Dahl rats [264]. Goto et.al

[264] showed that after EDRF inhibition, the relative contribution of EDHF to relaxation was significantly greater in HS dahl rats than in LS dahl rats. They suggested these EDHF like relaxations were contributed by large conductance calcium dependent potassium (BK_{Ca}) channels in HS dahl rats but not in LS dahl rats. In their experiments, Ach induced (endothelium dependent) relaxations and sodium nitroprusside or levcromakalim induced (endothelium independent) relaxations showed no difference in the two groups. They concluded that the upregulationof EDHF by increased BK_{Ca} activity appeared to compensate for the loss of NO in mesenteric arteries of LS Dahl rats. The ambiguity in the available literature has made it difficult to devise a precise conclusion and has encouraged us to design our experiments.

In our study, we observed that Ach fully relaxed the mesenteric arterioles in the LS rats. These relaxations were significantly compromised by 24% in HS rats. In addition, in the LS group, after L-NAME blockade the relaxations were compromised to 61%, suggesting a contribution of 39% of the relaxation to NO component and rest to EDHF mediated relaxation. On the other hand, in the HS group, after L-NAME blockade the relaxation were compromised to 48%. This implies 52% of the relaxation was dependent on NO component in hypertension.

In addition, we observed extracellular Ca^{2+} influx, and exogenous NO to reverse hypertension completely. Our previous RT-PCR data has clearly showed compromised eNOS expression in hypertensive Dahl rats. We observed α-2 receptor mediated agmatine relaxation were ~50% dependent on NO pathway. These relaxation were inhibited in hypertensive dahl rats, which resonates with the observed data from UK14304, a potent α-2 receptor agonist.

Our observations thus lead us to a conclusion that might suggest improved activity of NO -like parallel mechanisms that might try to mimic NO under hypertension. Another possibility is NO itself demonstrating hypersensitivity in hypertension. The presence of compensatory pathways and the effects of agonists and NO independent relaxation mechanisms may possibly mask the effect of NO contribution completely in hypertension. The coexistence of NO along with EDHF-like substances and endothelium independent relaxation mechanisms would confer compensatory flexibility under pathophysiological abnormality such as salt sensitive hypertension. These findings have intriguing implications with regards to the bioactivity of NO which is linked to salt sensitivity as a marker of increased cardiovascular risk.

Summary

In our study, we performed in-vitro experiments on isolated rat mesenteric arterioles to facilitate better understanding of NO activity in physiological and pathophysiological condition such as salt sensitive hypertension.

We showed that the frequency-dependent release of NO from the endothelium carried encoded information which could be translated into vascular tone. This frequency-dependent activity of NO resulted from the intracellular Ca^{2+} frequency dependence of the endothelium. This observation might have significant implications towards delivery of NO as a therapeutic target to alleviate hypertension. Incorporating the frequency aspect of NO release might improve the efficacy of NO activity in NO aided drugs. Further studies should explore the contribution of frequency of NO release in a diseased model. This study which was carried out with endogenous NO release can be extended to a direct administration of frequency-dependent delivery of NO.

Agmatine as a ligand was observed to relax the mesenteric arterioles. These relaxation were NO dependent and occurred via α-2 receptor activity. The observed potency of agmatine, a metabolite of L-arginine was 40 fold higher than L-arginine itself. This suggested us to propose a parallel pathway for L-arginine induced relaxation. Our initial finding with salt sensitive hypertensive model showed suppressed L-arginine and agmatine activity. We observed an improvement in the blood pressure for agmatine treated rats. The observed p values vs. high salt fed rats were

P value (low salt, high salt) = 0.0304

P value high salt, high salt + 2mg/ml agmatine) = 0.4232

Further investigation is required towards establishing agmatine as a potential anti-hypertensive agent. In addition, with vascular reactivity study, we identified contribution of EDRF, EDHF and receptor mediated activity in salt sensitive hypertension.

The vascular properties were identified to be altered in salt sensitive hypertension. We developed finite element models that described the biomechanics of rat mesentery. With inverse estimation approach we estimated the parameter values that described the differences in normotensive and hypertensive Dahl rats. Future work should look into integration of subcellular model with the experimental data to describe disease specific changes at microvascular level. The integration of subcellular data into computational model can allow the analysis of complex microcirculatory function in health and disease, hypothesis testing and as a guide for new experimentation.

Despite significant efforts and prior work in this area there is an incomplete understanding and limited quantitative information of the control mechanisms and effects of NO mediated pathway in regulating vascular tone. In this study, we contributed to elucidate the significance of NO related mechanisms involved in hypertension by designing in-vitro experiments assisted with mathematical models. Our efforts were towards guiding current efforts that optimize cardiovascular intervention and to assist development of new therapeutic strategies. This work shall prove to be beneficial in assisting efficient delivery of NO in the vasculature and minimize the risk while handling cardiovascular abnormality such as hypertension.

***

APPENDICES

Appendix A1: Vascular Reactivity Protocol

1.0   Purpose

This procedure describes the process to dissect, isolate, cannulate and verify the viability

of the isolated mesenteric artery. This procedure also verifies if the endothelial cells and

smooth muscle cells are intact.

2.0   Materials and Equipment

1. Cannulation chamber, Living Systems Instrumentation, VT, USA (Model CH1/SH)

2. Peristaltic pump (Model FC (Living Systems Instrumentation, VT, USA)

3. Pressure transducer (Model PT/F, Living Systems Instrumentation, VT)

4. Silicon tubings (Cole Parmer, IL)

5. Borosilicate glass cannulas (Model GC-12, Living Systems Instrumentation, VT)

6. Temperature controller (Model TC-01, Living Systems Instrumentation, VT, USA)

7. Perfusion pencil (8channel/16 channel, Autom8 Scinetific)

8. Dissecting microscope (Nikon, Model SMZ645, USA).

9. Motorized Inverted Research Microscope IX-81, USA

3.0   Reagents

NaCl, KCl, $CaCl_2$, $MgSO_4$, KH_2PO_4, HEPES, Glucose, Ach, NE, DI water, NaOH, Ethyl

alcohol.

Completed by (Initials/Date) _____ Verified by (Initials/Date) _____

4.0   Technician Signature Log

Print Name	Signature	Initials

5.0 **Procedure**

5.1 Handling the rat

 5.1.1 Obtain the rat from the animal facility on the day of the experiment. Animal care should be taken while transporting the animal. Covered cages accompanied food and water supply and carried in air conditioned vehicles.

 5.1.2 Care must be taken to avoid stress to the animal.

 5.1.3 Cages must be transported back to the animal facility within 24 hours.

5.2 Buffer preparation.

 5.2.1 Modified Krebs Ringer buffer used for the experiment is prepared with following salts composition:

 (inmM): NaCl 145, KCl 5, $CaCl_2$ 2.5, $MgSO_4$ 1.2, KH_2PO_4 1.2, HEPES 20, and Glucose 10.1.

 5.2.2 The buffer is titrated to pH of 7.4 with 1M NaOH.

 5.2.3 The buffer is maintained ice cold prior to the experiment.

5.3 Setting up the cannulation chamber, Living Systems Instrumentation, VT, USA (Model CH1/SH).

 5.3.1 The cannulation chabmer is thoroughly rinsed and cleaned with DI and 80% ethyl alcohol.

5.3.2   The vessel chamber allows three dimensional movements of cannulas. The taper tip glass cannulas are aligned in the chamber arms using screw and roller assembly on the cannulation chamber.

5.3.3   The chamber was connected with silicon tubings (Cole Parmer, IL) and and used borosilicate glass cannulas (Model GC-12, Living Systems Instrumentation, VT) with an internal tip diameter of 100-200 microns. The smooth beveled tip cannulas allow easy cannulation of the microvessel resulting in minimal damage to the endotheium. The smooth beveled tip cannulas allow easy cannulation of the microvessel resulting in minimal damage to the endotheium.   Two sutures are placed on each canula for tying the vessel on firm on the cannula.

5.3.4   Control solution is run through the tubings to confirm absence of air bubbles in the tubing lines.

5.3.5   Pressure transducer (Model PT/F, Living Systems Instrumentation, VT) is connected to the assembly along with the servo controller (Model PM/4, Living Systems Instrumentation, VT (pressure range: 0-200 mmHg)).

5.3.6   The pressure is maintained at 50 mmHg in closed position. Care is taken to assure lack of pressure drop. The entire assembly is maintained air tight.

5.3.7   Temperature controller (Model TC-01, Living Systems Instrumentation, VT, USA) is connected to assure 37C.

5.3.8   A peristaltic pump (Model FC (Living Systems Instrumentation, VT, USA) is used to maintain circulating fluids in the superfusion.

5.3.9   Driver pressure assembly is regulated with inlet air pressure. The driving pressure is adjusted using the pressure knob to maintain pressure drop of 50mmHg.

5.3.10 Solenoid valve assembly triggered automatically from the IPLAB or through manual valve switching allows instantaneous exchange of solutions.

5.3.11 The perfusion pencil (8channel/16 channel, Autom8 Scinetific) connected in the assembly allows instant switching of solution. The perfusion pencil is pierced in the assembly tubing. Care is taken to prevent air leakage.

5.4   Dissection of rat

5.4.1   Rats are euthanized in the CO_2 chamber by allowing CO_2 exposure for 3-5 minutes.

5.4.2   Rat is pinched in the leg with a forcep to ensure death.

5.4.3   Rat is placed on the dissection station, cleaned of abdominal hair and incision is made in the abdomen.

5.4.4   Mesenteric arcade is isolated from the rat abdomen and placed in ice cold buffer solution.

5.4.5   A ring of mesenteric arcade is separated in the pertidish with ice cold control.

5.4.6   The mesenteric arcade is placed firm with needles.

5.4.7   Mesenteric arterioles are identified for fat isolation.

5.5   Fat isolation

5.5.1   Extensive care is taken while isolating the fat from the arterioles.

5.5.2   Fat is 'cut' using a scissors and forcep under dissecting microscope (Model SMZ645).

5.5.3   'Cut' is very important word no 'pulling' or 'grabbing' of fat cells. Fat is 'cut' in the direction away from the arteriole and the vein without touching them.

5.5.4   After cleaning the fat, distinction is made between artery and a vein. The thicker vessel wall, normally with less blood is the artery. Vein the the inflated, more blood filled, thin vessel walled.

5.5.5   After identifying the distinction between the artery and the vein, the artery is kept for the experiment and vein is discarded.

5.6   Vessel Cannulation

5.6.1   The buffer in the cannulation chamber and the petri dish is replaced with cold buffer solution.

5.6.2   The cold solution prevents the artery from experiencing shock before while being cut.

5.6.3   The arteriole is cut in the pertidish and carefully lifted and placed in the cannulation chamber buffer.

5.6.4   The both ends of the arterioles are opened and cannulation is carried out one end at a time.

5.6.5   The pressure is lowered to 10 mmHg and blood is allowed to come out of the one end cannulated vessel.

5.6.6   The second end is cannulated and both ends are tied with sutures.

5.6.7   The vessel is stretched to avoid collapse. Extensive care is taken in the procedure to not touch the vessel except for the edge of the vessel.

5.6.8   After cannulation, the pressure is raised to 50mmHg and is allowed to equilibrate for 1 hr.

5.6.9   The vessel is tested for integrity as described below and vascular reactivity study is carried out

5.6.10 Images are acquired with an inverted microscope (Motorized Inverted Research Microscope IX-81, USA) acquisition protocol and IPLAB software.

5.6.11 Post analysis is carried out with IPLAB and MATLAB scripting.

5.7 NE agonist solution for constriction.

5.7.1 Superfuse cannulation chamber with NE (2μM) agonist solution for 5 minutes with a flow rate of 5 mL/min.

5.7.2 Image vessel with IP Lab software.

5.7.3 Open program.

5.7.4 Log in, adjust setting so that they read: Olympus lamp: on, Shutter: on, Camera: Bright field.

5.7.5 Set time to 5 minutes (300 sec.) with one image every 5 seconds.

5.7.6 Compare diameters of vessel from beginning to end of image capturing. Vessel should constrict by approximately 80%.

5.8 Ach solution for dilation

5.8.1 Perfuse vessel with 10 mM Ach for 5 minutes.

5.8.2 Image with IP Lab software.

5.8.3 Compare diameters of the vessel from beginning to end of image captureing. Vessel should dilate 90% in diameter.

Completed by (Initials/Date) _____ Verified by (Initials/Date) _____

Appendix A2: FURA-2AM Loading Protocol

1.0   Purpose

This procedure describes the process to load endothelial cells of the intact rat mesenteric arterioles with FURA 2-AM.

2.0   Materials and Equipment

1. Cannulation chamber, Living Systems Instrumentation, VT, USA (Model CH1/SH)

2. Peristaltic pump (Model FC (Living Systems Instrumentation, VT, USA)

3. Pressure transducer (Model PT/F, Living Systems Instrumentation, VT)

4. Silicon tubings (Cole Parmer, IL)

5. Borosilicate glass cannulas (Model GC-12, Living Systems Instrumentation, VT)

6. Temperature controller (Model TC-01, Living Systems Instrumentation, VT, USA)

7. Perfusion pencil (8channel/16 channel, Autom8 Scientific)

8. Dissecting microscope (Nikon, Model SMZ645, USA).

9. Motorized Inverted Research Microscope IX-81, USA

3.0   Reagents

Fura 2-AM, Pluronic Acid, anhydrous DMSO, Ach, 4Br-A23187, NaCl, KCl, $CaCl_2$, $MgSO_4$, KH_2PO_4, HEPES, Glucose, NE, DI water, NaOH, Ethyl alcohol.

Completed by (Initials/Date) _____ Verified by (Initials/Date) _____

4.0   Technician Signature Log

Print Name	Signature	Initials

5.0   Procedure

5.1   Preparation of FURA 2-AM

    5.1.1   All procedures involving dyes were conducted in dark to prevent dye autofluorescence.

    5.1.2   Fura 2-AM vial was allowed to reach room temperature before opening the vial.

    5.1.3   50 µL of cell grade anhydrous Dimethyl sulphoxide DMSO at a concentration of 1 mM.was mixed with 10% solution of Pluronic F127 in DMSO. (DMSO) was added to each vial containing 50 µg of fura 2-AM dye.

    5.1.4   Electric mixer was used to dissolve the dye in DMSO.

    5.1.5   The dyes were diluted to 10ml in control solution at room temperature to yield a dye concentration of 5 µM for Fura 2-AM and 0.05% Pluronic acid.

5.2   Loading FURA 2-AM (Endothelial cell loading)

    5.2.1   Solenoid valve operated perfusion system facilitated selective endothelial loading after delivery of Fura 2-AM into the lumen for 5 min at 37°C.

    5.2.2   This was followed by a 20 min washout with buffer solution to remove residual Fura 2-AM from the lumen.

    5.2.3   The chamber placed on the stage of a fluorescent microscope and cell loading was verified visually. After washout endothelial loading was visible on the luminal side of the artery in the focal plane.

5.2.4 Extra care is taken to prevent the movement of the vessel. This included smaller vessel for experiment and vessel placed very near to the cover slip. Such precautions greatly enhanced acquisition efficiency.

5.2.5 The changes in intracellular Ca^{2+} is observed by calculating the ratio of the light emitted through a 510 nm emission filter when the vessel was illuminated at 340 and 380 nm respectively.

5.3 Loading FURA 2-AM (Smooth Muscle cell loading)

5.3.1 Smooth Muscle loading can be achieved by following identical protocol by delivery of Fura 2-AM into the lumen for 20-30 min at $37^{o}C$.

5.4 Fluorescent Imaging

5.4.1 The arteriole was observed under UV light at 10X magnification.

5.4.2 The data was collected at 200 millisecond exposure time with 2x2 binning for excitation of Fura 2 loaded cells at both 340 and 380 nm.

5.4.3 Exposure time was varied depending upon the extent of dye loading but the proportions of individual exposure times were maintained. Preliminary studies examined the effect of changing the exposure time. Important imaging criterions like binning, camera gain, filter switch speed, and shutter wait time were determined empirically and maintained during all experiments. The parameters ensure optimum range of data collection, minimum vessel damage due to exposure, prevention of dye oversaturation and minimization of motion artifacts resulting from drift in focus.

Appendix A3: Microscopy

Nikon dissection microscope (Model SMZ645) was employed for microdissection i.e. removal of fat from the mesenteric microvessel and identifying artery from vein. The same microscope was also employed for adjusting the two cannulas at the same level, cannulating the microarteries and suturing the microarteries to the glass cannulas. Olympus fluorescent microscope (Motorized Inverted Research Microscope IX-81, USA) was used in bright field mode. The microscope components critical for bright field experiments were:

Olympus shutter, Olympus lamp and Camera

Olympus shutter was used to control exposure time of the light from Olympus lamp (IX-2 UCB) onto the vessel. The exposure time was set so that the vessel can be seen clearly on the screen and hence the diameter measurements can be performed using the IPLab4.0 software.The Olympus lamp (IX-2 UCB) was used to provide visible light to the vessel. The intensity of the light was controlled manually from the microscope or from the software IPLab4.0. Cooled mono 12 bit Retiga Q imaging camera (Model EXi)is employed for image acquisition. The camera was operated at a gain of 1557 and an offset of 2048. The gain and offset for the camera were maintained to acquire consistent and comparable results.

Objective

Objective with magnification of 4X bright field and 10X in fluorescent observation was used to record images for this study. The objectives have to be focused

to get a clear picture of the vessel. The focusing is done manually using the microscope.

The various specifications of the used objective are

Magnification	Numerical Aperture	Working distance (mm)	Depth of field
4X	0.16	8.2	55.5

Table 1: Important objective (4X) characteristics

IPLab 4 for Windows

Software IPLab 4.0 Windows version (Scanalytics, VA, USA) was used to control the microscope and the associated hardware. IPLab 4.0 allows control of shutter, filter wheel, camera and objectives. The diameter measurements were recorded with the help of the software manually as well as with the script for measuring diameter in bright field mode.

Appendix A5: Dahl Salt Sensitive Hypertension Protocol

1. Animal model

In 1962 Lewis Dahl developed the Dahl Salt-Sensitive (S) and Salt-Resistant (R) rat strains from Sprague Dawley rats which were bred on the basis of their blood pressures after being fed a high salt (8% NaCl) diet[2,3]. These strains developed by Dr. Dahl were designated as the Dahl Salt- Sensitive (S) and Salt-Resistant (R) Brookhaven outbred strain. The inbred strain of Dahl Salt Sensitive and Dahl Resistant rats were developed in 1985 by John Rapp from these Brookhaven rats[5]. They are designated as Dahl/SS/Jr. The Dahl salt sensitive rat is a rodent model of hypertension that exhibits many phenotypic traits common with hypertensive disease observed in human populations. Similarities include sodium sensitivity of hypertension, reduced renal function, elevated urinary excretion of protein and albumin, and a low plasma renin activity. Tubulointerstitial injury and the loss of Nitric Oxide Synthase (NOS) occur after birth and parallel the development of hypertension. It is suggested that the structural and functional changes that occur with renal injury in the Dahl/SS rat may contribute to the development of hypertension.

It has been demonstrated that the development of hypertension is accentuated in genetic models of hypertension depending on the diet being fed and it has been recommended that a AIN-76A diet with 4-8% salt works well in producing hypertension and kidney disease in a timely manner in the Dahl/SS rat. Additionally Mattson, *et al,* have shown that the source of protein, carbohydrate, fat, and/or other dietary components can have a

significant impact on the disease produced in experimental models of hypertension and renal disease.

The Dahl/SS rat has a low renin salt sensitive form of hypertension. It is associated with declining renal function.

2. Ordering the Animals and Diet:

ANIMALS:

The following vendor can be contacted for ordering the Dahl sensitive and the Dahl salt resistant rats:

Vendor 1: Harlan Teklad

http://www.harlan.com/contact_us/contact_us__North_America.hl

Call: 800-793-7287

3 – 4 weeks old SS/JrHsd rats

Price: $ 64.90 each

Shipping handling: $42.00

Vendor 2: Charles River

http://www.criver.com/en-US/Pages/home.aspx

Call to order: Charles River # 1-800-522-7287

Pricing as of 1st Dec 09

Salt Sensitive: $63.20 for one piece

Salt Resistant (SS-13BN) control rat: $63.20 for one piece

Housing: $13.30

Shipping: $27.15

DIET:

Vendor 1: Harlan Teklad

http://www.harlan.com/contact_us/contact_us__North_America.hl

Call: 800-483-5523

Formula

TD.90228	SodiumDeficientDiet
TD.96208	0.49%NaClDiet
TD.90229	1%NaClDiet
TD.92034	4%NaClDiet
TD.92012	8% NaCl Diet

Vendor 2: Research Diets

The following vendors can be contacted for ordering the diet

www.ResearchDiets.com

Call to order: Research Diet # 732-247-2390

D10001 (AIN-76A): price $ 362.5 (50 Ibs)

D05011703: Modified AIN-76A diet containing 4% added sodium chloride

1. American Institute of Nutrition. AIN report of the AIN ad hoc committee on standards for nutritional studies.J.Nutr. 107:1340-1348, 1977.

2. American Institute of Nutrition. AIN second report of the AIN ad hoc committee on standards for nutritional studies. J. Nutr. 110:1726, 1980.

3. Housing and Feeding Requirement for Rats

- In addition to the regular 5 Male Sprague Dwaley rats that we normally order, we require additional space for 8 Dahl salt sensitive rats.

- The rats are allowed initial acclimatization period for the to get adjusted to the new environment, these rats are maintained on diet standard diet.

- After an initial acclimatization for the rats to get adjusted to the new environment, At age of 42 days old, We separate the rats in two groups, the control rats are required to be fed the low salt TD.96208(0.5% NaCl) diet and the other 2 dahl salt sensitive, SS/JrHsd to be fed the TD.92034 (4% NaCl, High Salt) diet for 5 weeks. It should take 4-6 weeks for these rats to develop hypertension.

- We have to monitor the blood pressure during these 6 weeks (Ideally 1-2 times a week). The CODA system as described later shall be used to monitor the blood pressure. We are required to have a space for the measurement of blood pressure of the animals at the animal facility. A student from our lab shall be responsible for taking the blood pressure measurements.

- Starting from the beginning of week 6: we shall do one experiment per week sacrificing two rats at a time.

- At week 6: we thus sacrifice 2 high salt diet rats

- At the beginning of Week 5, we shall repeat the order cycle of 8 animals in two stages over four week period once again. Thus every two weeks henceforth we shall be ordering 4 animals and sacrificing 4 animals.

- Hence at the animal care facility, we require space for a maximum of 8 male Dahl salt sensitive SS/JrHsd rats in addition to the regular 5 outbread male Sprague Dwaley rats that we order at present. Thus we require a housing space for a maximum of 13 animals. In addition to this we as well require some space for the blood pressure system to record the blood pressure from these animals.

4. Monitoring the blood pressure Tail Cuff method:

Non-Invasive Blood Pressure Measurement:

The non-invasive blood pressure methodology consists of utilizing a tail-cuff placed on the tail to occlude the blood flow. Upon deflation, one of several types of non-invasive blood pressure sensors, placed distal to the occlusion cuff, can be utilized to monitor the blood pressure. There are three types of non-invasive blood pressure sensor technologies: photoplethysmography, piezoplethysmography and Volume Pressure Recording. Each method will utilize an occlusion tail-cuff as part of the procedure.

Volume Pressure Recording (VPR):

The Volume Pressure Recording sensor utilizes a specially designed differential pressure transducer to non-invasively measure the blood volume in the tail. Volume Pressure Recording will actually measure six blood pressure parameters simultaneously: systolic blood pressure, diastolic blood pressure, mean blood pressure, heart pulse rate, tail blood volume and tail blood flow.

Since Volume Pressure Recording utilizes a volumetric method to measure the blood flow and blood volume in the tail, there are no measurement artifacts related to ambient light; movement artifact is also greatly reduced. In addition, Volume Pressure Recording is not dependent on the animal's skin pigmentation. Dark-skinned animals have no negative effect on Volume Pressure Recording measurements. Very small, 10-gram C57/BL6 black mice are easily measured by the Volume Pressure Recording method.

Special attention is afforded to the length of the occlusion cuff with Volume Pressure Recording in order to derive the most accurate blood pressure readings.

Volume Pressure Recording is the most reliable, consistent and accurate method to non-invasively measure the blood pressure in mice as small as 10 grams to rats greater than 950 grams.

Rodent Holders

- The ideal animal holder should comfortably restrain the animal, create a low-stress environment and allow the researcher to constantly observe the animal's behavior.

- A trained rat or mouse should comfortably and quietly remain in the holder for several hours.

- It is very beneficial to incorporate a darkened nose cone into the rodent holder to limit the animal's view and reduce the level of animal stress. The animal's nose will protrude through the front of the nose cone allowing for comfortable breathing.

- The tail of the animal should be fully extended and exit through the rear hatch opening of the holder.

- The proper size animal holder is essential for proper blood pressure measurements. If the holder is too small for the animal, the limited lateral space will not allow the animal to breathe in a relaxed fashion. The animal will compensate by elongating its body, thereby creating a breathing artifact. A breathing artifact will cause excessive tail motion and undesirable blood pressure readings.

Animal Body Temperature

- A non-invasive blood pressure system should be designed to comfortably warm the animal, reduce the animal's stress and enhance blood flow to the tail.

- The rodent's core body temperature is very important for accurate and consistent blood pressure measurements. The animal must have adequate blood flow in the tail to acquire

a blood pressure signal. Thermo-regulation is the method by which the animal reduces its core body temperature, dissipates heat through its tail and generates tail blood flow.

- Anesthetized animals may have a lower body temperature than awake animals so additional care must be administered to maintain the animal's proper core body temperature. An infrared warming blanket or a re-circulating water pump with a warm water blanket is the preferred method to maintain the animal's proper core body temperature. The animal should be warm and comfortable but never hot. Extreme care must be exercised to never overheat the animal.

- Warming devices such as hot air heating chambers, heat lamps or heating platforms that apply direct heat to the animal's feet are not advisable to maintain the animal's core body temperature. These heating devices will overheat the animal and increase the animal's respiratory rate, thereby increasing the animal's stress level. These conditions will elicit poor thermo-regulatory responses and create inconsistent and inaccurate blood pressure readings.

- The animal body temperature is generally maintained at 32-35C

Environmental Temperature

- The proper room temperature is essential for accurate blood pressure measurements. The room temperature should be at or above 26°C. If the room temperature is too cool, such as below 22°C, the animal may not thermo-regulate, tail blood flow will be reduced and it may be difficult to obtain blood pressure signals. A cold steel table or a nearby air conditioning duct is undesirable during animal testing.

Animal Preparation for blood pressure measurement:

The animal should be placed in the holder at least 10 to 15 minutes prior to obtaining pressure measurements. Acclimated animals will provide faster BP measurements than non-acclimated animals. Proper animal handling is critical to consistent and accurate blood pressure measurements. A nervous, stressed animal may have diminished circulation in the tail.

Most rodents will quickly adapt to new conditions and feel comfortable in small, dark and confined spaces. Training is not necessary to obtain accurate blood pressure readings; however, some researchers prefer training sessions. Rodents can easily be trained in approximately three days, 15-minutes each day before beginning your experiment.

The animal should be allowed to enter the holder freely. After the animal is in the holder, adjust the nose cone so the animal is comfortable but not able to move excessively. The animal should never have its head bent sideways or its body compressed against the back hatch. The animal's temperature should be monitored throughout the experiment.

Measuring blood pressure using Volume-Pressure Recording (tail cuff method):

CODA non invasive blood pressure system enables the blood pressure measurements in rodents with the volume sensor recording that measure the tail volume blood changes when placed over the animal's tail.

1. Set up system:

- Use locations where the temperature is 20C or above avoid the locations near vibrations, freezers or air conditioning vents. Exposing the animals to loud noise or odors may stress the animals.

- Turn on the CODA Controller and then the warming platform to level 3. If the room temperature is above 25C start at level 1 or 2.

- Perform the controller diagnostics test,

- First open the CODA software, Select the CODA device by clicking on it.

- Click on Test Selected Device

- Select the cuffs and channels to test and click test

- After the controller diagnostic is complete close the diagnostic test window

- Select the CODA controller to use then click use these devices

- To setup the software Select Tools→Manage Personnel

- Next click on Researcher1 to Change the name to say Tushar

- Click on subsequent rows to add additional researchers

- Then click Save Data

- Click on the specimens tab to name the animal for easy identification or animal type and click Save

- Finally click on animal tab to select the animal type and sensitivity save data close.

- To begin a new experiment Select File→New→Experiment

- Give the experiment name, select the key researcher and select the begin date and click next

- The next step is to enter the basic session information. Start by entering the session name.

- Set acclimation cycles to 5 if you prefer not to include acclimation cycles set it to 0.

- Set the number of sets to 1, Time between sets to 30 secs for multiple sets, cycles per set to 20 cycles, and time between cycles to 5 secs then click next

- To begin specimen selection select specimen from the specimen pool and assign it to the first available channel and click next

- To set session parameters, set the maximum occlusion pressure to 250 mmHg, deflation time to 20 sec per rat, minimum volume to 15 μlitres, select the display style to one channel per graph. Click next

- Review the session script and click next DO NOT CLICK FINISH until you finish the animal preparation section which is described next.

2. Prepare the animals

- Before placing the animals in the holders, make sure that the size of the animal is such that it will be freely be able to enter the holder.

- Place each animal in the holder by picking it up by the tail and gently placing it in the rear of the holder which faces the open end of the nose cone. Carefully secure the rear hatch to the holder by turning the screw on the rear hatch. Be careful not to pinch the tail or other body parts while securing the hatch.

- Slide the nose cone to the hatch limiting the movement of the animal. The nose cone should be in a position to limit the animal from turning around while in the holder.

- Place the holder on the warming platform in the designated position. Allow the animal atleast 5 min to acclimatize to the holder.

- DO NOT TOUCH the animals while inside the holder. The increase contact could irritate the animal. NEVER leave the animal in the holder unattended.

- To properly place the occlusion tail cuff, thread the tail through the occlusion cuff and place the tail-cuff as close to the base of the tail as possible without force. After that thread the tail through the BPR sensor cuff; placing it within 2 mm of the occlusion cuff.

Secure the tubing and the occlusion cuff to the top rear of the holder. The occlusion tail cuff is inflated to impede the blood flow to the tail. The occlusion cuff is slowly deflated and the VPR tail cuff incorporating the specially designed sensor measures the physiological characteristics of the returning blood flow. As the blood returns to the tail the VPR sensor cuff measures the tail swelling as a result of the arterial pulsation from the blood flow.

- Systolic BP is automatically measured at the first appearance of the tail swelling, Diastolic BP is calculated when the increasing rate of swelling seizes in the tail.

- After all the animals are placed in the holders and their tails have been cuffed allow atleast 5 mins for the animals to thermo-regulate. Record the temperature frequently with the infrared thermometer. The animal temperature should be between 32-35C.

3. Data Collection and Processing:

- Now that the animals are ready, we can begin the experiment. Click FINISH to begin the experiment.

- The RED line indicates the deflation of the VPR sensor and the occlusion cuff. BLUE line represents the blood volume changes in the tail. The first deflection of the blue line minimum rate of change identifies the systolic blood pressure. The second inflection of the blue line the maximum rate of change identifies the diastolic blood pressure.

- When the experiment has ended remove the animals immediately from the cuffs and holders.

- A simple session summary report is displayed. The data collected in the experiment is saved as an excel file. There are several ways to process the data in the excel file. A common practice is to obtain the average and the standard deviation. Delete

115

measurements if the standard measurement is greater than 30. Additionally the rejected cycles may be viewed and the entire data can be exported to exel.

- Consult the User manual and the demonstration video on the following for more information:

- http://www.kentscientific.com/

  Use the following text when referencing the CODA system in your research:

  Blood pressure was non-invasively measured by determining the tail blood volume with a volume pressure recording sensor and an occlusion tail-cuff (CODA System, Kent Scientific, Torrington, CT)

Appendix A5: Real Time PCR Protocol

Homogenization

1. Remove RNA later from tube containing tissue (≤30 mg).

2. Add 600 µl of RLT buffer.

3. Homogenize using a sonicator (10 sec x 5 at 9 watts). Always rinse probe with chloroform first.

4. Centrifuge the lysate for 3 min at full speed.

5. Use supernant for RNA isolation.

RNA Isolation Protocol

1. Add 1 volume of 70% ethanol to the homogenized lysate and mix well by pipetting.

2. Transfer about 700 µl of each sample to RNeasy spin column and centrifuge at 10,000 g for 30 sec.

3. Add 700 µl Buffer RW1 to each column and spin at 10,000 g for 20 sec.

- For the next step use a new collecting tube.

4. Add 500 µl Buffer RPE to each column and spin at 10,000 g for 20 sec.

5. Add another 500 µl Buffer RPE to each column and this time spin at max speed for 2 min.

- **Critical step!** Make sure to remove all ethanol collected over the inner rim using a pipette tip, without touching the membrane.

6. Dry spin at max speed for another 5 min. Remove ethanol again.

- Begin setting vacuum centrifuge for Step 10

7. Place the column in a new 1.5 ml collection tube.

8. Add 40 µl RNase-free water at the center of membrane in column and let it sit for 1 min. Spin at max speed for 1 min.

9. Add another 40 µl water and spin again after 1 min incubation.

- Steps 8 and 9 are Elution steps

10. Discard the filter unit, keep tube and spin the tube alone in a vacuum centrifuge at 55 °C for 2 min to eliminate traces of leftover EtOH.

DNA digestion of RNA sample:

1. Mix the following in a microcentrifuge tube:

- 70 µl RNA sample + 10 µl Buffer RDD + 2.5 µl DNase I stock + 17.5 µl RNase free water = 100 µl.

2. Spin briefly and let sit at RT for 12 min.

3. Add 350 µl of RLT buffer

4. Add 450 µl of 70% ethanol to the above

Repeat RNA Isolation protocol to purify RNA.

Then take spectrophotometer readings for mRNA concentration.

1. Test for RNA/DNA quality:

- In control use 150 µl RNase-free water

- 3 µl sample + 147 µl H2O for sample reading

2. This reading should be 1.8-2.0 for a fairly pure RNA sample.

<u>First Strand cDNA synthesis by Superscript III RT</u>

1. Up to 5 µg of RNA in 0.5 ml PCR tubes with 3 simultaneous reactions

RNA   up to 5 µg

Random Hexamers   3 µl

dNTP	3μl
H2O	for a total of 13 μl

2. Incubate at 65˚C for 5 minutes.

3. Place on ice for 1 minute and spin briefly to collect sample.

4. In a 0.5 mL tubemix well the following:

10 x RT Buffer	6 μl
MgCl	12 μl
DTT	6 μl
RNaseOUT	3 μl
SuperScript IIIRT	3 μl
Total	**30 μl**

5. Add RNA mix   30 μl

6. Mix gently and collect by brief spin.

7. Transfer Tubes to thermocycler with settings:

    25°C, 10 minutes

    50°C, 50 minutes

    85°C, 5 minutes

8. Take tubes out and chill on ice.

9. Collect the reactions by a brief spin

10. Add 3 μl RNase H to each tube and incubate for 20 minutes AT 37°C in thermocycler.

cDNA Purification

1. Take 1 volume of cDNA sample and add 5 volumes of buffer PB

2. Pass through a column 750 μl each time. Spin at more than 10 000 rpm for 30 seconds

3. Wash with 750 µl of PE. Spin at less than 10 000 rpm for 30 seconds

4. Pipette out liquid from within the column

5. Dry spin for 10 minutes at 13.3 K and room temperature

6. Transfer column to a 1.5 ml micro fuge tube

7. Add 30 µl of RNase free water, let it sit for 1 min, then spin at 13.3 K for 1 minute at room temperature.

8. Repeat step 7 two more times.

9. Place sample on ice while taking the spectrophotometer readings.

RT-PCR Protocol

Materials Required

✓ Milli-Q water autoclaved

✓ Primers (Forward and Reverse)

✓ Master Mix

✓ cDNA

✓ 1.5 ml Eppendorf tubes

✓ 0.5 ml Eppendorf tubes

✓ RT-PCR tubes

Procedure

1. Spin primers in centrifuge for 30 seconds before diluting them.

a. Note: Use Milli-Q water autoclaved to dilute the primers

2. Add the necessary amount of water to each primer to obtain the necessary 100 µmol concentration.

3. Vortex them until mixed thoroughly

4. Add 12.5 µl of each primer and add 237.5 µl of milli-Q water (to prepare a **5 µmol working stock**)

5. General ratio for the preparation

Components	Ratio for 1x reaction (µl)
2x MM	10
cDNA	10 ng
Forward Primer (FP)	1
Reverse Primer (RP)	1
H$_2$O	Add for a total of 20
Total	**20**

6. Due to the specifications of the RT-PCR machine, 60 µl of the above mixture are needed to run each test consisting in 3 wells. It is advisable not to prepare exactly 60 µl just in case the pipettes are not exact enough. 70 µl are usually prepared to overcome this problem.

Components	Ratio for 3.5x reaction (µl)
2x MM	35
cDNA	30 ng
Forward Primer (FP)	3.5
Reverse Primer (RP)	3.5
H$_2$O	Add for total of 70
Total	**70**

7. In order to reduce the use of pipettes and thus the measurement error, prepare an initial mixture with the necessary amount of Master Mix, cDNA and water. Vortex mix by hand, then place in centrifuge for 30 seconds.

8. Separate into 3 aliquots and add 3.5 µl of forward primer and reverse primer to each aliquot. The volume in each Eppendorf tube should now be 70 µl.

9. Centrifuge for 30 seconds at less than 700 rpm

10. Add 20 µl aliquots to the PCR tubes

a. Note: **Crucial Step**

 i. When extracting the 20 µl, push solution in out of pipette tip until no bubbles arise from this procedure.

ii. When transferring the 20 µl into the PCR tubes make sure that the pipette is maintained pressed between each transfer to ensure that there is a small or no difference in the volumes of each well.

11. Spin the wells in the centrifuge <2500 rpm for about 2 minutes. Make sure that no residue is left on the walls of the tubes.

12. Run the RT-PCR machine.

Appendix A6: Biomechanics Principles

The arterioles are assumed to be a thin walled hyperelastic cylinder in 2D deformed in circumferential θ and axial z direction.

For a cylindrical vessel under inflation and axial stretching

1. For a cylindrical vessel under inflation and axial stretching, the equilibrium equation is

$$\frac{d\sigma_{rr}}{dr} + \frac{\sigma_{rr} - \sigma_{\theta\theta}}{r} = 0$$

From this equation and the boundary condition that the pressure at the outer surface is zero, the internal pressure is given as

$$p_i = \int_{r_r}^{r_0} \frac{\sigma_{rr} - \sigma_{\theta\theta}}{r} dr,$$

where r_i and r_0 are the inner and outer radius respectively.

2. The Green strain is defined as:

$$E_{\theta\theta} = \frac{1}{2}\left(\lambda_\theta^2 - 1\right),$$

$$E_{zz} = \frac{1}{2}\left(\lambda_z^2 - 1\right)$$

where $\lambda_\theta = D/D_0$ and $\lambda_z = L/L_0$ are the circumferential and axial stretch ratio and D and D_0 are the loaded and zero stress diameter; and L and L_0 are the axial lengths in loaded and no load state.

Assuming uniform density of vessel wall loaded and zero stress state; the First-PiolaKirchoff and Cauchy stress can be written as:

$$T_{\theta\theta} = \lambda_\theta S_{\theta\theta}$$

$$T_{zz} = \lambda_z S_{zz}$$

and

$$\sigma_{\theta\theta} = \lambda_\theta^2 S_{\theta\theta}$$
$$\sigma_{zz} = \lambda_z^2 S_{zz}$$

Where $S_{\theta\theta}$ and S_{zz} are the circumferential and axial second Piola-Kirchoff stresses respectively.

3. The relationship between stress strain

$$S = \frac{\partial W}{\partial E}$$

where

S – the second Piola-Kirchhoff stress tensor

E – Green-Lagrange strain tensor

W – strain energy density function

4. Energy function of soft biological tissues (Fung 1979)

Where the work function is given by

$$W = \frac{1}{2} c \left(e^Q - 1 \right),$$
$$Q = \frac{1}{2} a_{KLMN} E_{KL} E_{MN}.$$

Where

$$Q = c_1 E_{RR}^2 + c_2 E_{\Theta\Theta}^2 + c_3 E_{ZZ}^2 + 2C_4 E_{RR} E_{\Theta\Theta} + 2C_5 E_{ZZ} E_{\Theta\Theta} + 2C_6 E_{RR} E_{ZZ} + c_7 \left(E_{R\Theta}^2 + E_{\Theta R}^2 \right) + c_8 \left(E_{Z\Theta}^2 + E_{\Theta Z}^2 \right)$$
$$+ c_9 \left(E_{ZR}^2 + E_{RZ}^2 \right),$$

c1- c9: parameters of the strain energy function (Fung 1979)

Number of parameters – material

1 (2) – isotropic, incompressible, linear (nonlinear)

2 (3) – isotropic, compressible, linear (nonlinear)

9 (10) – orthotropic, compressible, linear (nonlinear)

For the constitutive relation to be used in a computational model, the convexity of strain energy function has to be satisfied to ensure the stability of loading. The strain energy W should be positive definite. To ensure this condition, the eigen values of the matrix

$$C = \begin{bmatrix} c_{11} & c_{12} & c_{13} \\ c_{12} & c_{22} & c_{23} \\ c_{13} & c_{23} & c_{33} \end{bmatrix},$$

have to be positive, the condition is equivalent to following the three equations

1. $c_{11} > 0,$
2. $c_{11} \cdot c_{22} - c_{12}^2 > 0$
3. $c_{11}\left(c_{22}c_{23} - c_{23}^2\right) - c_{12}\left(c_{12}c_{33} - c_{12}c_{23}\right) + c_{13}\left(c_{12}c_{23} - c_{13}c_{22}\right) > 0.$

$$***$$

References

[1] L. Gleibermann, Blood pressure and dietary salt in human populations, Ecology of Food and Nutrition 2 (1973) 143-156.

[2] M.H. Weinberger, Salt Sensitivity of Blood Pressure in Humans, Hypertension 27 (1996) 481-490.

[3] B. Joe, J.I. Shapiro, Molecular Mechanisms of Experimental Salt-Sensitive Hypertension, Journal of the American Heart Association 1 (2012).

[4] D. Serban, B. Nilius, P. Vanhoutte, The endothelial saga: the past, the present, the future, Pflügers Archiv European Journal of Physiology 459 (2010) 787-792.

[5] S. Moncada, E.A. Higgs, The discovery of nitric oxide and its role in vascular biology, British Journal of Pharmacology 147 (2006) S193-S201.

[6] R. Furchgott, Role of endothelium in responses of vascular smooth muscle, Circulation Research 53 (1983) 557-573.

[7] R.M.J. Palmer, D.S. Ashton, S. Moncada, Vascular endothelial cells synthesize nitric oxide from L-arginine, Nature 333 (1988) 664-666.

[8] L. Ignarro, Nitric oxide: biology and pathobiology Academic Press2000.

[9] R. Chen, M. Iwai, L. Wu, J. Suzuki, L.-J. Min, T. Shiuchi, T. Sugaya, H.-W. Liu, T.-X. Cui, M. Horiuchi, Important Role of Nitric Oxide in the Effect of Angiotensin-Converting Enzyme Inhibitor Imidapril on Vascular Injury, Hypertension 42 (2003) 542-547.

[10] K.-T. Kang, J.C. Sullivan, J.M. Sasser, J.D. Imig, J.S. Pollock, Novel Nitric Oxide Synthase–Dependent Mechanism of Vasorelaxation in Small Arteries From Hypertensive Rats, Hypertension 49 (2007) 893-901.

[11] G. Hodge, V. Ye, K. Duggan, Salt-sensitive hypertension resulting from nitric oxide synthase inhibition is associated with loss of regulation of angiotensin II in the rat, Experimental Physiology 87 (2002) 1-8.

[12] T.M. Gwathmey, B.M. Westwood, N.T. Pirro, L. Tang, J.C. Rose, D.I. Diz, M.C. Chappell, Nuclear angiotensin-(1–7) receptor is functionally coupled to the formation of nitric oxide, American Journal of Physiology - Renal Physiology 299 (2010) F983-F990.

[13] J.E. Hall, A.C. Guyton, M.W. Brands, Pressure-volume regulation in hypertension, Kidney Int Suppl 55 (1996) S35-41.

[14] J.A. Payne, B.T. Alexander, R.A. Khalil, Decreased Endothelium-Dependent NO-cGMP Vascular Relaxation and Hypertension in Growth-Restricted Rats on a High-Salt Diet, Hypertension 43 (2004) 420-427.

[15] P. Chen, P. Sanders, Role of nitric oxide synthesis in salt-sensitive hypertension in Dahl/Rapp rats, Hypertension 22 (1993) 812-818.

[16] JOHNSON, #160, R. A., FREEMAN, R. H., Sustained hypertension in the rat induced by chronic blockade of nitric oxide production, Nature Publishing Group, Basingstoke, ROYAUME-UNI, 1992.

[17] K.M. Gauthier-Rein, N.J. Rusch, Distinct Endothelial Impairment in Coronary Microvessels from Hypertensive Dahl Rats, Hypertension 31 (1998) 328-334.

[18] Y. Ozawa, K. Hayashi, T. Kanda, K. Homma, I. Takamatsu, S. Tatematsu, K. Yoshioka, H. Kumagai, S.H.U. Wakino, T. Saruta, Impaired nitric oxide- and endothelium-derived hyperpolarizing factor-dependent dilation of renal afferent arteriole in Dahl salt-sensitive rats, Nephrology 9 (2004) 272-277.

[19] J.M. Neutel, Effect of the renin-angiotensin system on the vessel wall: using ACE inhibition to improve endothelial function, J Hum Hypertens 18 (2004) 599-606.

[20] R.M. Touyz, Reactive Oxygen Species, Vascular Oxidative Stress, and Redox Signaling in Hypertension, Hypertension 44 (2004) 248-252.

[21] R. Rodrigo, J. Gonzalez, F. Paoletto, The role of oxidative stress in the pathophysiology of hypertension, Hypertens Res 34 (2011) 431-440.

[22] E. Schulz, T. Jansen, P. Wenzel, A. Daiber, T. Munzel, Nitric oxide, tetrahydrobiopterin, oxidative stress, and endothelial dysfunction in hypertension, Antioxid Redox Signal 10 (2008) 1115-26.

[23] M. Félétou, R. Köhler, P. Vanhoutte, Endothelium-derived Vasoactive Factors and Hypertension: Possible Roles in Pathogenesis and as Treatment Targets, Current Hypertension Reports 12 (2010) 267-275.

[24] I.M. Grumbach, W. Chen, S.A. Mertens, D.G. Harrison, A negative feedback mechanism involving nitric oxide and nuclear factor kappa-B modulates endothelial nitric oxide synthase transcription, Journal of Molecular and Cellular Cardiology 39 (2005) 595-603.

[25] G. Buga, J. Griscavage, N. Rogers, L. Ignarro, Negative feedback regulation of endothelial cell function by nitric oxide, Circulation Research 73 (1993) 808-812.

[26] N.E. Rogers, L.J. Ignarro, Constitutive nitric oxide synthase from cerebellum is reversibly inhibited by nitric oxide formed from L-arginine, Biochemical and Biophysical Research Communications 189 (1992) 242-249.

[27] N.D. Vaziri, X.Q. Wang, cGMP-Mediated Negative-Feedback Regulation of Endothelial Nitric Oxide Synthase Expression by Nitric Oxide, Hypertension 34 (1999) 1237-1241.

[28] R. Furchgott, P. Vanhoutte, Endothelium-derived relaxing and contracting factors, The FASEB Journal 3 (1989) 2007-2018.

[29] SCHMIDT, #160, H.H.H. W., LOHMANN, S. M., WALTER, U., The nitric oxide and cGMP signal transduction system : regulation and mechanism of action, Elsevier, Amsterdam, PAYS-BAS, 1993.

[30] T. Lincoln, T. Cornwell, Intracellular cyclic GMP receptor proteins, The FASEB Journal 7 (1993) 328-338.

[31] T.L. Cornwell, T.M. Lincoln, Regulation of intracellular Ca2+ levels in cultured vascular smooth muscle cells. Reduction of Ca2+ by atriopeptin and 8-bromo-cyclic GMP is mediated by cyclic GMP-dependent protein kinase, Journal of Biological Chemistry 264 (1989) 1146-1155.

[32] K. Furukawa, N. Ohshima, Y. Tawada-Iwata, M. Shigekawa, Cyclic GMP stimulates Na+/Ca2+ exchange in vascular smooth muscle cells in primary culture, Journal of Biological Chemistry 266 (1991) 12337-12341.

[33] D.M. Dudzinski, J. Igarashi, D. Greif, T. Michel, THE REGULATION AND PHARMACOLOGY OF ENDOTHELIAL NITRIC OXIDE SYNTHASE, Annual Review of Pharmacology and Toxicology 46 (2006) 235-276.

[34] W.C. Sessa, eNOS at a glance, Journal of Cell Science 117 (2004) 2427-2429.

[35] P.W. Shaul, REGULATION OF ENDOTHELIAL NITRIC OXIDE SYNTHASE: Location, Location, Location, Annual Review of Physiology 64 (2002) 749-774.

[36] Kone, Protein–protein interactions controlling nitric oxide synthases, Acta Physiologica Scandinavica 168 (2000) 27-31.

[37] P.M. Bauer, D. Fulton, Y.C. Boo, G.P. Sorescu, B.E. Kemp, H. Jo, W.C. Sessa, Compensatory Phosphorylation and Protein-Protein Interactions Revealed by Loss of Function and Gain of Function Mutants of Multiple Serine Phosphorylation Sites in Endothelial Nitric-oxide Synthase, Journal of Biological Chemistry 278 (2003) 14841-14849.

[38] J.B. Michel, O. Feron, D. Sacks, T. Michel, Reciprocal Regulation of Endothelial Nitric-oxide Synthase by Ca2+-Calmodulin and Caveolin, Journal of Biological Chemistry 272 (1997) 15583-15586.

[39] B. Vanhaesebroeck, S.J. Leevers, G. Panayotou, M.D. Waterfield, Phosphoinositide 3-kinases: A conserved family of signal transducers, Trends in Biochemical Sciences 22 (1997) 267-272.

[40] A. Chatterjee, J.D. Catravas, Endothelial nitric oxide (NO) and its pathophysiologic regulation, Vascular Pharmacology 49 134-140.

[41] M.A. Corson, N.L. James, S.E. Latta, R.M. Nerem, B.C. Berk, D.G. Harrison, Phosphorylation of Endothelial Nitric Oxide Synthase in Response to Fluid Shear Stress, Circulation Research 79 (1996) 984-991.

[42] R. Busse, I. Fleming, Pulsatile Stretch and Shear Stress: Physical Stimuli Determining the Production of Endothelium-Derived Relaxing Factors, Journal of Vascular Research 35 (1998) 73-84.

[43] K. Toda, E. Tatsumi, Y. Taenaka, T. Masuzawa, H. Takano, Sympathetic nerve activities in pulsatile and nonpulsatile systemic circulation in anesthetized goats, American Journal of Physiology - Heart and Circulatory Physiology 271 (1996) H15-H22.

[44] T.C. Bellamy, J. Garthwaite, Sub-second Kinetics of the Nitric Oxide Receptor, Soluble Guanylyl Cyclase, in Intact Cerebellar Cells, Journal of Biological Chemistry 276 (2001) 4287-4292.

[45] T.C. Bellamy, J. Garthwaite, Pharmacology of the nitric oxide receptor, soluble guanylyl cyclase, in cerebellar cells, British Journal of Pharmacology 136 (2002) 95-103.

[46] E.R. Derbyshire, M.A. Marletta, Biochemistry of Soluble Guanylate Cyclase

cGMP: Generators, Effectors and Therapeutic Implications. in: H.H.H.W. Schmidt, F. Hofmann, J.-P. Stasch, (Eds.), Springer Berlin Heidelberg2009, pp. 17-31.

[47] S.P.L. Cary, J.A. Winger, E.R. Derbyshire, M.A. Marletta, Nitric oxide signaling: no longer simply on or off, Trends in Biochemical Sciences 31 (2006) 231-239.

[48] J.W. Denninger, M.A. Marletta, Guanylate cyclase and the ·NO/cGMP signaling pathway, Biochimica et Biophysica Acta (BBA) - Bioenergetics 1411 (1999) 334-350.

[49] T.C. Bellamy, J. Wood, D.A. Goodwin, J. Garthwaite, Rapid desensitization of the nitric oxide receptor, soluble guanylyl cyclase, underlies diversity of cellular cGMP responses, Proceedings of the National Academy of Sciences 97 (2000) 2928-2933.

[50] R.H. Kramer, J.W. Karpen, Spanning binding sites on allosteric proteins with polymer-linked ligand dimers, Nature 395 (1998) 710-713.

[51] M. Négrerie, L. Bouzhir, J.-L. Martin, U. Liebl, Control of Nitric Oxide Dynamics by Guanylate Cyclase in Its Activated State, Journal of Biological Chemistry 276 (2001) 46815-46821.

[52] P. Condorelli, S.C. George, In Vivo Control of Soluble Guanylate Cyclase Activation by Nitric Oxide: A Kinetic Analysis, Biophysical journal 80 (2001) 2110-2119.

[53] I.R. Hutcheson, T.M. Griffith, Release of endothelium-derived relaxing factor is modulated both by frequency and amplitude of pulsatile flow, American Journal of Physiology - Heart and Circulatory Physiology 261 (1991) H257-H262.

[54] L.A. Juncos, J. Garvin, O.A. Carretero, S. Ito, Flow modulates myogenic responses in isolated microperfused rabbit afferent arterioles via endothelium-derived nitric oxide, The Journal of Clinical Investigation 95 (1995) 2741-2748.

[55] H. Gustafsson, Vasomotion and underlying mechanisms in small arteries. An in vitro study of rat blood vessels, Acta Physiol Scand Suppl 614 (1993) 1-44.

[56] J.R.H. Mauban, C. Lamont, C.W. Balke, W.G. Wier, Adrenergic stimulation of rat resistance arteries affects Ca2+ sparks, Ca2+ waves, and Ca2+oscillations, American Journal of Physiology - Heart and Circulatory Physiology 280 (2001) H2399-H2405.

[57] W.B. M. Sell, F. Markwardt, Desynchronising effect of the endothelium on intracellular Ca2+ concentration dynamics in vascular smooth muscle cells of rat mesenteric arteries, Cell Calcium 32 (2002) 105-120.

[58] G.B. Stefano, V. Prevot, P. Cadet, I. Dardik, Vascular pulsations stimulating nitric oxide release during cyclic exercise may benefit health: a molecular approach (review), Int J Mol Med 7 (2001) 119-29.

[59] J. Adams, J. Moore, M. Moreno, J. Coelho, J. Bassuk, D. Wu, Effects of Periodic Body Acceleration on the In Vivo Vasoactive Response to N-w-nitro–L-arginine and the In Vitro Nitric Oxide Production, Annals of Biomedical Engineering 31 (2003) 1337-1346.

[60] P. Cabrales, A.G. Tsai, J.A. Frangos, M. Intaglietta, Role of endothelial nitric oxide in microvascular oxygen delivery and consumption, Free Radical Biology and Medicine 39 (2005) 1229-1237.

[61] D.M. Hirai, S.W. Copp, L.F. Ferreira, T.I. Musch, D.C. Poole, Nitric oxide bioavailability modulates the dynamics of microvascular oxygen exchange during recovery from contractions, Acta Physiologica 200 (2010) 159-169.

[62] Z. Huang, J.G. Louderback, M. Goyal, F. Azizi, S.B. King, D.B. Kim-Shapiro, Nitric oxide binding to oxygenated hemoglobin under physiological conditions, Biochimica et Biophysica Acta (BBA) - General Subjects 1568 (2001) 252-260.

[63] D.B. Kim-Shapiro, A.N. Schechter, M.T. Gladwin, Unraveling the Reactions of Nitric Oxide, Nitrite, and Hemoglobin in Physiology and Therapeutics, Arteriosclerosis, Thrombosis, and Vascular Biology 26 (2006) 697-705.

[64] M.S. Joshi, T.B. Ferguson, T.H. Han, D.R. Hyduke, J.C. Liao, T. Rassaf, N. Bryan, M. Feelisch, J.R. Lancaster, Nitric oxide is consumed, rather than conserved, by reaction with oxyhemoglobin under physiological conditions, Proceedings of the National Academy of Sciences 99 (2002) 10341-10346.

[65] A.J. Gow, B.P. Luchsinger, J.R. Pawloski, D.J. Singel, J.S. Stamler, The oxyhemoglobin reaction of nitric oxide, Proceedings of the National Academy of Sciences 96 (1999) 9027-9032.

[66] R.M.J. Palmer, A.G. Ferrige, S. Moncada, Nitric oxide release accounts for the biological activity of endothelium-derived relaxing factor, Nature 327 (1987) 524-526.

[67] V.G. Kharitonov, M. Russwurm, D. Magde, V.S. Sharma, D. Koesling, Dissociation of Nitric Oxide from Soluble Guanylate Cyclase, Biochemical and Biophysical Research Communications 239 (1997) 284-286.

[68] V.G. Kharitonov, V.S. Sharma, D. Magde, D. Koesling, Kinetics of Nitric Oxide Dissociation from Five- and Six-Coordinate Nitrosyl Hemes and Heme Proteins, Including Soluble Guanylate Cyclase†, Biochemistry 36 (1997) 6814-6818.

[69] P.E. Brandish, W. Buechler, M.A. Marletta, Regeneration of the Ferrous Heme of Soluble Guanylate Cyclase from the Nitric Oxide Complex: Acceleration by Thiols and Oxyhemoglobin†, Biochemistry 37 (1998) 16898-16907.

[70] A. Margulis, A. Sitaramayya, Rate of deactivation of nitric oxide-stimulated soluble guanylate cyclase: influence of nitric oxide scavengers and calcium, Biochemistry 39 (2000) 1034-9.

[71] J.A. Winger, E.R. Derbyshire, M.A. Marletta, Dissociation of Nitric Oxide from Soluble Guanylate Cyclase and Heme-Nitric Oxide/Oxygen Binding Domain Constructs, Journal of Biological Chemistry 282 (2007) 897-907.

[72] N.M. Tsoukias, M. Kavdia, A.S. Popel, A theoretical model of nitric oxide transport in arterioles: frequency- vs. amplitude-dependent control of cGMP formation, Am J Physiol Heart Circ Physiol 286 (2004) H1043-56.

[73] J.E. Keeble, P.K. Moore, Pharmacology and potential therapeutic applications of nitric oxide-releasing non-steroidal anti-inflammatory and related nitric oxide-donating drugs, British Journal of Pharmacology 137 (2002) 295-310.

[74] T. Nakano, R. Tominaga, S. Morita, M. Masuda, I. Nagano, K.-i. Imasaka, H. Yasui, Impacts of pulsatile systemic circulation on endothelium-derived nitric oxide release in anesthetized dogs, Ann Thorac Surg 72 (2001) 156-162.

[75] R.J. Hendrickson, C. Cappadona, E.N. Yankah, J.V. Sitzmann, P.A. Cahill, E.M. Redmond, Sustained Pulsatile Flow Regulates Endothelial Nitric Oxide Synthase and Cyclooxygenase Expression in Co-Cultured Vascular Endothelial and Smooth Muscle Cells, Journal of Molecular and Cellular Cardiology 31 (1999) 619-629.

[76] A. MacKenzie, R.M. Wadsworth, Extracellular L-arginine is required for optimal NO synthesis by eNOS and iNOS in the rat mesenteric artery wall, British Journal of Pharmacology 139 (2003) 1487-1497.

[77] J.K. Stechmiller, B. Childress, L. Cowan, Arginine Supplementation and Wound Healing, Nutrition in Clinical Practice 20 (2005) 52-61.

[78] M.K. Angele, S.M. Nitsch, R.A. Hatz, P. Angele, T. Hernandez-Richter, M.W. Wichmann, I.H. Chaudry, F.W. Schildberg, L-arginine: a unique amino acid for improving depressed wound immune function following hemorrhage, Eur Surg Res 34 (2002) 53-60.

[79] S.M. Morris, Arginine: beyond protein, The American Journal of Clinical Nutrition 83 (2006) 508S-512S.

[80] E. Mocchegiani, G. Nistico, L. Santarelli, N. Fabris, Effect of L-arginine on thymic function. Possible role of L-arginine: Nitric oxide (no) pathway, Archives of Gerontology and Geriatrics 19 (1994) 163-170.

[81] C.C. Carson, 3rd, Erectile dysfunction: diagnosis and management with newer oral agents, Proc (Bayl Univ Med Cent) 13 (2000) 356-60.

[82] G. Wu, F.W. Bazer, T.A. Davis, S.W. Kim, P. Li, J. Marc Rhoads, M. Carey Satterfield, S.B. Smith, T.E. Spencer, Y. Yin, Arginine metabolism and nutrition in growth, health and disease, Amino Acids 37 (2009) 153-68.

[83] J. Appleton, Arginine: clinical potential of a semi-essential amino acid. (Arginine), Alternative Medicine Review 7 (2002) 512(11).

[84] S.M. Bode-Böger, F. Scalera, L.J. Ignarro, The l-arginine paradox: Importance of the l-arginine/asymmetrical dimethylarginine ratio, Pharmacology & Therapeutics 114 (2007) 295-306.

[85] L.J. Ignarro, Nitric oxide : biology and pathobiology, Academic Press, San Diego, 2000.

[86] D.S. Bredt, S.H. Snyder, Isolation of nitric oxide synthetase, a calmodulin-requiring enzyme, Proceedings of the National Academy of Sciences of the United States of America 87 (1990) 682-685.

[87] M.E. Gold, P.A. Bush, L.J. Ignarro, Depletion of arterial L-arginine causes reversible tolerance to endothelium-dependent relaxation, Biochemical and Biophysical Research Communications 164 (1989) 714-721.

[88] R.M.J. Palmer, D.D. Rees, D.S. Ashton, S. Moncada, L-arginine is the physiological precursor for the formation of nitric oxide in endothelium-dependent relaxation, Biochemical and Biophysical Research Communications 153 (1988) 1251-1256.

[89] M.S. Joshi, T.B. Ferguson, F.K. Johnson, R.A. Johnson, S. Parthasarathy, J.R. Lancaster, Receptor-mediated activation of nitric oxide synthesis by arginine in endothelial cells, Proceedings of the National Academy of Sciences 104 (2007) 9982-9987.

[90] S.M. Morris, Enzymes of Arginine Metabolism, The Journal of Nutrition 134 (2004) 2743S-2747S.

[91] L.H. Wei, A.T. Jacobs, S.M. Morris, Jr., L.J. Ignarro, IL-4 and IL-13 upregulate arginase I expression by cAMP and JAK/STAT6 pathways in vascular smooth muscle cells, Am J Physiol Cell Physiol 279 (2000) C248-56.

[92] M.T. Jay, S. Chirico, R.C. Siow, K.R. Bruckdorfer, M. Jacobs, D.S. Leake, J.D. Pearson, G.E. Mann, Modulation of vascular tone by low density lipoproteins: effects on L-arginine transport and nitric oxide synthesis, Exp Physiol 82 (1997) 349-60.

[93] G. García-Cardeña, P. Oh, J. Liu, J.E. Schnitzer, W.C. Sessa, Targeting of nitric oxide synthase to endothelial cell caveolae via palmitoylation: implications for nitric oxide signaling, Proceedings of the National Academy of Sciences of the United States of America 93 (1996) 6448-6453.

[94] K.K. McDonald, S. Zharikov, E.R. Block, M.S. Kilberg, A Caveolar Complex between the Cationic Amino Acid Transporter 1 and Endothelial Nitric-oxide Synthase May Explain the "Arginine Paradox", Journal of Biological Chemistry 272 (1997) 31213-31216.

[95] Y. Gao, B. Gumusel, G. Koves, A. Prasad, Q. Hao, A. Hyman, H. Lippton, Agmatine: A novel endogenous vasodilator substance, Life Sciences 57 (1995) PL83-PL86.

[96] D.J. Reis, S. Regunathan, Agmatine: An Endogenous Ligand at Imidazoline Receptors Is a Novel Neurotransmittera, Annals of the New York Academy of Sciences 881 (1999) 65-80.

[97] S.R. Donald J Reis, Is agmatine a novel neurotransmitter in brain?, Trends in Pharmacological Sciences 21 (2000) 187-193.

[98] W. Raasch, U. Schafer, J. Chun, P. Dominiak, Biological significance of agmatine, an endogenous ligand at imidazoline binding sites, Br J Pharmacol 133 (2001) 755-80.

[99] C.A. Fairbanks, K.L. Schreiber, K.L. Brewer, C.-G. Yu, L.S. Stone, K.F. Kitto, H.O. Nguyen, B.M. Grocholski, D.W. Shoeman, L.J. Kehl, S. Regunathan, D.J. Reis, R.P. Yezierski, G.L. Wilcox, Agmatine reverses pain induced by inflammation, neuropathy, and spinal cord injury, Proceedings of the National Academy of Sciences of the United States of America 97 (2000) 10584-10589.

[100] N. Wu, R.-B. Su, J. Li, Agmatine and Imidazoline Receptors: Their Role in Opioid Analgesia, Tolerance and Dependence, Cellular and Molecular Neurobiology 28 (2008) 629-641.

[101] S. Regunathan, Agmatine: Biological Role and Therapeutic Potentials in Morphine Analgesia and Dependence. in: R.S. Rapaka, W. Sadée, (Eds.), Drug Addiction, Springer New York2008, pp. 625-634.

[102] S. Hong, J. Lee, C. Kim, G.J. Seong, Agmatine protects retinal ganglion cells from hypoxia-induced apoptosis in transformed rat retinal ganglion cell line, BMC Neuroscience 8 (2007) 81.

[103] W. Raasch, S. Regunathan, G. Li, D.J. Reis, Agmatine, the bacterial amine, is widely distributed in mammalian tissues, Life Sciences 56 (1995) 2319-2330.

[104] S. Regunathan, C. Youngson, W. Raasch, H. Wang, D.J. Reis, Imidazoline receptors and agmatine in blood vessels: a novel system inhibiting vascular smooth muscle proliferation, J Pharmacol Exp Ther 276 (1996) 1272-82.

[105] J.J. Morrissey, S. Klahr, Agmatine activation of nitric oxide synthase in endothelial cells, Proc Assoc Am Physicians 109 (1997) 51-7.

[106] G. Li, S. Regunathan, C. Barrow, J. Eshraghi, R. Cooper, D. Reis, Agmatine: an endogenous clonidine-displacing substance in the brain, Science 263 (1994) 966-969.

[107] U. Raasch W Fau - Schafer, F. Schafer U Fau - Qadri, P. Qadri F Fau - Dominiak, P. Dominiak, Agmatine, an endogenous ligand at imidazoline binding sites, does not antagonize the clonidine-mediated blood pressure reaction.

[108] D.J. Reis, G.E.N. Li, S. Regunathan, Endogenous Ligands of Imidazoline Receptors: Classic and Immunoreactive Clonidine-Displacing Substance and Agmatine, Annals of the New York Academy of Sciences 763 (1995) 295-313.

[109] M.J. Mulvany, C. Aalkjaer, Structure and function of small arteries, Physiol Rev 70 (1990) 921-61.

[110] R.H. Cox, Contribution of salt to arterial wall changes in DOCA hypertension in the rat, J Hypertens 5 (1987) 611-9.

[111] R.H. Cox, Changes in the expression and function of arterial potassium channels during hypertension, Vascul Pharmacol 38 (2002) 13-23.

[112] G.L. Baumbach, D.D. Heistad, Remodeling of cerebral arterioles in chronic hypertension, Hypertension 13 (1989) 968-72.

[113] A.M. Briones, J.M. González, B. Somoza, J. Giraldo, C.J. Daly, E. Vila, M. Carmen González, J.C. McGrath, S.M. Arribas, Role of Elastin in Spontaneously Hypertensive Rat Small Mesenteric Artery Remodelling, The Journal of Physiology 552 (2003) 185-195.

[114] A.M. Heagerty, C. Aalkjaer, S.J. Bund, N. Korsgaard, M.J. Mulvany, Small artery structure in hypertension. Dual processes of remodeling and growth, Hypertension 21 (1993) 391-7.

[115] J.P. Rapp, Dahl salt-susceptible and salt-resistant rats. A review, Hypertension 4 (1982) 753-63.

[116] M.P. Blaustein, J. Zhang, L. Chen, B.P. Hamilton, How does salt retention raise blood pressure?, American Journal of Physiology - Regulatory, Integrative and Comparative Physiology 290 (2006) R514-R523.

[117] T. QUASCHNING, L.V. D'USCIO, S. SHAW, H.-J. GRÖNE, F. RUSCHITZKA, T.F. LÜSCHER, Vasopeptidase Inhibition Restores Renovascular Endothelial Dysfunction in Salt-Induced Hypertension, Journal of the American Society of Nephrology 12 (2001) 2280-2287.

[118] W.C. Sessa, Regulation of endothelial derived nitric oxide in health and disease, Memórias do Instituto Oswaldo Cruz 100 (2005) 15-18.

[119] D.B.M. Philip J. Kadowitz, (Ed.), Nitric oxide and the regulation of the peripheral circulation, Birkhauser Boston2000.

[120] F.L.M. Ricciardolo, L. Vergnani, S. Wiegand, F. Ricci, N. Manzoli, A. Fischer, S. Amadesi, R. Fellin, P. Geppetti, Detection of Nitric Oxide Release Induced by Bradykinin in Guinea Pig Trachea and Main Bronchi Using a Porphyrinic Microsensor, Am. J. Respir. Cell Mol. Biol. 22 (2000) 97-104.

[121] C.N. Hall, J. Garthwaite, What is the real physiological NO concentration in vivo?, Nitric Oxide 21 (2009) 92-103.

[122] M.J. Berridge, M.D. Bootman, H.L. Roderick, Calcium signalling: dynamics, homeostasis and remodelling, Nat Rev Mol Cell Biol 4 (2003) 517-529.

[123] R.E. Dolmetsch, R.S. Lewis, Signaling between intracellular Ca2+ stores and depletion-activated Ca2+ channels generates [Ca2+]i oscillations in T lymphocytes, The Journal of General Physiology 103 (1994) 365-388.

[124] R.E. Dolmetsch, R.S. Lewis, C.C. Goodnow, J.I. Healy, Differential activation of transcription factors induced by Ca2+ response amplitude and duration, Nature 386 (1997) 855-8.

[125] P. De Koninck, H. Schulman, Sensitivity of CaM Kinase II to the Frequency of Ca2+ Oscillations, Science 279 (1998) 227-230.

[126] K.U. Bayer, P. De Koninck, H. Schulman, Alternative splicing modulates the frequency-dependent response of CaMKII to Ca(2+) oscillations, EMBO J 21 (2002) 3590-7.

[127] R.E. Dolmetsch, K. Xu, R.S. Lewis, Calcium oscillations increase the efficiency and specificity of gene expression, Nature 392 (1998) 933-936.

[128] S. Kupzig, D. Bouyoucef, G.E. Cozier, P.J. Cullen, Studying the spatial and temporal regulation of Ras GTPase-activating proteins, Methods Enzymol 407 (2006) 64-82.

[129] S. Kupzig, S.A. Walker, P.J. Cullen, The frequencies of calcium oscillations are optimized for efficient calcium-mediated activation of Ras and the ERK/MAPK cascade, Proceedings of the National Academy of Sciences of the United States of America 102 (2005) 7577-7582.

[130] J.M. Bradshaw, Y. Kubota, T. Meyer, H. Schulman, An ultrasensitive Ca2+/calmodulin-dependent protein kinase II-protein phosphatase 1 switch facilitates specificity in postsynaptic calcium signaling, Proceedings of the National Academy of Sciences 100 (2003) 10512-10517.

[131] J.F. Perez, M.J. Sanderson, The Contraction of Smooth Muscle Cells of Intrapulmonary Arterioles Is Determined by the Frequency of Ca2+ Oscillations Induced by 5-HT and KCl, The Journal of General Physiology 125 (2005) 555-567.

[132] M.J. Sanderson, Y. Bai, J. Perez-Zoghbi, Ca(2+) oscillations regulate contraction of intrapulmonary smooth muscle cells, Adv Exp Med Biol 661 (2010) 77-96.

[133] A. Strahonja-Packard, M.J. Sanderson, Intercellular Ca(2+) waves induce temporally and spatially distinct intracellular Ca(2+) oscillations in glia, Glia 28 (1999) 97-113.

[134] J.F. Perez-Zoghbi, Y. Bai, M.J. Sanderson, Nitric oxide induces airway smooth muscle cell relaxation by decreasing the frequency of agonist-induced Ca2+ oscillations, The Journal of General Physiology 135 (2010) 247-259.

[135] D.M. Kaye, S.D. Wiviott, J.-L. Balligand, W.W. Simmons, T.W. Smith, R.A. Kelly, Frequency-Dependent Activation of a Constitutive Nitric Oxide Synthase and Regulation

of Contractile Function in Adult Rat Ventricular Myocytes, Circulation Research 78 (1996) 217-224.

[136] C. Salazar, A. Zaccaria Politi, T. Höfer, Decoding of Calcium Oscillations by Phosphorylation Cycles: Analytic Results, Biophysical journal 94 (2008) 1203-1215.

[137] B. Knoke, M. Marhl, S. Schuster, Selective Regulation of Protein Activity by Complex Ca<sup>2+</sup> Oscillations: A Theoretical Study

Mathematical Modeling of Biological Systems, Volume I. in: A. Deutsch, L. Brusch, H. Byrne, G.d. Vries, H. Herzel, (Eds.), Birkhäuser Boston2007, pp. 11-22.

[138] M. Marhl, V. Grubelnik, Role of cascades in converting oscillatory signals into stationary step-like responses, Biosystems 87 (2007) 58-67.

[139] J. Sneyd, J. Keizer, M.J. Sanderson, Mechanisms of calcium oscillations and waves: a quantitative analysis, FASEB J 9 (1995) 1463-72.

[140] V. Brezina, I.V. Orekhova, K.R. Weiss, Control of time-dependent biological processes by temporally patterned input, Proceedings of the National Academy of Sciences 94 (1997) 10444-10449.

[141] G. Dupont, G. Houart, P. De Koninck, Sensitivity of CaM kinase II to the frequency of Ca2+ oscillations: a simple model, Cell Calcium 34 (2003) 485-497.

[142] D. Gall, E. Baus, G. Dupont, Activation of the Liver Glycogen Phosphorylase by Ca2+Oscillations: a Theoretical Study, Journal of Theoretical Biology 207 (2000) 445-454.

[143] J. Hoyer, R. Köhler, A. Distler, Mechanosensitive Ca2+ oscillations and STOC activation in endothelial cells, The FASEB Journal 12 (1998) 359-366.

[144] G. Grynkiewicz, M. Poenie, R.Y. Tsien, A new generation of Ca2+ indicators with greatly improved fluorescence properties, Journal of Biological Chemistry 260 (1985) 3440-3450.

[145] J.C. Falcone, L. Kuo, G.A. Meininger, Endothelial cell calcium increases during flow-induced dilation in isolated arterioles, American Journal of Physiology - Heart and Circulatory Physiology 264 (1993) H653-H659.

[146] H.J. Knot, K.M. Lounsbury, J.E. Brayden, M.T. Nelson, Gender differences in coronary artery diameter reflect changes in both endothelial Ca2+ and ecNOS activity, American Journal of Physiology - Heart and Circulatory Physiology 276 (1999) H961-H969.

[147] S. Dimmeler, I. Fleming, B. Fisslthaler, C. Hermann, R. Busse, A.M. Zeiher, Activation of nitric oxide synthase in endothelial cells by Akt-dependent phosphorylation, Nature 399 (1999) 601-605.

[148] L. Hadri, R. Bobe, Y. Kawase, D. Ladage, K. Ishikawa, F. Atassi, D. Lebeche, E.G. Kranias, J.A. Leopold, A.M. Lompré, L. Lipskaia, R.J. Hajjar, SERCA2a gene transfer

enhances eNOS expression and activity in endothelial cells, Molecular therapy : the journal of the American Society of Gene Therapy 18 (2010) 1284-1292.

[149] A.J. Kanai, H.C. Strauss, G.A. Truskey, A.L. Crews, S. Grunfeld, T. Malinski, Shear Stress Induces ATP-Independent Transient Nitric Oxide Release From Vascular Endothelial Cells, Measured Directly With a Porphyrinic Microsensor, Circulation Research 77 (1995) 284-293.

[150] L.A. Birder, M.L. Nealen, S. Kiss, W.C. de Groat, M.J. Caterina, E. Wang, G. Apodaca, A.J. Kanai, Beta-adrenoceptor agonists stimulate endothelial nitric oxide synthase in rat urinary bladder urothelial cells, J Neurosci 22 (2002) 8063-70.

[151] M.G.V. Petroff, S.H. Kim, S. Pepe, C. Dessy, E. Marban, J.-L. Balligand, S.J. Sollott, Endogenous nitric oxide mechanisms mediate the stretch dependence of Ca2+ release in cardiomyocytes, Nat Cell Biol 3 (2001) 867-873.

[152] M.J. Berridge, The AM and FM of calcium signalling, Nature 386 (1997) 759-760.

[153] P.E. RAPP, M.J. BERRIDGE, The Control of Transepithelial Potential Oscillations in the Salivary Gland of Calliphora Erythrocephala, Journal of Experimental Biology 93 (1981) 119-132.

[154] P. Tompa, R. Töth-Boconádi, P. Friedrich, Frequency decoding of fast calcium oscillations by calpain, Cell Calcium 29 (2001) 161-170.

[155] N.M. Woods, K.S.R. Cuthbertson, P.H. Cobbold, Repetitive transient rises in cytoplasmic free calcium in hormone-stimulated hepatocytes, Nature 319 (1986) 600-602.

[156] A. Kapela, A. Bezerianos, N.M. Tsoukias, A mathematical model of Ca2+ dynamics in rat mesenteric smooth muscle cell: Agonist and NO stimulation, Journal of Theoretical Biology 253 (2008) 238-260.

[157] E. Stankevicius, V. Lopez-Valverde, L. Rivera, A.D. Hughes, M.J. Mulvany, U. Simonsen, Combination of Ca2+ -activated K+ channel blockers inhibits acetylcholine-evoked nitric oxide release in rat superior mesenteric artery, Br J Pharmacol 149 (2006) 560-72.

[158] H. Shimokawa, H. Yasutake, K. Fujii, M.K. Owada, R. Nakaike, Y. Fukumoto, T. Takayanagi, T. Nagao, K. Egashira, M. Fujishima, A. Takeshita, The Importance of the Hyperpolarizing Mechanism Increases as the Vessel Size Decreases in Endothelium-Dependent Relaxations in Rat Mesenteric Circulation, Journal of Cardiovascular Pharmacology 28 (1996) 703-711.

[159] G. Garcia-Cardena, P. Oh, J. Liu, J.E. Schnitzer, W.C. Sessa, Targeting of nitric oxide synthase to endothelial cell caveolae via palmitoylation: implications for nitric oxide signaling, Proc Natl Acad Sci U S A 93 (1996) 6448-6453.

[160] S. Regunathan, C. Youngson, W. Raasch, H. Wang, D.J. Reis, Imidazoline receptors and agmatine in blood vessels: a novel system inhibiting vascular smooth muscle proliferation, Journal of Pharmacology & Experimental Therapeutics 276 (1996) 1272-1282.

[161] G.M. Gilad, V.H. Gilad, J.M. Rabey, Arginine and ornithine decarboxylation in rodent brain: coincidental changes during development and after ischemia, Neurosci Lett 216 (1996) 33-6.

[162] G. Li, S. Regunathan, C.J. Barrow, J. Eshraghi, R. Cooper, D.J. Reis, Agmatine: an endogenous clonidine-displacing substance in the brain, Science 263 (1994) 966-969.

[163] M.M. Shafaroudi, M. McBride, C. Deighan, A. Wokoma, J. Macmillan, C.J. Daly, J.C. McGrath, Two "knockout" mouse models demonstrate that aortic vasodilatation is mediated via alpha2a-adrenoceptors located on the endothelium, J.Pharmacol.Exp.Ther.2005.Aug.;314.(2.):804.-10.Epub.2005.May.5. 314 (2005) 804-810.

[164] J.P. Hieble, D.C. Kolpak, Mediation of the hypotensive action of systemic clonidine in the rat by alpha 2-adrenoceptors, Br J Pharmacol 110 (1993) 1635-9.

[165] M.S. Joshi, T.B. Ferguson, Jr., F.K. Johnson, R.A. Johnson, S. Parthasarathy, J.R. Lancaster, Jr., Receptor-mediated activation of nitric oxide synthesis by arginine in endothelial cells, Proc Natl Acad Sci U S A 104 (2007) 9982-7.

[166] J.J. Morrissey, S. Klahr, Agmatine activation of nitric oxide synthase in endothelial cells, Proceedings of the Association of American Physicians 109 (1997) 51-57.

[167] M. Satoh, Y. Haruna, S. Fujimoto, T. Sasaki, N. Kashihara, Telmisartan improves endothelial dysfunction and renal autoregulation in Dahl salt-sensitive rats, Hypertens Res 33 (2010) 135-42.

[168] E. Moura, C.E. Pinto, M.P. Serrao, J. Afonso, M.A. Vieira-Coelho, Adrenal alpha(2)-adrenergic receptors in the aging normotensive and spontaneously hypertensive rat, Neurobiol Aging 33 (2012) 969-78.

[169] J. Park, J.J. Galligan, G.D. Fink, G.M. Swain, Alterations in sympathetic neuroeffector transmission to mesenteric arteries but not veins in DOCA-salt hypertension, Auton Neurosci 152 (2010) 11-20.

[170] M. Feng, S. Whitesall, Y. Zhang, M. Beibel, L. D'Alecy, K. DiPetrillo, Validation of volume-pressure recording tail-cuff blood pressure measurements, Am J Hypertens 21 (2008) 1288-91.

[171] B.R. Duling, R.W. Gore, R.G. Dacey, Jr., D.N. Damon, Methods for isolation, cannulation, and in vitro study of single microvessels, Am J Physiol 241 (1981) H108-116.

[172] S. Taylor, M. Wakem, G. Dijkman, M. Alsarraj, M. Nguyen, A practical approach to RT-qPCR—Publishing data that conform to the MIQE guidelines, Methods 50 (2010) S1-S5.

[173] U.E. Gibson, C.A. Heid, P.M. Williams, A novel method for real time quantitative RT-PCR, Genome Research 6 (1996) 995-1001.

[174] K.H. Nam, S.H. Lee, J. Lee, Differential Expression of ADC mRNA during Development and upon Acid Stress in Soybean (Glycine max) Hypocotyls, Plant and Cell Physiology 38 (1997) 1156-1166.

[175] N. Yarlett, W.R. Waters, J.A. Harp, M.J. Wannemuehler, M. Morada, J. Bellcastro, S.J. Upton, L.J. Marton, B.J. Frydman, Activities of dl-α-Difluoromethylarginine and Polyamine Analogues against Cryptosporidium parvum Infection in a T-Cell Receptor Alpha-Deficient Mouse Model, Antimicrobial Agents and Chemotherapy 51 (2007) 1234-1239.

[176] K.L. Christensen, M.J. Mulvany, Perindopril changes the mesenteric pressure profile of conscious hypertensive and normotensive rats, Hypertension 23 (1994) 325-8.

[177] B.J. Falloon, S.J. Bund, J.R. Tulip, A.M. Heagerty, In vitro perfusion studies of resistance artery function in genetic hypertension, Hypertension 22 (1993) 486-95.

[178] Y. Ozawa, K. Hayashi, T. Kanda, K. Homma, I. Takamatsu, S. Tatematsu, K. Yoshioka, H. Kumagai, S. Wakino, T. Saruta, Impaired nitric oxide- and endothelium-derived hyperpolarizing factor-dependent dilation of renal afferent arteriole in Dahl salt-sensitive rats, Nephrology (Carlton) 9 (2004) 272-7.

[179] M. Hermann, G. Camici, A. Fratton, D. Hurlimann, F.C. Tanner, J.P. Hellermann, M. Fiedler, J. Thiery, M. Neidhart, R.E. Gay, S. Gay, T.F. Luscher, F. Ruschitzka, Differential effects of selective cyclooxygenase-2 inhibitors on endothelial function in salt-induced hypertension, Circulation 108 (2003) 2308-11.

[180] J.A. Payne, B.T. Alexander, R.A. Khalil, Decreased endothelium-dependent NO-cGMP vascular relaxation and hypertension in growth-restricted rats on a high-salt diet, Hypertension 43 (2004) 420-7.

[181] S. Fujii, L. Zhang, J. Igarashi, H. Kosaka, L-arginine reverses p47phox and gp91phox expression induced by high salt in Dahl rats, Hypertension 42 (2003) 1014-20.

[182] R.C. Blantz, J. Satriano, F. Gabbai, C. Kelly, Biological effects of arginine metabolites, Acta Physiol Scand 168 (2000) 21-5.

[183] S. Regunathan, J.E. Piletz, Regulation of inducible nitric oxide synthase and agmatine synthesis in macrophages and astrocytes, Ann N Y Acad Sci 1009 (2003) 20-9.

[184] M.J. Lortie, W.F. Novotny, O.W. Peterson, V. Vallon, K. Malvey, M. Mendonca, J. Satriano, P. Insel, S.C. Thomson, R.C. Blantz, Agmatine, a bioactive metabolite of arginine. Production, degradation, and functional effects in the kidney of the rat, Journal of Clinical Investigation 97 (1996) 413-420.

[185] A.V. Santhanam, S. Viswanathan, M. Dikshit, Activation of protein kinase B/Akt and endothelial nitric oxide synthase mediates agmatine-induced endothelium-dependent relaxation, Eur.J.Pharmacol.2007.Jun.29.;. . (2007).

[186] I.F. Musgrave, A. Van Der Zypp, M. Grigg, C.J. Barrow, Endogenous imidazoline receptor ligands relax rat aorta by an endothelium-dependent mechanism, Ann N Y Acad Sci 1009 (2003) 222-7.

[187] C. Ledent, J.M. Vaugeois, S.N. Schiffmann, T. Pedrazzini, M. El Yacoubi, J.J. Vanderhaeghen, J. Costentin, J.K. Heath, G. Vassart, M. Parmentier, Aggressiveness, hypoalgesia and high blood pressure in mice lacking the adenosine A2a receptor, Nature 388 (1997) 674-8.

[188] F.K. Johnson, R.A. Johnson, K.J. Peyton, W. Durante, Arginase inhibition restores arteriolar endothelial function in Dahl rats with salt-induced hypertension, Am J Physiol Regul Integr Comp Physiol 288 (2005) R1057-62.

[189] Y. Hirano, M. Tsunoda, T. Shimosawa, H. Matsui, T. Fujita, T. Funatsu, Suppression of catechol-O-methyltransferase activity through blunting of alpha2-adrenoceptor can explain hypertension in Dahl salt-sensitive rats, Hypertens Res 30 (2007) 269-78.

[190] W.R. Dunn, S.M. Gardiner, Structural and Functional Properties of Isolated, Pressurized, Mesenteric Resistance Arteries From a Vasopressin-Deficient Rat Model of Genetic Hypertension, Hypertension 26 (1995) 390-396.

[191] M.J.C.S. Jeroen van den Akker, Erik N.T.P. Bakker, Ed vanBavel, Small Artery Remodeling: Current Concepts and Questions, Journal of Vascular Research 47 (2010) 183-202.

[192] M. Mulvany, Small artery remodeling in hypertension, Current Hypertension Reports 4 (2002) 49-55.

[193] G.K. Owens, P.S. Rabinovitch, S.M. Schwartz, Smooth muscle cell hypertrophy versus hyperplasia in hypertension, Proceedings of the National Academy of Sciences 78 (1981) 7759-7763.

[194] R.M. Lee, C.R. Triggle, Morphometric study of mesenteric arteries from genetically hypertensive Dahl strain rats, Blood Vessels 23 (1986) 199-224.

[195] H.D. Intengan, G. He, E.L. Schiffrin, Effect of Vasopressin Antagonism on Structure and Mechanics of Small Arteries and Vascular Expression of Endothelin-1 in Deoxycorticosterone Acetate–Salt Hypertensive Rats, Hypertension 32 (1998) 770-777.

[196] H.D. Intengan, E.L. Schiffrin, Mechanical properties of mesenteric resistance arteries from Dahl salt-resistant and salt-sensitive rats: role of endothelin-1, J Hypertens 16 (1998) 1907-12.

[197] H.D. Intengan, E.L. Schiffrin, Structure and mechanical properties of resistance arteries in hypertension: role of adhesion molecules and extracellular matrix determinants, Hypertension 36 (2000) 312-8.

[198] A. Shirwany, K.T. Weber, Extracellular Matrix Remodeling in Hypertensive Heart Disease, Journal of the American College of Cardiology 48 (2006) 97-98.

[199] C.G. Brilla, B. Maisch, K.T. Weber, Myocardial collagen matrix remodelling in arterial hypertension, Eur Heart J 13 Suppl D (1992) 24-32.

[200] A.M. Briones, F.E. Xavier, S.M. Arribas, M.C. González, L.V. Rossoni, M.J. Alonso, M. Salaices, Alterations in structure and mechanics of resistance arteries from ouabain-induced hypertensive rats, American Journal of Physiology - Heart and Circulatory Physiology 291 (2006) H193-H201.

[201] M.A. Boegehold, T.A. Kotchen, Effect of dietary salt on the skeletal muscle microvasculature in Dahl rats, Hypertension 15 (1990) 420-6.

[202] M.A. Boegehold, Microvascular changes associated with high salt intake and hypertension in Dahl rats, Int J Microcirc Clin Exp 12 (1993) 143-56.

[203] A. Benetos, H. Bouaziz, P. Albaladejo, D. Guez, M.E. Safar, Carotid Artery Mechanical Properties of Dahl Salt-Sensitive Rats, Hypertension 25 (1995) 272-277.

[204] S. Kinlay, M.A. Creager, M. Fukumoto, H. Hikita, J.C. Fang, A.P. Selwyn, P. Ganz, Endothelium-Derived Nitric Oxide Regulates Arterial Elasticity in Human Arteries In Vivo, Hypertension 38 (2001) 1049-1053.

[205] J. Bellien, J. Favre, M. Iacob, J. Gao, C. Thuillez, V. Richard, R. Joannides, Arterial stiffness is regulated by nitric oxide and endothelium-derived hyperpolarizing factor during changes in blood flow in humans, Hypertension 55 (2010) 674-80.

[206] Y. Cao, H. Li, F.T. Mu, O. Ebisui, J.W. Funder, J.P. Liu, Telomerase activation causes vascular smooth muscle cell proliferation in genetic hypertension, FASEB J 16 (2002) 96-8.

[207] M. Iglarz, R.M. Touyz, F. Amiri, M.-F. Lavoie, Q.N. Diep, E.L. Schiffrin, Effect of Peroxisome Proliferator–Activated Receptor-α and -γ Activators on Vascular Remodeling in Endothelin-Dependent Hypertension, Arteriosclerosis, Thrombosis, and Vascular Biology 23 (2003) 45-51.

[208] J. Bellien, R. Joannides, M. Iacob, P. Arnaud, C. Thuillez, Calcium-Activated Potassium Channels and NO Regulate Human Peripheral Conduit Artery Mechanics, Hypertension 46 (2005) 210-216.

[209] J.-S. Li, E.L. Schiffrin, Effect of Calcium Channel Blockade or Angiotensin-Converting Enzyme Inhibition on Structure of Coronary, Renal, and Other Small Arteries in Spontaneously Hypertensive Rats, Journal of Cardiovascular Pharmacology 28 (1996) 68-74.

[210] J.G. Dickhout, R.M.K.W. Lee, Increased medial smooth muscle cell length is responsible for vascular hypertrophy in young hypertensive rats, American Journal of Physiology - Heart and Circulatory Physiology 279 (2000) H2085-H2094.

[211] U.C. Garg, A. Hassid, Nitric oxide-generating vasodilators and 8-bromo-cyclic guanosine monophosphate inhibit mitogenesis and proliferation of cultured rat vascular smooth muscle cells, J Clin Invest 83 (1989) 1774-7.

[212] S.M.L. Wallace, Yasmin, C.M. McEniery, K.M. Mäki-Petäjä, A.D. Booth, J.R. Cockcroft, I.B. Wilkinson, Isolated Systolic Hypertension Is Characterized by Increased Aortic Stiffness and Endothelial Dysfunction, Hypertension 50 (2007) 228-233.

[213] D.M.-. ASTM, Standard Test Method for Tensile Properties of Polymer Matrix Composite Materials, Book of Standards Volume 15.03, 2008.

[214] Y.C. Fung, Biomechanics : mechanical properties of living tissues, Springer-Verlag, New York, 1993.

[215] Y. Huo, Y. Cheng, X. Zhao, X. Lu, G.S. Kassab, Biaxial vasoactivity of porcine coronary artery, American Journal of Physiology - Heart and Circulatory Physiology 302 (2012) H2058-H2063.

[216] W. Zhang, C. Wang, G.S. Kassab, The mathematical formulation of a generalized Hooke's law for blood vessels, Biomaterials 28 (2007) 3569-3578.

[217] G.L. Baumbach, M.A. Hajdu, Mechanics and composition of cerebral arterioles in renal and spontaneously hypertensive rats, Hypertension 21 (1993) 816-26.

[218] C.B. Neylon, Potassium channels and vascular proliferation, Vascular Pharmacology 38 (2002) 35-41.

[219] L.A. Pardo, Voltage-Gated Potassium Channels in Cell Proliferation, Physiology 19 (2004) 285-292.

[220] X.-L. Shi, G.-L. Wang, Z. Zhang, Y.-J. Liu, J.-H. Chen, J.-G. Zhou, Q.-Y. Qiu, Y.-Y. Guan, Alteration of Volume-Regulated Chloride Movement in Rat Cerebrovascular Smooth Muscle Cells During Hypertension, Hypertension 49 (2007) 1371-1377.

[221] S.N. Orlov, J. Tremblay, P. Hamet, Altered beta-adrenergic regulation of Na-K-Cl cotransport in cultured smooth muscle cells from the aorta of spontaneously hypertensive rats. Role of the cytoskeleton network, Am J Hypertens 8 (1995) 739-47.

[222] E.J. Mackie, T. Scott-Burden, A.W. Hahn, F. Kern, J. Bernhardt, S. Regenass, A. Weller, F.R. Buhler, Expression of tenascin by vascular smooth muscle cells. Alterations in hypertensive rats and stimulation by angiotensin II, Am J Pathol 141 (1992) 377-88.

[223] W.F. Jackson, Potassium channels in the peripheral microcirculation, Microcirculation 12 (2005) 113-27.

[224] L. Cartin, K.M. Lounsbury, M.T. Nelson, Coupling of Ca2+ to CREB Activation and Gene Expression in Intact Cerebral Arteries From Mouse, Circulation Research 86 (2000) 760-767.

[225] M.J. Mulvany, W. Halpern, Contractile properties of small arterial resistance vessels in spontaneously hypertensive and normotensive rats, Circ Res 41 (1977) 19-26.

[226] B.I. Levy, J.B. Michel, J.L. Salzmann, M. Azizi, P. Poitevin, M. Safar, J.P. Camilleri, Effects of chronic inhibition of converting enzyme on mechanical and structural

properties of arteries in rat renovascular hypertension, Circulation Research 63 (1988) 227-39.

[227] B.I. Levy, J.B. Michel, J.L. Salzmann, P. Poitevin, M. Devissaguet, E. Scalbert, M.E. Safar, Long-term effects of angiotensin-converting enzyme inhibition on the arterial wall of adult spontaneously hypertensive rats, The American Journal of Cardiology 71 (1993) E8-E16.

[228] P. Laurant, R.M. Touyz, E.L. Schiffrin, Effect of pressurization on mechanical properties of mesenteric small arteries from spontaneously hypertensive rats, J Vasc Res 34 (1997) 117-25.

[229] L. Hu, R.D. Manning, Role of nitric oxide in regulation of long-term pressure-natriuresis relationship in Dahl rats, American Journal of Physiology - Heart and Circulatory Physiology 268 (1995) H2375-H2383.

[230] P.Y. Chen, P.W. Sanders, L-arginine abrogates salt-sensitive hypertension in Dahl/Rapp rats, J Clin Invest 88 (1991) 1559-67.

[231] K. Nakanishi, N. Hara, Y. Nagai, Salt-sensitive hypertension in conscious rats induced by chronic nitric oxide blockade, Am J Hypertens 15 (2002) 150-6.

[232] L. Raij, Nitric oxide, salt sensitivity, and cardiorenal injury in hypertension, Semin Nephrol 19 (1999) 296-303.

[233] A. Miyoshi, H. Suzuki, M. Fujiwara, M. Masai, T. Iwasaki, Impairment of endothelial function in salt-sensitive hypertension in humans, Am J Hypertens 10 (1997) 1083-90.

[234] H. Hayakawa, L. Raij, The Link Among Nitric Oxide Synthase Activity, Endothelial Function, and Aortic and Ventricular Hypertrophy in Hypertension, Hypertension 29 (1997) 235-241.

[235] E. Bragulat, A.d.l. Sierra, M.T. Antonio, A. Coca, Endothelial Dysfunction in Salt-Sensitive Essential Hypertension, Hypertension 37 (2001) 444-448.

[236] S. Taddei, A. Virdis, P. Mattei, L. Ghiadoni, I. Sudano, A. Salvetti, Defective l-Arginine–Nitric Oxide Pathway in Offspring of Essential Hypertensive Patients, Circulation 94 (1996) 1298-1303.

[237] B. Tesfamariam, M.L. Ogletree, Dissociation of endothelial cell dysfunction and blood pressure in SHR, American Journal of Physiology - Heart and Circulatory Physiology 269 (1995) H189-H194.

[238] R.K. Dubey, M.A. Boegehold, D.G. Gillespie, M. Rosselli, Increased nitric oxide activity in early renovascular hypertension, American Journal of Physiology - Regulatory, Integrative and Comparative Physiology 270 (1996) R118-R124.

[239] L. Linder, W. Kiowski, F.R. Bühler, T.F. Lüscher, Indirect evidence for release of endothelium-derived relaxing factor in human forearm circulation in vivo. Blunted response in essential hypertension, Circulation 81 (1990) 1762-7.

143

[240] J. Li, R.D. Bukoski, Endothelium-dependent relaxation of hypertensive resistance arteries is not impaired under all conditions, Circulation Research 72 (1993) 290-6.

[241] W. Lockette, Y. Otsuka, O. Carretero, The loss of endothelium-dependent vascular relaxation in hypertension, Hypertension 8 (1986) II61-6.

[242] A.I. Soloviev, A.V. Parshikov, A.V. Stefanov, Evidence for the involvement of protein kinase C in depression of endothelium-dependent vascular responses in spontaneously hypertensive rats, J Vasc Res 35 (1998) 325-31.

[243] F. Pourageaud, J.L. Freslon, Impaired endothelial relaxations induced by agonists and flow in spontaneously hypertensive rat compared to Wistar-Kyoto rat perfused coronary arteries, J Vasc Res 32 (1995) 190-9.

[244] B. Tesfamariam, W. Halpern, Endothelium-dependent and endothelium-independent vasodilation in resistance arteries from hypertensive rats, Hypertension 11 (1988) 440-4.

[245] H.I. Chen, C.T. Hu, Endogenous nitric oxide on arterial hemodynamics: a comparison between normotensive and hypertensive rats, American Journal of Physiology - Heart and Circulatory Physiology 273 (1997) H1816-H1823.

[246] E. Nava, G. Noll, T.F. Lüscher, Increased Activity of Constitutive Nitric Oxide Synthase in Cardiac Endothelium in Spontaneous Hypertension, Circulation 91 (1995) 2310-2313.

[247] C.-T. Hu, K.-C. Chang, C.-Y. Wu, H.I. Chen, Acute effects of nitric oxide blockade with L-NAME on arterial haemodynamics in the rat, British Journal of Pharmacology 122 (1997) 1237-1243.

[248] M. Félétou, P.M. Vanhoutte, Endothelium-Derived Hyperpolarizing Factor, Arteriosclerosis, Thrombosis, and Vascular Biology 26 (2006) 1215-1225.

[249] R.P. Brandes, F.-H. Schmitz-Winnenthal, M. Félétou, A. Gödecke, P.L. Huang, P.M. Vanhoutte, I. Fleming, R. Busse, An endothelium-derived hyperpolarizing factor distinct from NO and prostacyclin is a major endothelium-dependent vasodilator in resistance vessels of wild-type and endothelial NO synthase knockout mice, Proceedings of the National Academy of Sciences 97 (2000) 9747-9752.

[250] Y. Nishikawa, D.W. Stepp, W.M. Chilian, Nitric oxide exerts feedback inhibition on EDHF-induced coronary arteriolar dilation in vivo, American Journal of Physiology - Heart and Circulatory Physiology 279 (2000) H459-H465.

[251] J. Bauersachs, R.d. Popp, M. Hecker, E. Sauer, I. Fleming, R. Busse, Nitric Oxide Attenuates the Release of Endothelium-Derived Hyperpolarizing Factor, Circulation 94 (1996) 3341-3347.

[252] L.A. Schildmeyer, R.M. Bryan, Jr., Effect of NO on EDHF response in rat middle cerebral arteries, Am J Physiol Heart Circ Physiol 282 (2002) H734-8.

[253] S. Chauhan, A. Rahman, H. Nilsson, L. Clapp, R. MacAllister, A. Ahluwalia, NO contributes to EDHF-like responses in rat small arteries: a role for NO stores, Cardiovascular Research 57 (2003) 207-216.

[254] H.R. Chang, R.P. Lee, C.Y. Wu, H.I. Chen, Nitric oxide in mesenteric vascular reactivity: a comparison between rats with normotension and hypertension, Clin Exp Pharmacol Physiol 29 (2002) 275-80.

[255] C.S. Bockman, I. Gonzalez-Cabrera, P.W. Abel, Alpha-2 adrenoceptor subtype causing nitric oxide-mediated vascular relaxation in rats, Journal of Pharmacology and Experimental Therapeutics 278 (1996) 1235-43.

[256] K.F. Ng, S.W. Leung, R.Y. Man, P.M. Vanhoutte, Endothelium-derived hyperpolarizing factor mediated relaxations in pig coronary arteries do not involve Gi/o proteins, Acta Pharmacol Sin 29 (2008) 1419-24.

[257] C.S. Flordellis, M. Castellano, R. Franco, V.I. Zannis, H. Gavras, Expression of multiple alpha 2-adrenergic receptor messenger RNA species in rat tissues, Hypertension 15 (1990) 881-7.

[258] D.E. Handy, C.S. Flordellis, N.N. Bogdanova, M.R. Bresnahan, H. Gavras, Diverse tissue expression of rat alpha 2-adrenergic receptor genes, Hypertension 21 (1993) 861-5.

[259] E. Kintsurashvili, I. Gavras, C. Johns, H. Gavras, Effects of antisense oligodeoxynucleotide targeting of the alpha(2B)-adrenergic receptor messenger RNA in the central nervous system, Hypertension 38 (2001) 1075-80.

[260] K.P. Makaritsis, C. Johns, I. Gavras, H. Gavras, Role of alpha(2)-adrenergic receptor subtypes in the acute hypertensive response to hypertonic saline infusion in anephric mice, Hypertension 35 (2000) 609-13.

[261] P.W. Sanders, Salt-sensitive hypertension: Lessons from animal models, American Journal of Kidney Diseases 28 (1996) 775-782.

[262] M.S. Zhou, H. Kosaka, R.X. Tian, Y. Abe, Q.H. Chen, H. Yoneyama, A. Yamamoto, L. Zhang, L-Arginine improves endothelial function in renal artery of hypertensive Dahl rats, J Hypertens 19 (2001) 421-9.

[263] R. Schubert, U. Krien, I. Wulfsen, D. Schiemann, G. Lehmann, N. Ulfig, R.W. Veh, J.R. Schwarz, H. Gago, Nitric Oxide Donor Sodium Nitroprusside Dilates Rat Small Arteries by Activation of Inward Rectifier Potassium Channels, Hypertension 43 (2004) 891-896.

[264] K. Goto, Y. Kansui, H. Oniki, T. Ohtsubo, K. Matsumura, T. Kitazono, Upregulation of endothelium-derived hyperpolarizing factor compensates for the loss of nitric oxide in mesenteric arteries of dahl salt-sensitive hypertensive rats, Hypertens Res 35 (2012) 849-854.

[265] I.C. Villar, C.M. Panayiotou, A. Sheraz, M. Madhani, R.S. Scotland, M. Nobles, B. Kemp-Harper, A. Ahluwalia, A.J. Hobbs, Definitive role for natriuretic peptide receptor-C in

mediating the vasorelaxant activity of C-type natriuretic peptide and endothelium-derived hyperpolarising factor, Cardiovasc Res 74 (2007) 515-25.

[266] S.D. Chauhan, H. Nilsson, A. Ahluwalia, A.J. Hobbs, Release of C-type natriuretic peptide accounts for the biological activity of endothelium-derived hyperpolarizing factor, Proceedings of the National Academy of Sciences 100 (2003) 1426-1431.

[267] P. Ortiz, B.A. Stoos, N.J. Hong, D.M. Boesch, C.F. Plato, J.L. Garvin, High-Salt Diet Increases Sensitivity to NO and eNOS Expression But Not NO Production in THALs, Hypertension 41 (2003) 682-687.

[268] G.J. Lagaud, P.L. Skarsgard, I. Laher, C. van Breemen, Heterogeneity of endothelium-dependent vasodilation in pressurized cerebral and small mesenteric resistance arteries of the rat, J Pharmacol Exp Ther 290 (1999) 832-9.

[269] A.G. Stewart, P.J. Piper, Vasodilator actions of acetylcholine, A23187 and bradykinin in the guinea-pig isolated perfused heart are independent of prostacyclin, Br J Pharmacol 95 (1988) 379-84.

[270] T. Nagao, S. Illiano, P.M. Vanhoutte, Heterogeneous distribution of endothelium-dependent relaxations resistant to NG-nitro-L-arginine in rats, Am J Physiol 263 (1992) H1090-4.

[271] M.R. Tschudi, S. Mesaros, T.F. Luscher, T. Malinski, Direct in situ measurement of nitric oxide in mesenteric resistance arteries. Increased decomposition by superoxide in hypertension, Hypertension 27 (1996) 32-5.

[272] S.J. Parsons, A. Hill, G.J. Waldron, F. Plane, C.J. Garland, The relative importance of nitric oxide and nitric oxide-independent mechanisms in acetylcholine-evoked dilatation of the rat mesenteric bed, Br J Pharmacol 113 (1994) 1275-80.

[273] A.T. Chaytor, D.H. Edwards, L.M. Bakker, T.M. Griffith, Distinct hyperpolarizing and relaxant roles for gap junctions and endothelium-derived H2O2 in NO-independent relaxations of rabbit arteries, Proceedings of the National Academy of Sciences 100 (2003) 15212-15217.

[274] N. Boulebda, A. Gairard, Characterization of endothelium-derived relaxing factor involvement in the potentiating effect of parathyroidectomy on norepinephrine-induced rat aortic contraction, Fundam Clin Pharmacol 8 (1994) 43-53.

[275] S. Rajagopalan, S. Kurz, T. Munzel, M. Tarpey, B.A. Freeman, K.K. Griendling, D.G. Harrison, Angiotensin II-mediated hypertension in the rat increases vascular superoxide production via membrane NADH/NADPH oxidase activation. Contribution to alterations of vasomotor tone, J Clin Invest 97 (1996) 1916-23.

[276] U. Landmesser, S. Dikalov, S.R. Price, L. McCann, T. Fukai, S.M. Holland, W.E. Mitch, D.G. Harrison, Oxidation of tetrahydrobiopterin leads to uncoupling of endothelial cell nitric oxide synthase in hypertension, The Journal of Clinical Investigation 111 (2003) 1201-1209.

146

[277] M.J. Somers, K. Mavromatis, Z.S. Galis, D.G. Harrison, Vascular Superoxide Production and Vasomotor Function in Hypertension Induced by Deoxycorticosterone Acetate–Salt, Circulation 101 (2000) 1722-1728.

[278] M. Feletou, P.M. Vanhoutte, A.H. Weston, G. Edwards, EDHF and endothelial potassiun channels: IKCa and SKCa, Br J Pharmacol 140 (2003) 225; author reply 226.

[279] R.H.P. Hilgers, R.C. Webb, Reduced expression of SKCa and IKCa channel proteins in rat small mesenteric arteries during angiotensin II-induced hypertension, American Journal of Physiology - Heart and Circulatory Physiology 292 (2007) H2275-H2284.

[280] Q.-H. Chen, M.A. Andrade, A.S. Calderon, G.M. Toney, Hypertension Induced by Angiotensin II and a High Salt Diet Involves Reduced SK Current and Increased Excitability of RVLM Projecting PVN Neurons, Journal of Neurophysiology 104 (2010) 2329-2337.

[281] S. Dal-Ros, C. Bronner, C. Schott, M.O. Kane, M. Chataigneau, V.B. Schini-Kerth, T. Chataigneau, Angiotensin II-Induced Hypertension Is Associated with a Selective Inhibition of Endothelium-Derived Hyperpolarizing Factor-Mediated Responses in the Rat Mesenteric Artery, Journal of Pharmacology and Experimental Therapeutics 328 (2009) 478-486.

[282] U. Onaka, K. Fujii, I. Abe, M. Fujishima, Antihypertensive Treatment Improves Endothelium-Dependent Hyperpolarization in the Mesenteric Artery of Spontaneously Hypertensive Rats, Circulation 98 (1998) 175-182.

[283] Y. Takeda, A. Zhu, T. Yoneda, M. Usukura, H. Takata, M. Yamagishi, Effects of Aldosterone and Angiotensin II Receptor Blockade on Cardiac Angiotensinogen and Angiotensin-Converting Enzyme 2 Expression in Dahl Salt-Sensitive Hypertensive Rats, American Journal of Hypertension 20 (2007) 1119-1124.

[284] M.S. Zhou, E.A. Jaimes, L. Raij, Benazepril combined with either amlodipine or hydrochlorothiazide is more effective than monotherapy for blood pressure control and prevention of end-organ injury in hypertensive Dahl rats, J Cardiovasc Pharmacol 48 (2006) 857-61.

[285] M.S. Zhou, A.G. Adam, E.A. Jaimes, L. Raij, In salt-sensitive hypertension, increased superoxide production is linked to functional upregulation of angiotensin II, Hypertension 42 (2003) 945-51.

[286] O.A. Sofola, A. Knill, R. Hainsworth, M. Drinkhill, Change in endothelial function in mesenteric arteries of Sprague-Dawley rats fed a high salt diet, J Physiol 543 (2002) 255-60.

VITA

TUSHAR V. GADKARI

2007 – Present	PhD Candidate, Department of Biomedical Engineering, Florida International University, Miami, USA
2005 – 2007	M.A.Sc, Electrical and Computer Engineering Department, McMaster University, Hamilton, Ontario, Canada
2000 – 2004	B.E, Instrumentation Engineering, Mumbai University, Mumbai, India.

PEER-REVIEWED PUBLICATIONS

T.V. Gadkari, Kapela A, N.M.Tsoukais, "Determination of Mechanical Parameters of Rat Mesenteric Arterioles in Dahl Salt Sensitive hypertension: A Theoretical and Experimental study." (manuscript in preparation to be submitted Annals of Biomedical Engineering).

T.V. Gadkari, N.M. Tsoukias, "Regulation of arteriolar diameter by the frequency of endothelial Ca2+ transients." (manuscript submitted to Microcirculation Journal).

T. Gadkari, N. Cortes, K.J. Madrasi, N.M. Tsoukias, and M.S. Joshi, "Agmatine Induced NO Dependent Rat Mesenteric Artery Relaxation and its Impairment in Salt-Sensitive Hypertension." Nitric Oxide, (manuscript accepted for publication).

K.J. Madrasi, T. Gadkari, M.S. Joshi, K. Kavallieratos and N. Tsoukias. "Glutathiyl radical as an intermediate in glutathione nitrosation" Free Radical Biology and Medicine 53 (2012) 1968-1976.

CONFERENCE PROCEEDINGS

A. Kapela, T. Gadkari, and N. M. Tsoukias, "A multiscale computational model of microcirculatory vasoreactivity: Linking subcellular events to macroscale responses in health and disease," FASEB J., vol. 23:627.12, 2009.

Tushar Gadkari, Nikolaos Tsoukias, and Mahesh S. Joshi, Agmatine Produced by Arginine Decarboxylase Activity Causes NO Dependent Rat Mesenteric Artery Relaxation, FASEB 2011

Tushar Gadkari, Zenith Acosta, Nikolaos Tsoukias, and Mahesh S Joshi, Agmatine-mediated rat mesenteric artery relaxation via NO synthesis, FASEB J, Apr 2010; 24: 984.23

Tushar Gadkari, Zenith Acosta, and Nikolaos Tsoukias, Nitric Oxide dependent signaling in vasorelaxation: Effect of transient Nitric Oxide release, BMES Annual meeting, Oct 2009, 2192

Kapela, A., Gadkari, T., Nagaraja, S. and Tsoukias, N. M, Multiscale Mathematical Modeling of Microvascular Tone Regulation in 25th Southern Biomedical Engineering Conference May 2009, Vol. 24, IFMBE Proceedings 297-298 (Springer Berlin Heidelberg, 2009